AD-A119 460 TRW DEFENSE AND SPACE SYSTEMS GROUP REDONDO BEACH CA F/G 20/5
DIRECTED BEAM ALIGNMENT SYSTEM TESTING PROGRAM.(U)
JUN 79 R F GATES DAAK40-79-C-0018
UNCLASSIFIED TRW-33556 NL

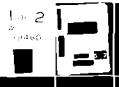

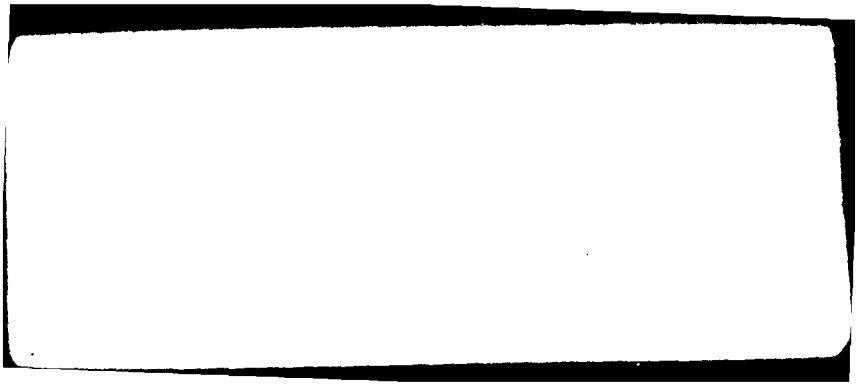

Sales No.: 33556

[redacted]

DIRECTED BEAM ALIGNMENT SYSTEM TESTING PROGRAM

FINAL REPORT

JUNE 4, 1979

CONTRACT No. DAAK-40-78-C-0018 79 CDRL A003

Prepared by R F Gates
R. F. Gates

Approved by P E Kendall
P. E. Kendall

PREPARED FOR

U.S. ARMY MISSLE RESEARCH AND DEVELOPMENT COMMAND

HIGH ENERGY LASER SYSTEMS PROJECT OFFICE

RED STONE ARSENAL

ALABAMA 35809

TRW
DEFENSE AND SPACE SYSTEMS GROUP

page 79 has been removed from this document and it is no longer proprietary.
9 Aug 82
David J. Klug
COTR

SECURITY CLASSIFICATION OF THIS PAGE (When Data Entered)

REPORT DOCUMENTATION PAGE		READ INSTRUCTIONS BEFORE COMPLETING FORM
1. REPORT NUMBER	2. GOVT ACCESSION NO. AD-A119460	3. RECIPIENT'S CATALOG NUMBER
4. TITLE (and Subtitle) Directed Beam Alignment System		5. TYPE OF REPORT & PERIOD COVERED Final Dec 78-Jun 79
		6. PERFORMING ORG. REPORT NUMBER 33556
7. AUTHOR(s) Robert F. Gates		8. CONTRACT OR GRANT NUMBER(s) DAAK40-79-C-0018
9. PERFORMING ORGANIZATION NAME AND ADDRESS TRW, One Space Park, Redondo Beach, CA 90278		10. PROGRAM ELEMENT, PROJECT, TASK AREA & WORK UNIT NUMBERS 63314A
11. CONTROLLING OFFICE NAME AND ADDRESS US Army MICOM, DRSMI-RHS, Redstone Arsenal, AL 35898		12. REPORT DATE 4 Jun 79
		13. NUMBER OF PAGES 109
14. MONITORING AGENCY NAME & ADDRESS(if different from Controlling Office) Same as 11		15. SECURITY CLASS. (of this report) UNCLAS
		15a. DECLASSIFICATION/DOWNGRADING SCHEDULE N/A

16. DISTRIBUTION STATEMENT (of this Report)

UNLIMITED

DISTRIBUTION STATEMENT A
Approved for public release;
Distribution Unlimited

17. DISTRIBUTION STATEMENT (of the abstract entered in Block 20, if different from Report)

UNLIMITED

DISTRIBUTION STATEMENT A
Approved for public release;
Distribution Unlimited

18. SUPPLEMENTARY NOTES

19. KEY WORDS (Continue on reverse side if necessary and identify by block number)

Coordinate Alignment Systems; Remote Coordinate Alignment

20. ABSTRACT (Continue on reverse side if necessary and identify by block number)

A technique has been developed for six-degree-or-freedom coordinate frame alignment between remote battlefield vehicles. It was developed specifically for a High Energy Laser Weapon application which must hand off a target from a radar vehicle to a laser vehicle to milliradian accuracy. Laboratory hardware was used from rooftops in Redondo Beach to validate the concept experimentally. In a field environment, an alignment should take less than 30 sec, work to ranges beyond 3 km, and work in visibilities less than 4 km.

DD FORM 1 JAN 73 1473 EDITION OF 1 NOV 65 IS OBSOLETE UNCLASSIFIED

SECURITY CLASSIFICATION OF THIS PAGE (When Data Entered)

ACKNOWLEDGMENTS

The following people assisted in the preparation of the material presented in this report: O. Imai, O. W. Momary, R. C. Howe, J. Nella, J. V. Flannery, L. G. Horn, L. Danielson. Thanks are also due to D. Gray, HELSPO technical monitor for his helpful suggestions during the performance of the contract.

Sales No.: 33556

TABLE OF CONTENTS

		PAGE
1.0	Introduction	1
	1.1 State of the Problem	2
	1.2 Summary	2
2.0	DBAS Principles	4
	2.1 Purpose of DBAS	4
	2.1.1 Handover Based on DBAS Alignment	7
	2.2 Conceptual Implementation of DBAS	8
3.0	Breadboard	13
	3.1 Receiver	13
	3.1.1 Optics	13
	3.1.2 Detector	14
	3.1.3 Electronics	14
	3.1.4 Breadboard Design Package	21
	3.2 Transmitter	21
	3.3 Laboratory Measurements	23
	3.3.1 Geometric Measurements	23
	3.3.2 Radiometric Measurements	31
4.0	Experimental Results	35
	4.1 Tests	35
	4.1.1 Tests Results	37
	4.2 Verification	40
5.0	Conceptual Design	44
	5.1 Operation	55

TABLE OF CONTENTS (Continued)

PAGE

5.2 Transmitter 63

5.2.1 Laser. 63

5.2.2 Optics 64

5.3 Receiver. 65

5.3.1 Optics 65

5.3.2 Detector 67

5.4 Electronics 69

5.5 Unique Problems 73

6.0 Development Recommendations. 75

6.1 Detailed Experimental Prototype Schedule. 77

6.2 Cost Estimates. 77

Appendix A

Scattering Phonomenology. 80

Appendix B

Two Gimbal DBAS Equations 88

Appendix C

Test Plan and Errata Sheet. 90

LIST OF FIGURES

		PAGE
Figure 1.	DBAS Parameters	3
Figure 2.	DBAS Components	5
Figure 3.	DBAS Geometry for Range and Altitude Determinations	11
Figure 4.	Typical Spectral Responsivity	15
Figure 5.	DBAS Breadboard Post Amplifier	18
Figure 6.	DBAS Breadboard Signal Processing	19
Figure 7.	Bouwers Concentric Optical System	22
Figure 8.	Fiber Optics Slits As Seen Through Telescope Lens	25
Figure 9.	Slit Misalignment	26
Figure 10.	Slit Angle with Respect to Vertical	29
Figure 11.	True Slit Width	31
Figure 12.	L.A. Local Area Map	36
Figure 13.	Angular Slit Sensitivity	41
Figure 14.	R6 Parking Lot Verification Geometry and Measurements	42
Figure 15.	Building 82 Verification Geometry and Measurements	42a
Figure 16.	Detector Arrangement	45
Figure 17.	Basic Block Diagram of Optical Receiver Unit	47
Figure 18.	Basic Block Diagram for Laser Transmitter Unit	48
Figure 19.	Block Diagram of Combined Unit	49
Figure 20.	Double Gimbal Set Configuration	50
Figure 21.	X-Y Gimbal Set Configuration	52

LIST OF FIGURES (Continued)

PAGE

Figure 22. Final Configuration. 53

Figure 23. Basic Block Diagram of Final Concept 54

Figure 24(a) DBAS Functional Flow 58

Figure 24(b) DBAS Functional Flow (Continued) 59

Figure 24(c) DBAS Functional Flow (Continued) 60

Figure 24(d) DBAS Functional Flow (Continued) 61

Figure 24(e) DBAS Functional Flow (Continued) 62

Figure 25. Transmitter Optical Schematic. 64

Figure 26. Receiver Optical Schematic 66

Figure 27. Detector Spectral Response 68

Figure 28. Pulse Sequence Timing Diagrams 70

Figure 29. Level Sensor 72

Figure 30. Recommended DBAS Development Schedule. 76

Figure 31. Experimental Prototype Schedule. 78

Figure A-1. Aerosol Scattering Geometry 81

Figure A-2. Predicted Intensity at the Receiver 87

LIST OF TABLES

		PAGE
Table 1.	Test Summary	3
Table 2.	APD Module Characteristics	16
Table 3.	Analog Electronics Specification	20
Table 4.	Transmitter Characteristics.	23
Table 5.	D.B.A.S. Sensor Geometric Measurements	32
Table 6.	Summary of DBAS Radiometric Measurements	34
Table 7.	R6 Parking Lot Test Summary.	38
Table 8.	Building 82 Test Summary	38
Table 9.	Test Summary	43
Table 10.	Laser Performance Parameters	63
Table 11.	Optical Specifications	65
Table 12.	Detector Specification	67
Table 13.	Experimental Prototype Cost Estimate	79

1.0 INTRODUCTION

TRW instituted a High Energy Laser Weapons System (HELWS) fire control project in 1977 as a portion of the total Independent Research and Development (IR&D) effort. As a part of this project, a scheme for providing fast, accurate, and reliable inter-vehicle alignment information (where the vehicles were not necessarily in view of each other) was investigated. This preliminary concept made use of clinometers, magnetic compasses, altimeters, pulsed laser transmitters, and laser pulse backscatter receivers at each of the vehicles. Later, a simpler system was conceived using only the pulsed laser transmitter and the laser pulse backscatter sensors. This simplified version, known as DBAS (an acronym for Directed Beam Alignment System) was constructed in breadboard form and tested by TRW in 1978, also on company funds.

The present contract provided for the following tasks:

- o Preparation of a test plan describing the experiments and conditions for testing of the breadboard DBAS.
- o Review meeting with HELSPO personnel to review test plan
- o Testing and Demonstration of the breadboard
- o Technical briefing at MIRADCOM on test results
- o A top level conceptual design for a militarized automated DBAS
- o Establishment of guidelines for developing the operational version of DBAS
- o Preparation of the Final Report
- o Final technical briefing at MIRADCOM to review project results

1.1 STATEMENT OF THE PROBLEM

It is expected that High Energy Laser Weapons will be employed to protect rear-area high value assets. In this type of deployment there may be several laser weapons and an acquisition radar located within a 9 square km area about the asset. These vehicles will be at random orientations relative to each other, with pitch and roll angles of the vehicles being as large as 10 degrees, and may not be visible to each other. Knowledge of the relative alignment of a weapon vehicle's inertial frame of reference with respect to the inertial frame of reference of the acquisition radar is necessary, so that the threat coordinates can be transferred from the radar to the laser weapons precision tracker with sufficient accuracy so that the threat will be within the trackers relatively small field-of-view. Thus, some trade-offs exist between the precision of the alignment and the HEL weapons optical tracker's search field, with the required alignment accuracy varying inversely with the tracker's field-of-view. Normally, this means that the alignment accuracy requirement is not in the precision surveying category, i.e., orientation accuracies of one or two milliradians, and position accuracies to 10 or so meters appear to be sufficient. The breadboard described in Section 3 was designed to provide a test bed to experimentally verify the feasibility of using DBAS for this purpose.

1.2 SUMMARY

The test program proved the feasibility of using the DBAS for providing range, elevation, and angular data for use in an overall intervehicle alignment coordinate transformation system. Table 1 shows the results of tests from two different locations at TRW's Space Park complex. The details of these tests are contained in Section 4.0.

Some difficulties were experienced during the test period with bad weather, which caused the testing period to be longer than originally scheduled. However some of the difficulties encountered helped to identify some practical problems with an operational system, and thus provided insight into the conceptual design of a future system. The useful range of the system was found to be a function of the visibility. Visibility between 3 and ten kilometers appeared to give the best results. By best results is meant the most consistent signal reception. When the weather was extremely clear, the signals were sporadic, the same was true when the visibility was less than 3 kilometers.

Based upon the experience with the breadboard, a conceptual design for a militarized version has evolved. Section 5 covers this design in detail.

Recommendations for further development are given in Section 6 along with schedule and cost data for an experimental prototype.

TABLE I - TEST SUMMARY

		MEASUREMENTS (METERS)		DIFFERENCE (METERS)	
TEST	PARAMETER	DBAS	SURVEY	MEASURED	THEORETICAL ONE SIGMA
A	RANGE	590.7	592.5	1.8	6
	ELEVATION	13.9	5.1	8.8	20
B	RANGE	1185.1	1193.4	8.3	6
	ELEVATION	-21.8	-4.9	16.9	20

2.0 DBAS PRINCIPLES

2.1 PURPOSE OF DBAS

The basic problem that the DBAS concept addresses is that of determining the relative alignment - both positional and rotational - of two remote vehicles separated by up to 3 km. The primary operational obstacle to the process of establishing this alignment is that a clear line of sight between the two vehicles is generally not available.

With respect to the illustration in Figure 1, the alignment problem consists of establishing:

θ_T and ϕ_T, the pitch and roll angles respectively of the vehicle on which the DBAS transmitter is mounted

θ_R and ϕ_R, the pitch and roll angles respectively of the vehicle on which the DBAS receiver is mounted

A_ρ, the bearing angle from the DBAS receiver to the DBAS transmitter

ζ, the bearing angle from the DBAS transmitter to the DBAS receiver

ρ_H, the horizontal range between the two vehicles

ρ_V, the altitude difference between the two vehicles

Then the position components of the receiver vehicle, expressed in the transmitter vehicle coordinate set, are

$$\begin{bmatrix} \rho_{XR} \\ \rho_{YR} \\ \rho_{ZR} \end{bmatrix}_{TV} = \left[T_T\right] \begin{bmatrix} \rho_H \cdot \cos\zeta \\ \rho_H \cdot \sin\zeta \\ -\rho_V \end{bmatrix} \qquad (1)$$

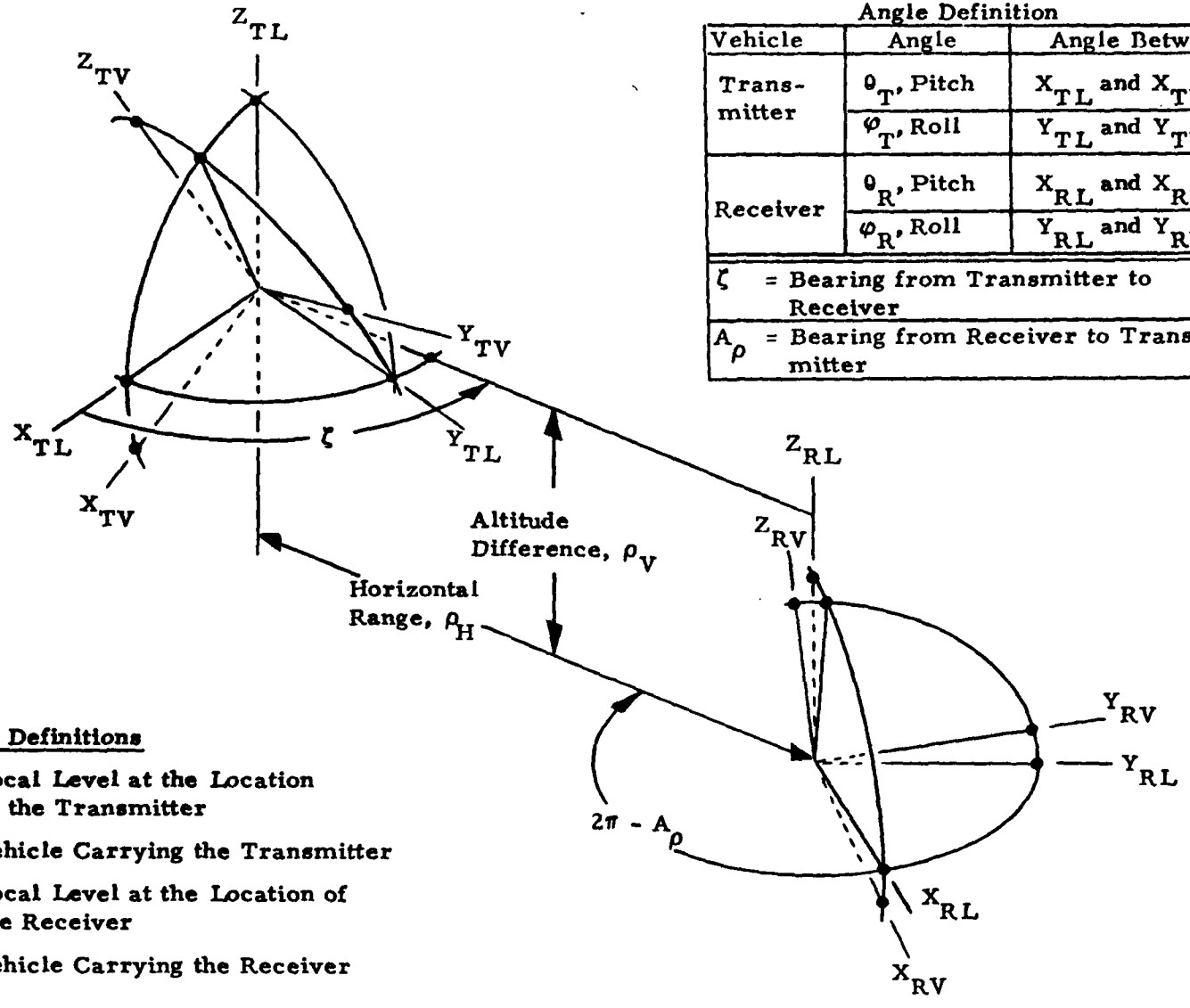

Angle Definition

Vehicle	Angle	Angle Between
Transmitter	θ_T, Pitch	X_{TL} and X_{TV}
	φ_T, Roll	Y_{TL} and Y_{TV}
Receiver	θ_R, Pitch	X_{RL} and X_{RV}
	φ_R, Roll	Y_{RL} and Y_{RV}
ζ = Bearing from Transmitter to Receiver		
A_ρ = Bearing from Receiver to Transmitter		

Subscript Definitions

TL - Local Level at the Location of the Transmitter

TV - Vehicle Carrying the Transmitter

RL - Local Level at the Location of the Receiver

RV - Vehicle Carrying the Receiver

FIGURE 1. DBAS PARAMETERS

where $\left[T_T\right]$ = coordinate transformation matrix between the transmitter vehicle and its reference local level set

$$\left[T_T\right] = \begin{bmatrix} \cos\theta_T & 0 & -\sin\theta_T \\ \sin\phi_T \cdot \sin\theta_T & \cos\phi_T & \sin\phi_T \cdot \cos\theta_T \\ \cos\phi_T \cdot \sin\theta_I & -\sin\phi_T & \cos\phi_T \cdot \cos\theta_T \end{bmatrix} \tag{2}$$

Conversely, the transmitter vehicle location in the receiver vehicle coordinate set is

$$\begin{bmatrix} \rho_{XT} \\ \rho_{YT} \\ \rho_{ZT} \end{bmatrix}_{RV} = \left[T_R\right] \begin{bmatrix} \rho_H \cos A_\rho \\ \rho_H \sin A_\rho \\ \rho_V \end{bmatrix} \tag{3}$$

$$\text{where } \left[T_R\right] = \begin{bmatrix} \cos\theta_R & 0 & -\sin\theta_R \\ \sin\phi_R \cdot \sin\theta_R & \cos\phi_R & \sin\phi_R \cdot \cos\theta_R \\ \cos\phi_R \cdot \sin\theta_R & -\sin\phi_R & \cos\phi_R \cdot \cos\theta_R \end{bmatrix} \tag{4}$$

The rotation matrix from the transmitter vehicle to the receiver vehicle is

$$\left[T_{RT}\right] = \left[T_R\right] \cdot \begin{bmatrix} -\cos(A_\rho - \zeta) & \sin(A_\rho - \zeta) & 0 \\ -\sin(A_\rho - \zeta) & -\cos(A_\rho - \zeta) & 0 \\ 0 & 0 & 1 \end{bmatrix} \cdot \left[T_T\right]^T \tag{5}$$

In the above development, the implicit assumption has been made that the local verticals at the two sites are parallel to each other (i.e., that the dot product $\underline{Z}_{TL} \cdot \underline{Z}_{RL} = 1.0$). For a maximum separation of 3 km, this is a reasonable assumption inasmuch as for 3 km,

$$\underline{Z}_{TL} \cdot \underline{Z}_{RL} = \cos \alpha = 0.999999889, \text{ and}$$

$$\underline{Z}_{TL} \cdot \underline{Z}_{RL} = \sin \alpha = 0.00047, \text{ or}$$

the maximum error contribution is less than 0.5 mrad.

2.1.1 Handover Based on DBAS Alignment

Assume that the DBAS transmitter is located on a radar van, that the DBAS receiver is mounted on a remotely located vehicle with an electro-optical tracker, and that it is desired to handover the radar tracking to the electro-optical tracker. Let the measured radar quantities with respect to the radar vehicle coordinate set (X_{TV}, Y_{TV}, Z_{TV}) be

R, radar range

A, azimuth from X_{TV}, measured in $X_{TV}Y_{TV}$ plane

E, elevation measured from $X_{TV}Y_{TV}$ plane

$\dot{R}$, radar range rate

Further, let the estimated angular rates (based on track filter processing) be

$\dot{A}$, azimuth rate

$\dot{E}$, elevation rate

Then the corresponding quantities at the electro-optical tracker site, measured with respect to the electro-optical vehicle coordinate set (X_{RV}, Y_{RV}, Z_{RV}) are

$$\begin{bmatrix} r \cdot \cos e \cdot \cos a \\ r \cdot \cos e \cdot \sin a \\ r \cdot \sin e \end{bmatrix} = \left[T_{RT}\right]^T \begin{bmatrix} R \cdot \cos E \cdot \cos A - \rho_{XR} \\ R \cdot \cos E \cdot \sin A - \rho_{YR} \\ R \cdot \sin E - \rho_{ZR} \end{bmatrix} \quad (6)$$

$$\begin{bmatrix} \dot{r} \\ \dot{a} \\ \dot{e} \end{bmatrix} = \begin{bmatrix} \cos e \cdot \cos a & \cos e \cdot \sin a & \sin e \\ \frac{-\sin a}{r \cdot \cos e} & \frac{\cos a}{r \cdot \cos e} & 0 \\ \frac{\sin e \cdot \cos a}{r} & \frac{-\sin e \cdot \sin a}{r} & \frac{\cos e}{r} \end{bmatrix} \cdot \left[T_{RT}\right]^{T} \cdot \begin{bmatrix} \cos E \cdot \cos A & -R \cdot \cos E \cdot \sin A & -R \cdot \sin E \cdot \cos A \\ \cos E \cdot \sin A & -R \cdot \cos E \cdot \cos A & -R \cdot \sin E \cdot \sin A \\ \sin E & 0 & R \cos E \end{bmatrix} \begin{bmatrix} \dot{R} \\ \dot{A} \\ \dot{E} \end{bmatrix} \quad (7)$$

2.2 CONCEPTUAL IMPLEMENTATION OF DBAS

A possible layout of the DBAS components required to establish the parameters in equations (1) through (5) is illustrated in Figure 2. It should be emphasized that the layout illustrated (with four gimbal mounts at both the transmitter and receiver locations and with "upper" and "lower" receiver windows) is only for the purposes of describing the DBAS concept; the DBAS preliminary design discussed in Section 5.0 is much simplified, utilizing only two axis gimbals at each location and a single optical window to provide all the essential functions and capabilities.

As shown in Figure 2, a two axis base is mounted on each of the vehicles involved in the alignment process. When the instrument mounting plate is leveled, the gimbal readouts provide the vehicle pitch and roll angles, θ_i and ϕ_i (i = T or R) with respect to local level.

At the radar vehicle, the DBAS transmitter is mounted on the leveled mounting plate and similarly, a DBAS receiver is mounted at each location of an electro-optical tracker*. The DBAS transmitter is triggered to output

*Although this discussion has been made application-specific to the case where handover from a radar tracker to remote electro-optical trackers is desired, DBAS can be used for any remote alignment, position fixing application.

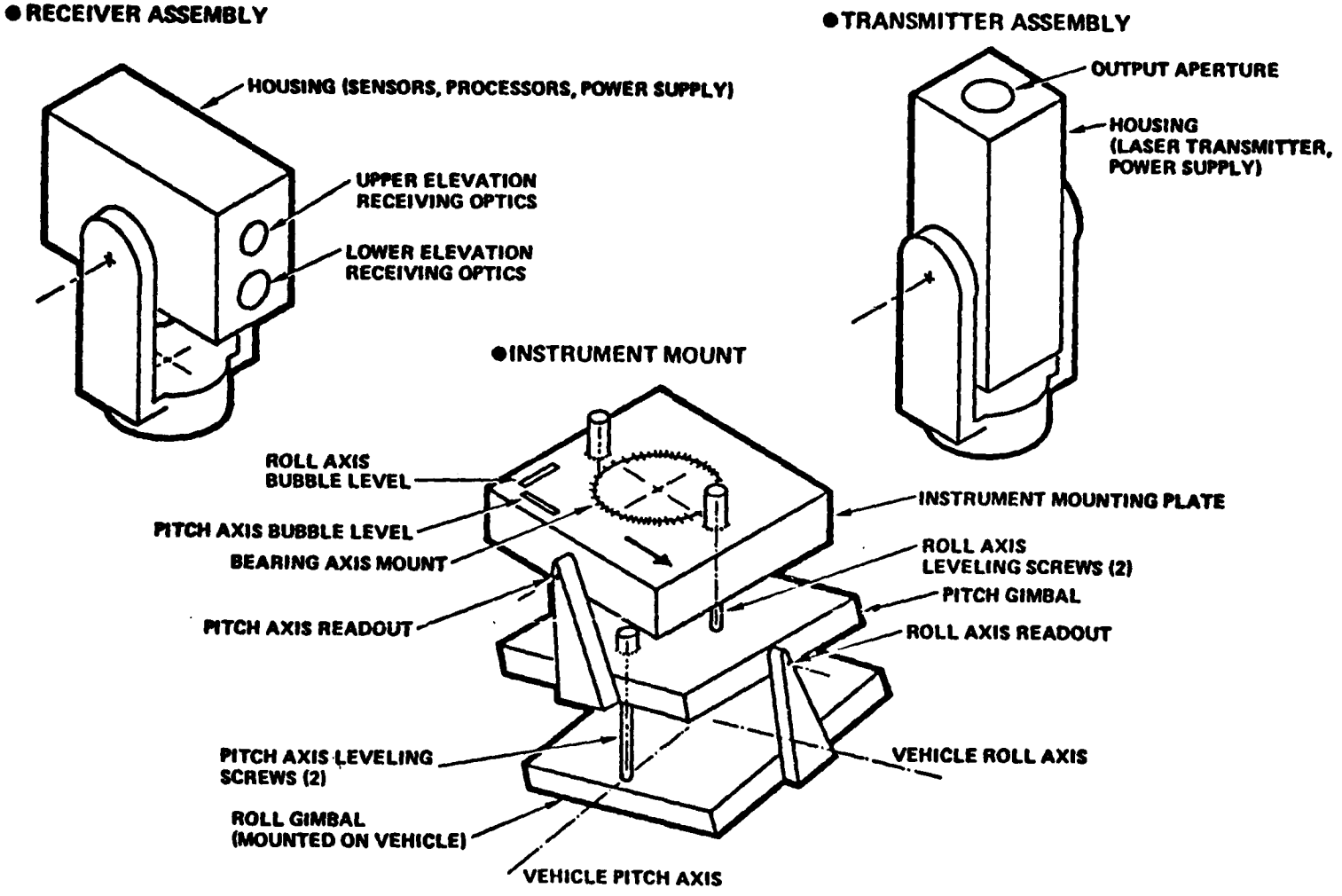

FIGURE 2. DBAS COMPONENTS

a stream of laser pulses (approximately 25 nanosecond pulses at 10 pps) at 90° elevation. The DBAS receiver senses the backscatter from these laser pulses.

At each receiver location, the receiver is set at an elevation angle such that the "lower" window optical axis clears any obstructions between the receiver and the general direction of the transmitter. The "lower" optical axis is then at angle E_1 above the horizontal and the "upper" optical axis is at a fixed angle above E_1, or $E_2 = E_1 + \Delta E$. Subsequently,

(i) The receiver is programmed for an azimuth search until an indication is received that the receiver optical axis is pointing directly at the vertically projected laser pole. This point can be indicated by (a) the nulling of "left" and "right" detectors in the "lower" window, (b) the use of a three slit detection scheme (see Section 3.1), or (c) averaging azimuth readings at signal fade-in and fade-out (see Section 5.0).

(ii) At this point, the bearing A_ρ from the receiver to the transmitter is determined and the diagram of Figure 3(a) applies.

(iii) Sensed backscatter signals from one pulse, first from Point A and then from Point B, are received in the "lower" and "upper" windows respectively. The time difference of arrival, Δt_o, is proportional to (AB + BO) - AO.

(iv) Then the horizontal range is

$$\rho_H = \frac{c \cdot \Delta t_o \cdot \cos E_1 \cdot \cos E_2}{\sin(E_2 - E_1) + \cos E_1 - \cos E_2} \qquad (8)$$

where c = speed of light

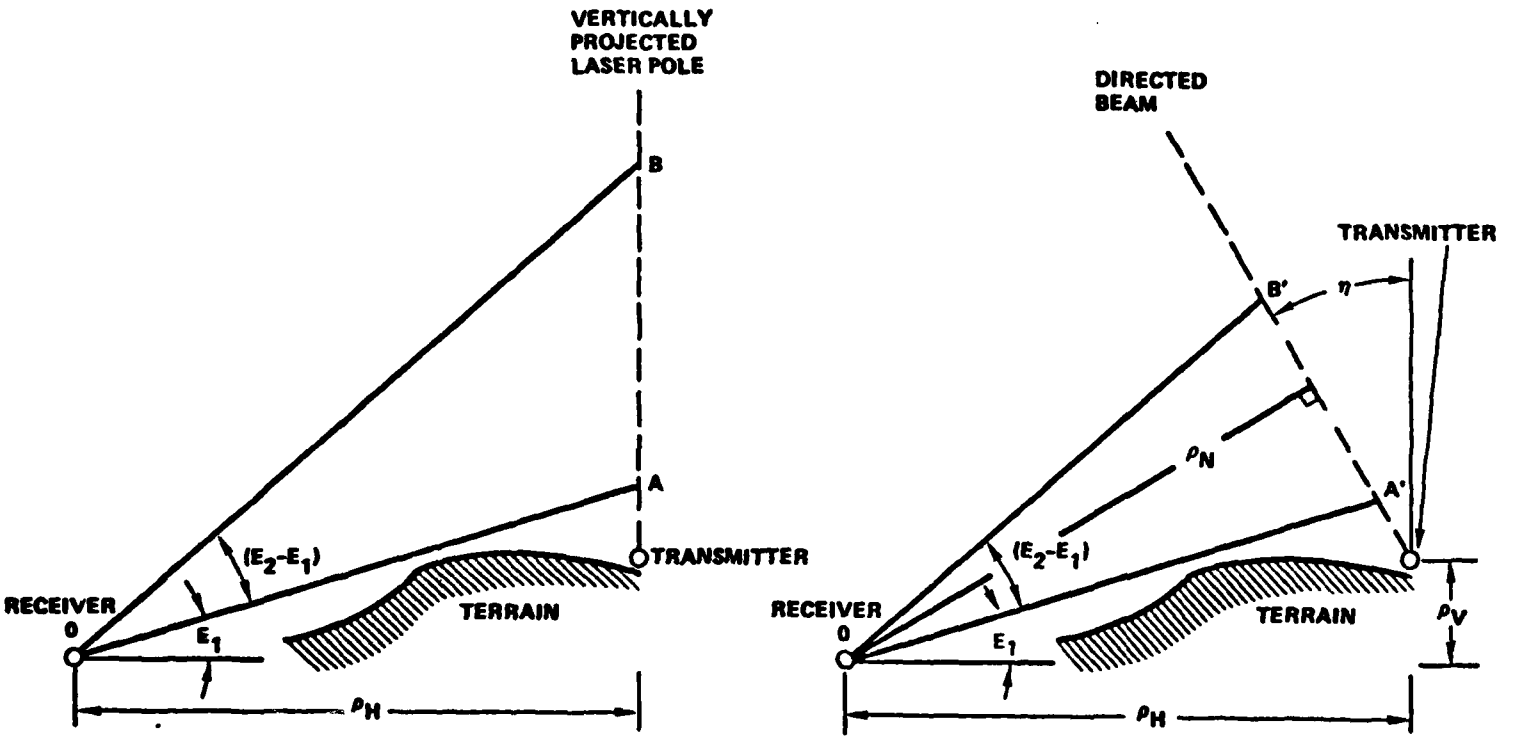

FIGURE 3. DBAS GEOMETRY FOR RANGE AND ALTITUDE DETERMINATIONS

(v) The receiver orientation is locked at A_ρ and E_1

(vi) The DBAS transmitted beam is now tilted down by angle η from zenith and rotated in azimuth about vertical

(vii) Via communication from the receiver to the transmitter, transmitter azimuth rotation is stopped when receiver again indicates "centering".

(viii) At this point, the bearing ζ from transmitter to receiver is determined and the diagram of Figure 3(b) applies.

(ix) The time difference of arrival Δt_N is now proportional to $(A'B' + B'O) - A'O$ and the beam normal range ρ_N is

$$\rho_N = \frac{c\,\Delta t_N \cdot \cos(E_1-\eta)\,\cos(E_2-\eta)}{\sin(E_2-E_1) + \cos(E_1-\eta) - \cos(E_2-\eta)} \tag{9}$$

(x) The vertical separation is computed as

$$\rho_V = (\rho_N - \rho_H \cos\eta)/\sin\eta \tag{10}$$

Thus all the parameters required in equations (1) through (5) are established at the end of Step (x). Note that all receivers of a multi-unit deployment can be proceeding simultaneously down through Step (v). From Step (vi) to (viii), the transmitter must be directed sequentially in azimuth to each receiver in the total deployment. When fully automated, the time required for alignment between one radar vehicle and up to three remote electro-optical trackers is expected to be under one minute.

3.0 BREADBOARD

In this section the DBAS breadboard receiver is described. Details of the geometric and radiometric laboratory measurements are presented, and the transmitter characteristics are shown for the TRW ruby laser which was used in the tests.

3.1 RECEIVER

Receiver design characteristics were developed from analyses of the expected signal and background levels (see Appendix A). The design and component selection were based on a conservative approach with the minimum cost for the breadboard receiver. Standard rotary tables were used for the azimuth and elevation mounts, giving an accuracy of about 20 seconds of arc in the readout of each axis. To perform the measurements, the receiver and mounts were attached to a flat plate equipped with levelling screws and the assembly was transferred to a van for transporting between measurement sites.

3.1.1 Optics

A Bouwers concentric telescope design was selected for the breadboard optical system. This design provides the high light gathering capability (7 inch f/1.0) and good imaging (< 3 mr blur over $\pm 10^{o}$) required for the field measurements. Off-the-shelf optical systems were also considered but these were rejected on the basis of insufficient focal plane illumination, poorer image quality, and/or cost.

The optical system consists of a spherical primary mirror, a corrector lens, an aperture stop at the center of curvature, and fiber optics bundles for transferring the light from the curved focal plane

to the silicon detectors. The primary mirror is 12 inches in diameter and the corrector has a diameter of 8 inches. Fiber optics were used to transfer the rectangular image at the focal plane to a circular image at the detector.

The image characteristics of the telescope were analyzed by means of a computer program in which three angles of incidence were considered, on-axis, 6.7 degrees off-axis, and 9.4 degrees off-axis. The maximum deviation of the 0.6943 μm rays is about ± 10 micrometers, which translates to an angular blur of ± 1.4 mrad. Imagery is somewhat better at the field edges, ± 0.6 mrad.

A 5 inch diameter spectral filter used for the tests was mounted in front of the entrance aperture. The filter has a spectral bandpass of about 50 Å, centered about the ruby wavelength.

3.1.2 *Detector*

The avalanche photodiode (APD) selected for the breadboard receiver is ideally suited for high frequency operation and offers a substantial gain in signal-to-noise ratio over other detector types. In addition, this detector offers response to either ruby laser (.6943 μm), or Nd:yag laser radiation (1.06 μm). The detector module is an RCA C30911E, containing an integral light pipe and a hybrid preamplifier supplied in a single modified 12-lead TO-8 package. A typical spectral response is shown in Figure 4. Device characteristics are shown in Table 2.

3.1.3 Electronics

Electronics design for the breadboard receiver consists of the three APD detector/preamplifier modules, custom post amplifiers

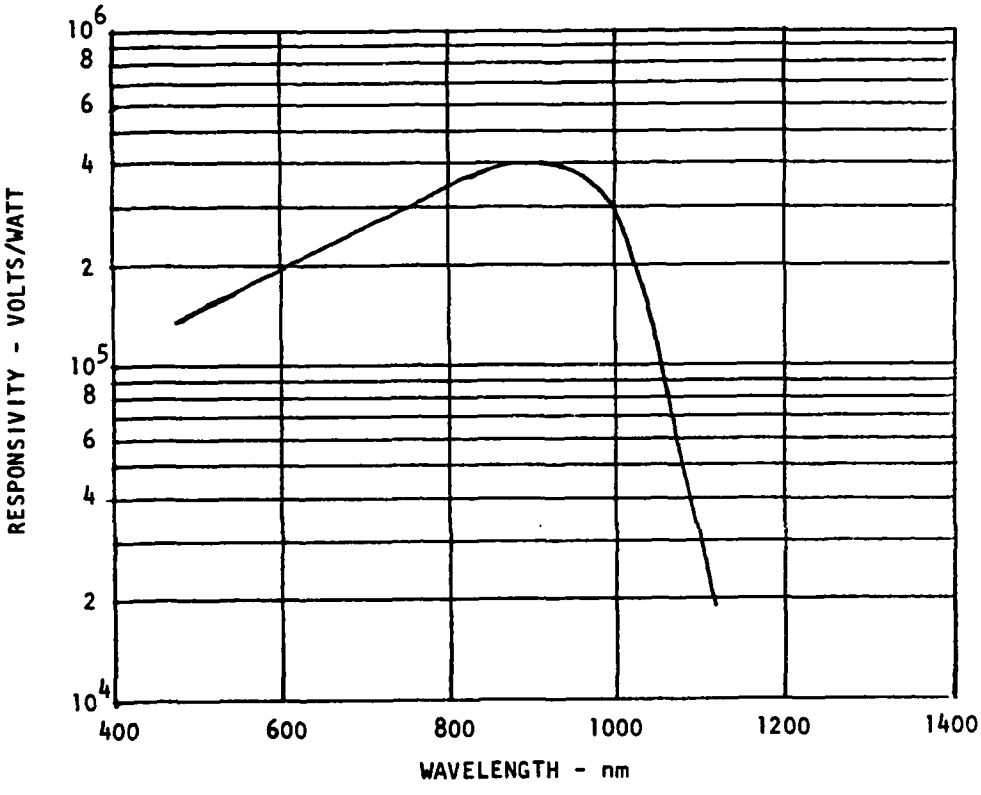

FIGURE 4. TYPICAL SPECTRAL RESPONSIVITY

and high voltage power supplies, and two HP5345 Time Interval Counters. The goals of the electronic implementation were:

- o Maintain the APD module rise time through the post amplifiers to the counter inputs.
- o Design for minimum signal distortion and delay to preserve time measurement accuracy.
- o Maintain an overall time interval accuracy of $\pm$ 5 ns; this includes $\pm$ 2 ns counter accuracy and variable delays in the detector channels.

Table 2

APD Module Characteristics

Parameter	Typical Value	Units
Temperature Coefficient	2.2	$V/^{o}C$
Responsivity		
0.900 μm	2×10^5	V/W
1.06 μm	5×10^4	
Noise Equivalent Power		
f = 100 kHz, Δf = 1.0 Hz		
0.900 μm	0.075	pW/(Hz)1/2
1.06 μm	0.30	
Output Spectral Noise		
Voltage Density		
f = 100 kHz - 100 MHz	15	nV/(Hz)1/2
Δf= 1.0 Hz		
Output Impedance	25	Ohms
System Bandwidth (3dB)	20	MHz
Rise Time	22	ns
Linear Output Voltage Swing	0.7	V
Output Offset Voltage	- 1.5	V
Supply Current	4.0	mA

The APD modules contain low noise, wide bandwidth (40 MHz) hybrid preamplifiers to reduce the effects of stray capacitance and pickup. The post amplifiers were designed to maintain the signal rise time and increase the signal level to interface with the counters.

The outputs of the post amplifiers are connected to the HP5345 trigger inputs in such a way as to measure the time intervals Δt_1 and Δt_2. Trigger level control is provided for each input to provide optimum detection. With the use of external logic and counter controls, a range gate or time window is created to reduce false alarms.

The post amplifier design is shown in Figure 5, and a simplified block diagram of the signal processing is shown in Figure 6. The diagram shows a HP 9852A calculator which was not used in the tests. The calculator could be used to receive time interval data, average the results, and calculate range, altitude, and azimuth. During the tests, time interval data were recorded by hand, since only a relatively low pulse rate was available from the transmitter. The analog electronics specifications are shown in Table 3.

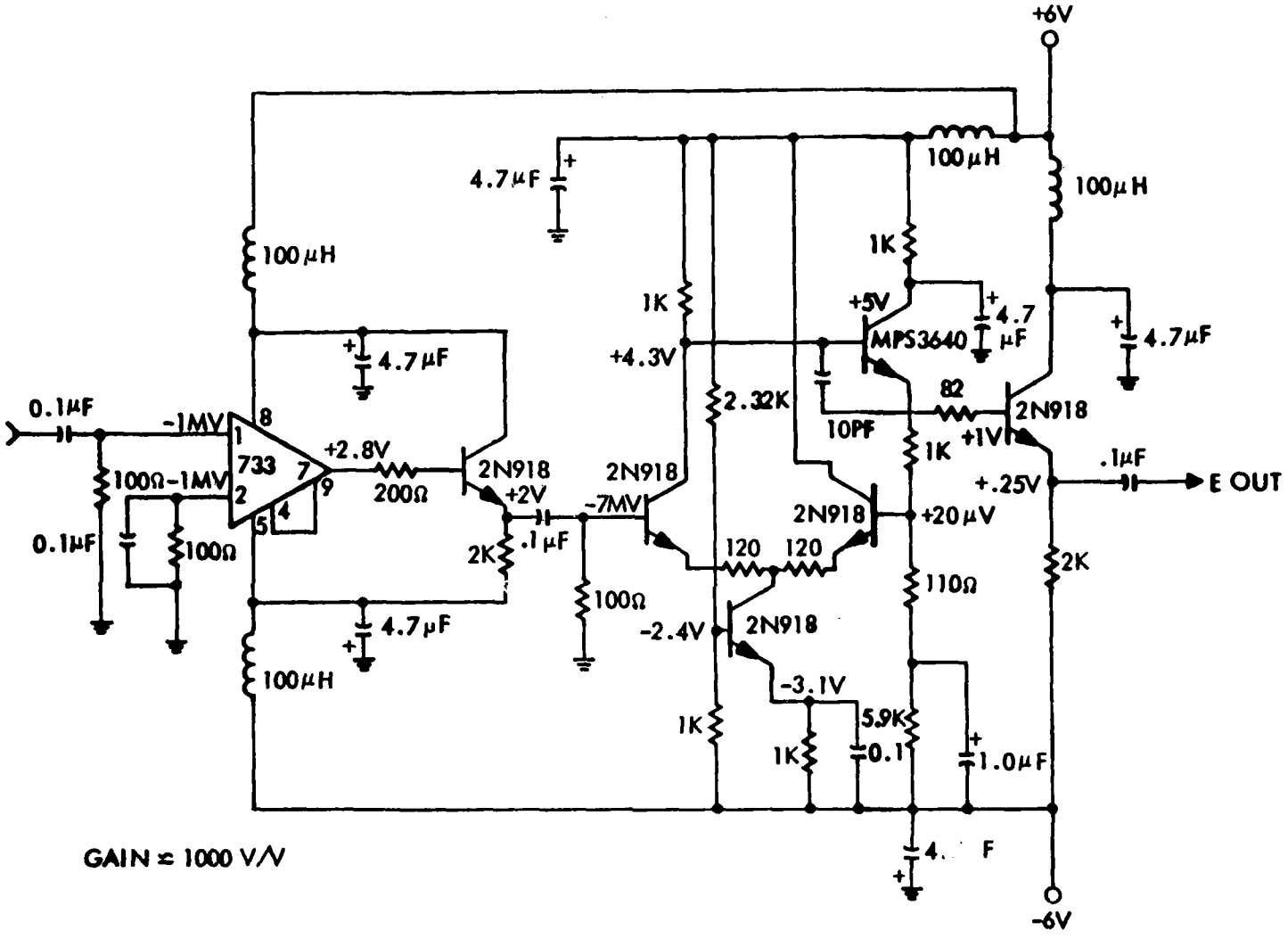

FIGURE 5. DBAS BREADBOARD POST AMPLIFIER

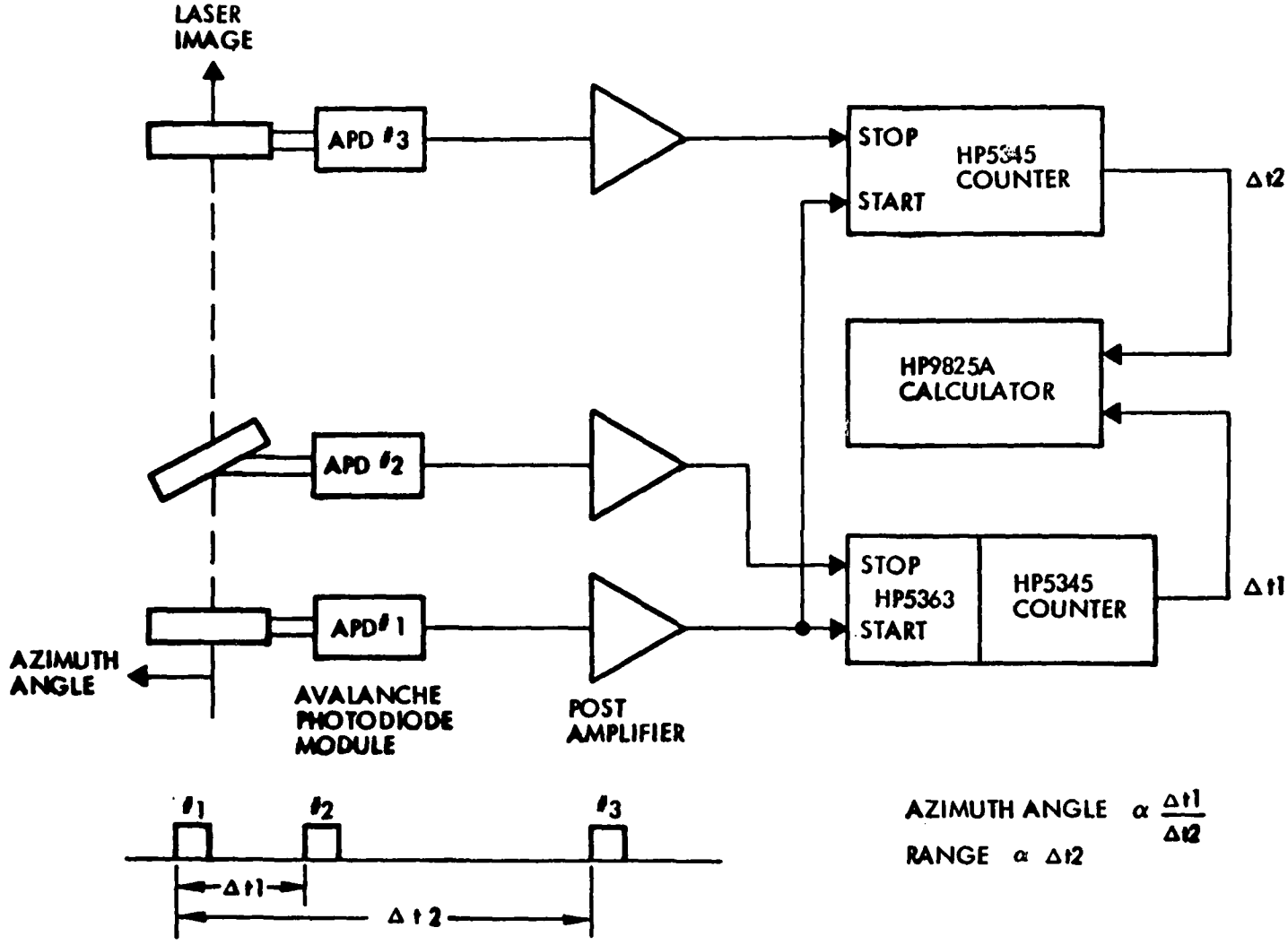

FIGURE 6. DBAS BREADBOARD SIGNAL PROCESSING

TABLE 3

ANALOG ELECTRONICS SPECIFICATION

GAIN:

APD	–	0.43 A/W @ .69 μm
PREAMPLIFIER	–	2×10^5 V/A
POSTAMPLIFIER	–	1000 V/V
END-TO-END GAIN	–	8.6×10^7 V/W @ .69 μm

AC CHARACTERISTICS:

BW	–	10 MHZ (NOISE BANDWIDTH ≈ 14 MHz)
RISETIME	–	20 NSEC

NOISE:

APD MODULE	–	15 - 30 $nV/\sqrt{Hz}$
OUTPUT NOISE	–	50 TO 100 mV RMS
NEP	–	0.6 TO 1.2 nW

3.1.4 Breadboard Design Package

The optical system described in 3.1.1 was packaged in a cylindrical housing with provision for focus adjustment through translation of the corrector element. Space was provided within the telescope for the three APD modules just inside the aperture plate. Figure 7 shows the arrangement. In operation, two 6 volt power supplies (HP 721A) were used to drive the APD bias supply circuits, and the entire package was attached to a plate with azimuth and elevation rotary mounts and independent levelling pads.

3.2 TRANSMITTER

The laser transmitter which was used for the tests was originally developed at TRW for a holographic demonstration program. This was the only available device for use in the DBAS test program which most nearly met the requirements. A special fixture was provided for directing the beam in the vertical direction and for tilting the beam at an angle of 30 degrees from the vertical. This fixture was adapted to a rotary stage to permit fine adjustment of the azimuth angle prior to tilting the beam. Since there was no azimuth-elevation mount for the transmitter, the rotary stage could not be used effectively. The transmitter characteristics are shown below in Table 4.

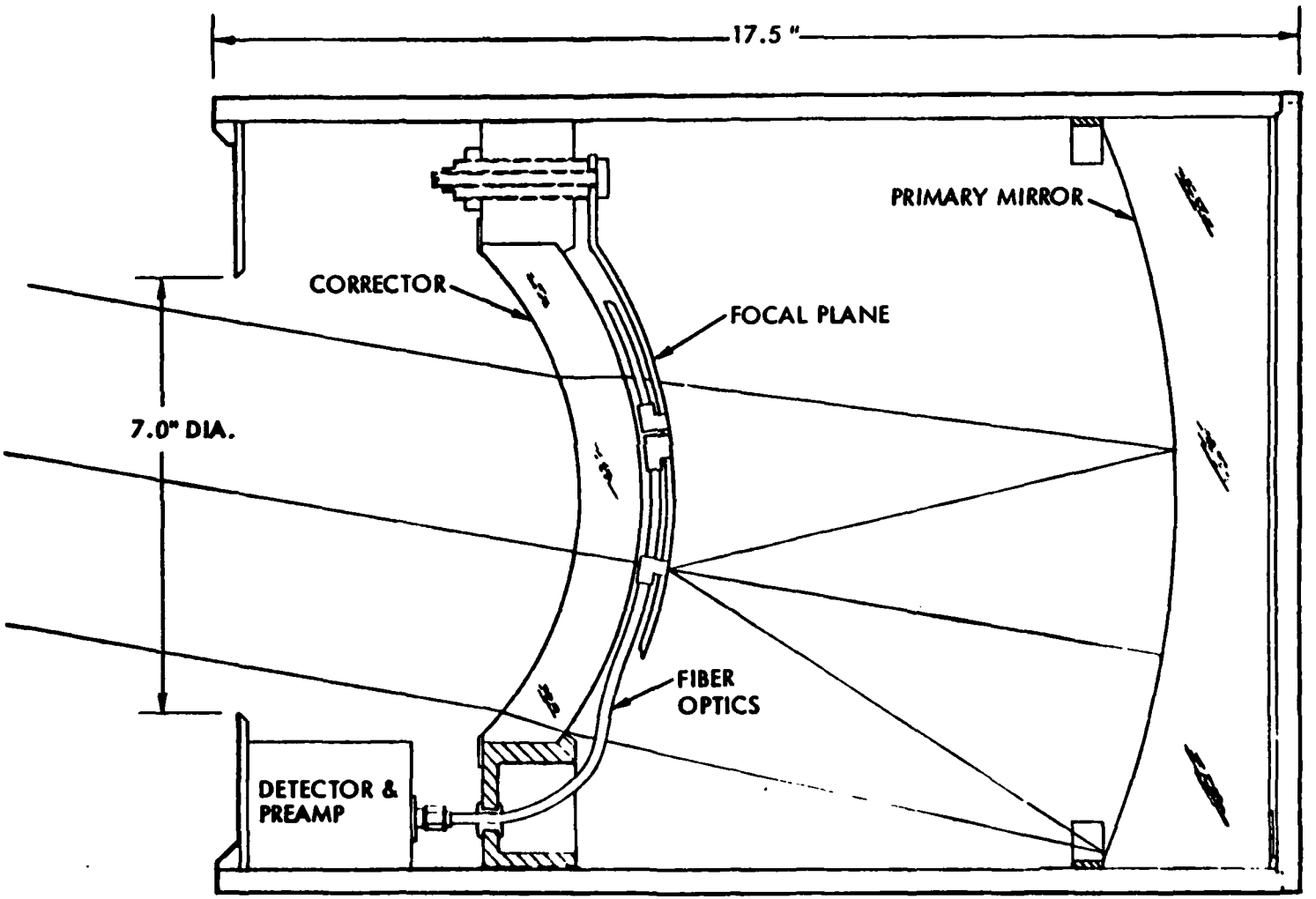

FIGURE 7. BOUWERS CONCENTRIC OPTICAL SYSTEM

TABLE 4

TRANSMITTER CHARACTERISTICS

Laser Type	Ruby
Wavelength	0.6943 μm
Pulse Repetition Rate	6 ppm
Pulse Energy	100 - 200 mJoules
Pulse Duration	25 ns
Beam Diameter	6 mm
Beam Divergence	2 mrad

3.3 LABORATORY MEASUREMENTS

To serve as an aid in the interpretation of the field test data, and to provide for checkout of the telescope assembly, the breadboard sensor was tested in the laboratory for geometric and radiometric response.

3.3.1 Geometric Measurements

The following measurements describe the position, dimensions, and alignment of the three fiber optic slits which are mounted behind the telescope lens. These measurements were taken by rotating the telescope so that a collimated He-Ne laser beam would contact the fiber optic slits at various points. The position of the laser beam

on the slit was monitored by oscilloscope and by viewing the beam through the lens of the telescope. The relative positions of these fiber optic slits, as seen through the telescope lens, are illustrated in Figure 8. The lower, upper, and diagonal fiber optic slits are connected to the channel 1, channel 2, and channel 3 sensors, respectively.

Azimuth Measurements for the Upper and Lower Slits

To find the left azimuth measurement for the upper slit, the following steps were taken. The telescope was rotated upward along the elevation axis until the laser beam was focused on the upper slit as seen through the telescope lens. Then verification of the laser beam's position was made on the oscilloscope screen. The next step was to rotate the telescope clockwise along the azimuth axis until the beam was seen at the left edge of the upper slit. This edge position was also verified on the oscilloscope screen. The length of the upper slit was found by subtracting the left azimuth reading from the right azimuth reading. This length is $1^{o}50'$. Using the same procedure, the lower slit length was determined to also be $1^{o}50'$.

In comparing the left edge readings of the upper and lower slits, a difference of 5' was found. The same 5' difference was obtained when comparing the right edge readings of the upper and lower slits. This suggests that the fiber optic axis is rotated 5' counterclockwise (as seen through the telescope lens) with respect to the laser beam (see Figure 9).

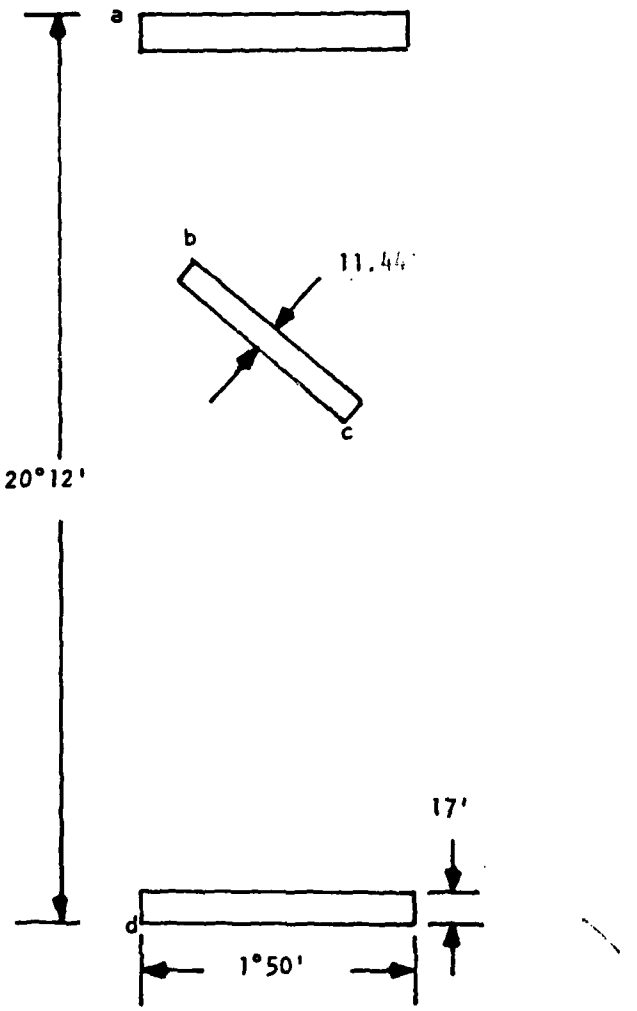

FIGURE 8. FIBER OPTICS SLITS AS SEEN THROUGH TELESCOPE LENS

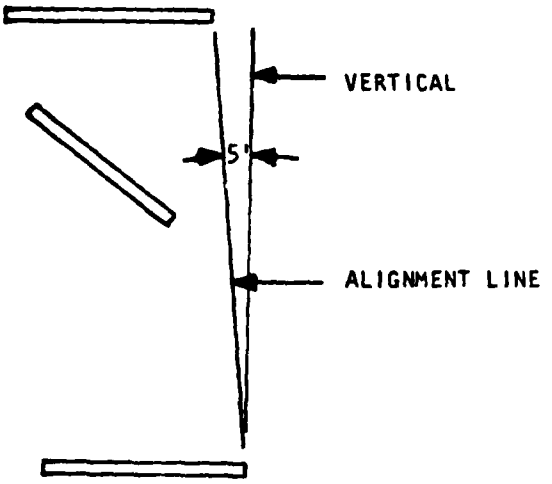

FIGURE 9. SLIT MISALIGNMENT

Height and Width Measurements for the Upper and Lower Slits

To find the elevation height of the upper slit, the oscilloscope was first connected to the channel 2 sensor. Then the telescope was rotated upward until the beam was focused on the upper slit and a channel 1 signal was registered on the oscilloscope. The oscilloscope was then rotated further upward along the elevation axis until this waveform signal reverted to a horizontal line. This point was on the upper edge of the slit. The above procedure was repeated three times at different points on the slit and an average of these measurements was taken. The height obtained was $259^{\circ}55'$ (see point a on Figure 8). To find the elevation measurement for the lower edge of the lower slit, the oscillo-

scope was connected to the channel 1 sensor. Next, the telescope was rotated downward until the beam contacted the slit, and then the method described above was employed. The average of the three measurements was $280^{\circ}7'$ (see point d on Figure 8) By subtracting the upper edge of the upper slit from the lower edge of the lower slit, a separation of $20^{\circ}12'$ was obtained.

The Width Along the Azimuth Axis of the Diagonal Slit

To obtain this measurement, several steps were taken. First, the oscilloscope was connected to the channel 3 detector. Next, the telescope was rotated clockwise along the azimuth axis until the beam was to the left of the diagonal slit (as seen through the telescope lens). Then, the telescope was rotated counterclockwise along the same axis until the channel 3 signal registered on the oscilloscope screen. The azimuth measurement at this point was noted. Then the telescope was rotated further along the same axis to the point at which the channel 3 signal disappeared from the oscilloscope screen. The azimuth at this point was taken. Then the former azimuth measurement was subtracted from the latter azimuth measurement, yielding a slit width along the azimuth axis of 12'. The telescope was then rotated slightly upward along the elevation axis and the same procedure was repeated to obtain a second slit width of 12'. The above procedure was repeated two more times to obtain two slit widths of 11' and 12'. Four width measurements were averaged to yield an azimuth slit width measurement of 12'.

Diagonal Slit Position Measurements

To find the coordinates of the uppermost point of the diagonal slit (see point b on Figure 8), the following steps were taken. First, the telescope was rotated to a point just above the uppermost point of the diagonal slit. At this point, there was no channel 3 signal registering on the scope. Then the telescope was rotated one minute downward on the elevation axis (in order that the laser beam would contact the fiber optic axis at a point one minute lower). Next, the telescope was rotated back and forth along the azimuth axis to determine whether the oscilloscope signal would change. This procedure was repeated until a point was found at which the beam made contact with the beam made contact with the fiber optic slit (i.e., where a channel 3 signal registered on the oscilloscope screen). Azimuth and elevation measurements were noted for this point.

azimuth = $30^{\circ}40'$

elevation = $262^{\circ}17'$

To find the lowest point of the diagonal slit, the telescope was rotated until the laser beam was just below the slit. At this point, a channel 3 signal was not registering on the oscilloscope screen. This time the telescope was rotated upward one minute. Then it was swept back and forth along the azimuth axis. No signal change was noticed. This procedure was repeated until a channel 3 signal registered on the oscilloscope. The azimuth and

elevation measurements were noted at this point.

azimuth = $31^{o}29'$

elevation = $265^{o}2'$

The Angle that the Diagonal Slit Makes With the Vertical

To find this angle θ (see Figure 10), the following steps were taken. First, a point on the right edge of the diagonal slit between points b and c was chosen and the laser beam was focused there. This point is designated as point A. Its azimuth and elevation measurements are the abscissa and ordinate, respectively, in the following parenthesis:

A = $(31^{o}15', 264^{o}0')$

Next, the telescope was rotated one degree upward along the elevation

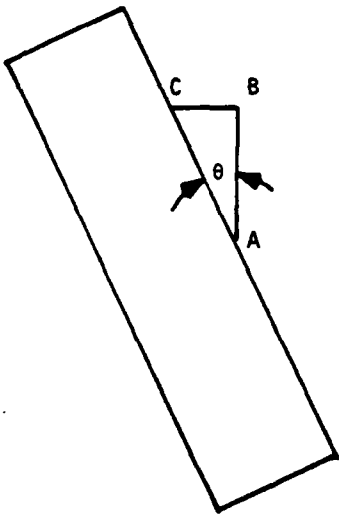

FIGURE 10. SLIT ANGLE WITH RESPECT TO VERTICAL

axis (and the laser beam is rotated one degree upward). This point, designated as point B, has the following coordinates:

$$B = (31^{\circ}15', 263^{\circ}0')$$

Next, the telescope was rotated clockwise until the laser beam contacted the edge of the fiber optic slit. This point, designated as point c, has the coordinates listed below:

$$C = (30^{\circ}56', 263^{\circ}0')$$

From these measurements, the dimensions of the right triangle Δ ABC can be obtained:

$$|\overline{AB}| = 1^{\circ} = 60'$$

$$|\overline{BC}| = 19'$$

Then the angle is obtained from:

$$\theta = \text{Arc tan } (19'/60')$$

$$\theta = 17.57^{\circ} \text{ or } 17^{\circ}34'.$$

<u>The True Width of the Diagonal Slit</u>

The true width of the diagonal slit (see "x" in Figure 11) can now be derived. From Figure 11 it is apparent that: (the azimuth width) (cos θ) = true width of the diagonal slit or

$$12' \cos 17.57^{\circ} = X$$

therefore

$$X = 11.44'.$$

Table 5 summarizes the geometric measurements

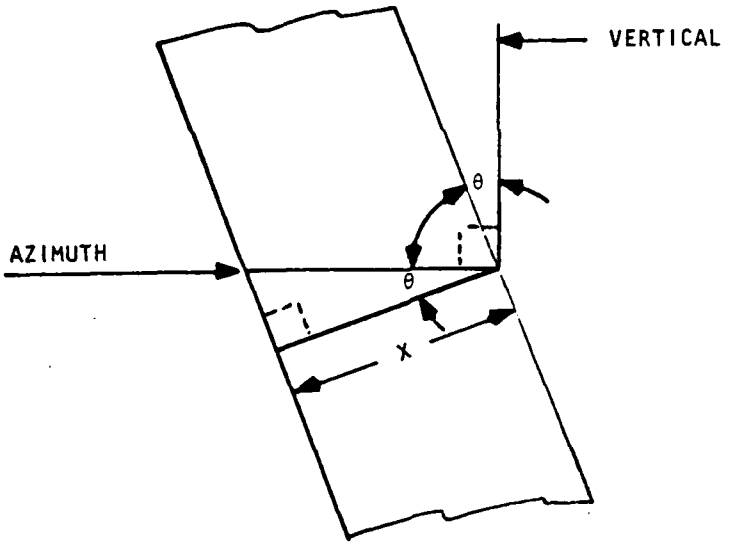

FIGURE 11. TRUE SLIT WIDTH

3.3.2 Radiometric Measurements

In order to obtain a measure of the sensor's radiometric response, it was necessary to provide a signal of known irradiance which is at or near the wavelength of operation. To accomplish this, a calibrated detector was used with a HeNe laser source (0.6328 μm). Because of the frequency response of the electronics, it was necessary to chop the laser beam. The highest chopping frequency available was about 30 kHz, which is within the bandpass of the post amplifier. The laser beam was expanded to a diameter of about 5 cm and directed toward the telescope aperture. A reading at the aperture gave the magnitude of the input radiant power

TABLE 5

D.B.A.S. Sensor Geometric Measurements

Dimension	Diagonal Slit	Upper Slit	Lower Slit
Left Edge (Azimuth Reading)		30^{o} 6'	30^{o} 11'
Right Edge (Azimuth)		31^{o} 56'	32^{c} 1'
Length		1^{o} 50'	1^{o} 50'
Height Measurements (Elevation Reading)		259^{o} 55'	280^{o} 7'
Coordinates of Upper and Lower Points of Diagonal Slit (Azimuth Elevation)	b = (30^{o} 40', 262^{o} 17') c = (31^{o} 29', 265^{o} 2')		
True Width	11.44'	17'	17'
Azimuth Width	12'		
Angle θ For Diagonal Slit	17.57^{o} or 17^{o} 34'		

Difference in alignment between upper and lower slit = 5'.

Difference between point a and point d (separation) = 20^{o} 12'.

which was collected and focussed on the fiber optic slits. From a reading of the signal voltage in response to the laser input, and an estimate of the optical transmission losses through the telescope, a value for detector responsivity was derived. This measurement was then compared with the manufacturer's data by using the curve of relative spectral response to estimate responsivity at the HeNe laser wavelength. The input power at the aperture was 9.72×10^{-8} W, producing a broadband signal of 3.90 V p-p. The transmission of the optical system is estimated to be 0.54, which includes a factor of 0.6 for the fiber link. With the post amplifier gain of 1000, the responsivity is determined from,

$$R = (V_s/G)\ (1/P\tau)$$

where

V_s = signal volts

G = amplifier gain

P = input power

τ = optical transmission

and

$$R = 7.4 \times 10^4 \text{ volts/watt}$$

From the detector data, typical response at a wavelength of 0.900 μm is 2×10^5 V/W. From the curve of relative response one can estimate,

$$R_{.6328}/R_{.9000} = 0.55$$

and a predicted value of 1.10×10^5 V/W results for the responsivity of a

typical device. In the absence of a signal, the wideband noise was 0.066 volts rms. From this value, the peak signal to rms noise ratio (SNR) for the measurement was 59. The radiant power at the detector is

$$P_D = P\tau = 5.25 \times 10^{-8} \text{ W}$$

and the detector noise equivalent power (NEP) can be determined from

$$NEP = P_D/SNR = 8.9 \times 10^{-10} \text{ W}$$

The telescope noise equivalent flux density (NEFD) is a measure of the irradiance at the aperture which produces a signal-to-noise ratio of unity.

$$NEFD = NEP/A_c\tau = 6.65 \times 10^{-12} \text{ w/cm}^2$$

where A_c is the area of the collecting aperture (248 cm^2).

All of the above values are derived from the measurement at 0.6328μm using the HeNe laser. It is necessary to scale these values for other wavelengths from a spectral response curve. The results of the radiometric measurements are summarized in Table 6.

TABLE 6

Summary of DBAS Radiometric Measurements*

Responsivity	7.4×10^4 V/W
RMS Noise (14 KhZ Bandwidth)	67 mV
Noise Equivalent Power	8.9×10^{-10} W
Noise Equivalent Flux Density	6.65×10^{-12} W/cm^2

* Wavelength = 0.6328 μm

4.0 EXPERIMENTAL RESULTS

The test plan (Appendix C) gives a detailed explanation of how the tests were to be conducted on the DBAS. In this section the highlight of the test plan are reviewed.

4.1 TESTS

The primary equipment used for the DBAS tests consisted of a Ruby laser and the DBAS breadboard, both discussed in Section 3. The laser was located on the roof of Building R1 as shown in the map in Figure 12. The DBAS breadboard was mounted in the back compartment of a commercial van, so that when the rear doors of the van were open, the receiver could "look" out through the opening. In normal operation, the van was driven to a selected site and blocked up off of the ground so that it could not move or rock. The platform that the DBAS receiver was mounted on was manually leveled using a precision laboratory bubble level. The same bubble level was used to level the laser transmitter unit.

Some variations in the test plan were required because of the bad weather that was experienced. The first attempt at making a measurement with the van located on the roof of Building 82 was negative. It was not possible, in one days operation, to locate the backscattered laser beam. Therefore the van was moved to the Building R6 parking lot from which it was possible to see the laser located on the Building R1 roof. At this time it was discovered that the alignment telescope on the receiver was not properly aligned with the boresight axis of the receiver. After aligning the telescope with the

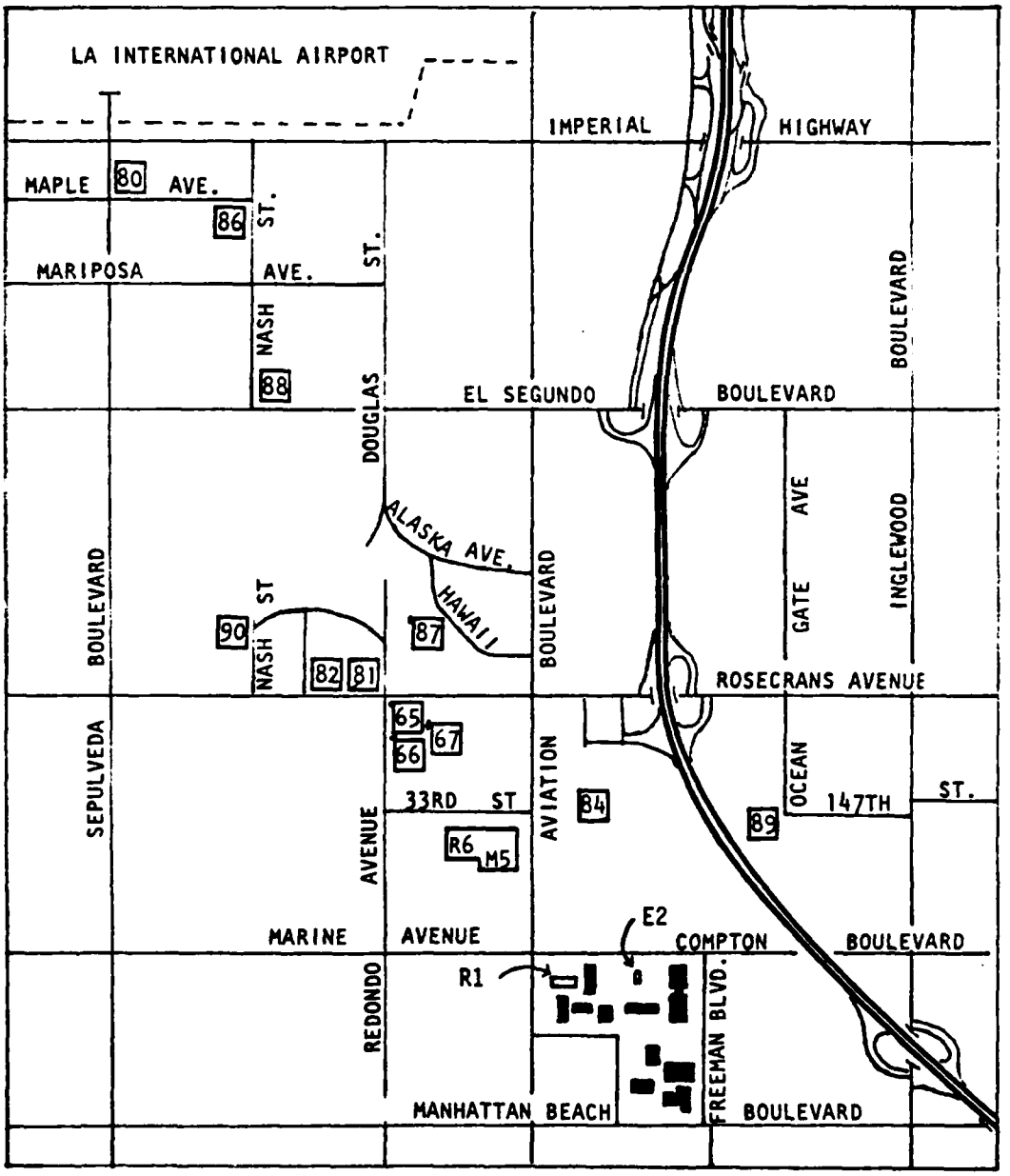

FIGURE 12. L.A. LOCAL AREA MAP

receiver and sighting on the laser, measurements were obtained from the DBAS instrument. Since the equipment was set up, a series of tests were ran at this location.

The van was then moved back to the roof of Building 82 set up and an azimuth search made for the laser backscatter. Within minutes the beam was acquired and measurements obtained.

As mentioned earlier, many delays were experienced because of the excessively rainy weather during the scheduled test period. Since the ruby laser used as a transmitter was designed for laboratory use, it could not be left on the roof. Consequently, it had to be moved from the lab to the roof each time it was to be used. Therefore, it was necessary to be fairly certain that several hours of good weather were available, before any measurements could be attempted.

4.1.1 Tests Results

The results for the R6 parking tests are summarized in Table 7, while the results for the Building 82 tests are summarized in Table 8. Table 8(a) shows the raw data for the timing measurements from Building 82.

In addition to range testing, a series of measurements were made of the time increment between the lower slit pulse and the slanted slit pulse to determine azimuth sensitivity. Figure 13 shows a plot of this time increment versus azimuth angle at one elevation angle from the roof of Building 82. It is interesting to note that the width of the slit as determined by the lab measurements agrees remarkably well with this curve. Also note that the affect of the edge of the slit is noticable in this plot, indicating that the optical system was very well focussed.

TABLE 7 - R6 PARKING LOT TEST SUMMARY

DATA

ELEVATION ANGLE = 11° 40'

Δt_o = 870×10^{-9} SEC

Δt_η = 460×10^{-9} SEC

η = 30°

RESULTS

RANGE = 590.66 METERS

ELEVATION = 13.93 METERS

TABLE 8 - BUILDING 82 TEST SUMMARY

DATA

ELEVATION ANGLE = 10° 10'

Δt_o = 1690×10^{-9} SEC

Δt_η = 903×10^{-9} SEC

η = 30°

RESULTS

RANGE = 1185.06 METERS

ELEVATION = 21.82 METERS

TABLE 8(a) - TIMING DATA FOR BUILDING 82 TEST TAKEN ON 2/22/79

WITH BEAM VERTICAL (nanoseconds)	WITH BEAM TILTED 30° (nanoseconds)
1674	904
1678	902
1688	910
1698	898
1704	898
1684	900
1712	908
1682	904
1688	908
1688	896
1689	904
1700	906
$\bar{x}$ = 1690	$\bar{x}$ = 903
σ = 11.1	σ = 4.5

4.2 VERIFICATION

The results summarized in the last section needed to be verified by an independent set of measurements. The test plan (Appendix C) contains a derivation for verification based upon surveying techniques. Figure 14 shows the R6 parking lot verification geometry, the theodolite measurements and the calculated results for horizontal range. This compares favorably with the DBAS results.

Figure 15 shows the Building 82 to R1 geometry. Since a theodolite was used for making the angular measurements, instead of the DBAS receiver mount, and it was not possible to see from 82 to R1 becuase of the intervening M5-R6 complex, another surveying technique was utilized. Baselines were laid out at both locations and measurements made of the baseline lengths. The theodolite was set up at the points identified in the figure as A, B, C, T, and X and angular measurements made that are listed in the figure. Using these measurements and straightforward geometry enabled the distance from the receiver to the transmitter to be calculated. In this case the range measurement was not as close as it was in the R6 tests, but still reasonably close. Table 9 summarizes the results of the testing and verification.

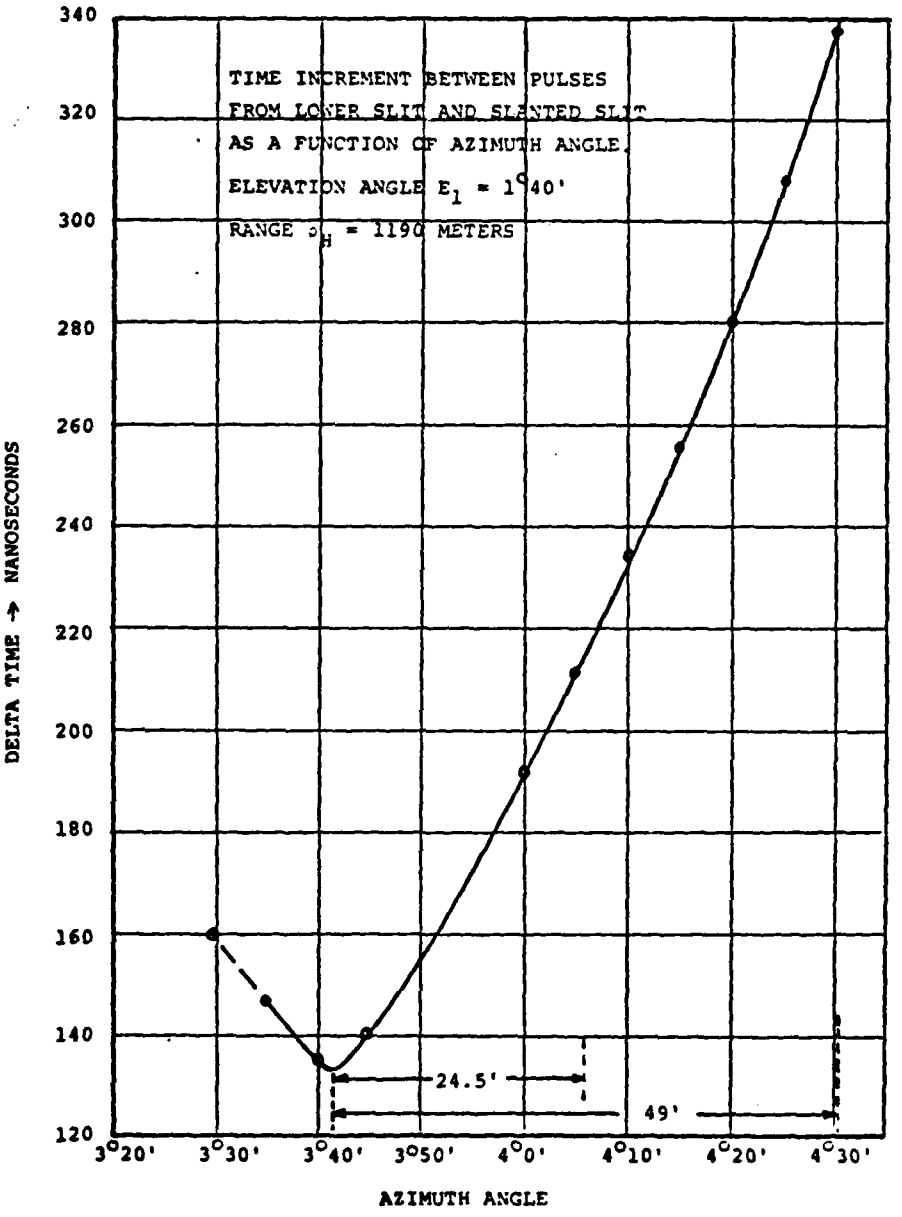

FIGURE 13. ANGULAR SLIT SENSITIVITY

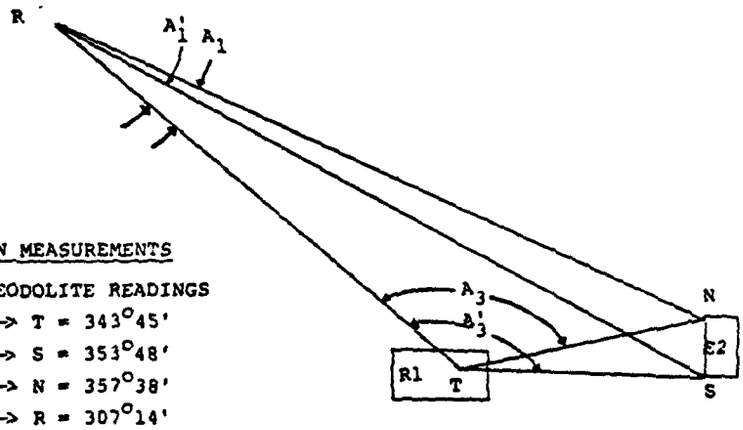

RAW MEASUREMENTS

THEODOLITE READINGS

R → T = 343°45'
R → S = 353°48'
R → N = 357°38'
T → R = 307°14'
T → N = 82°20'
T → S = 95°03'
$\overline{NS}$ = 60.96 METERS

CONVERTED DATA

A_3' = 147.81667°
A_3' = 135.10000°
A_1' = 10.05000°
A_1 = 13.88333°

CALCULATED RESULTS

$\overline{RT}$ = 592.46 METERS
$\overline{TS}$ = 244.41 METERS
TN = 275.88 METERS

FIGURE 14. R6 PARKING LOT VERIFICATION GEOMETRY AND MEASUREMENTS

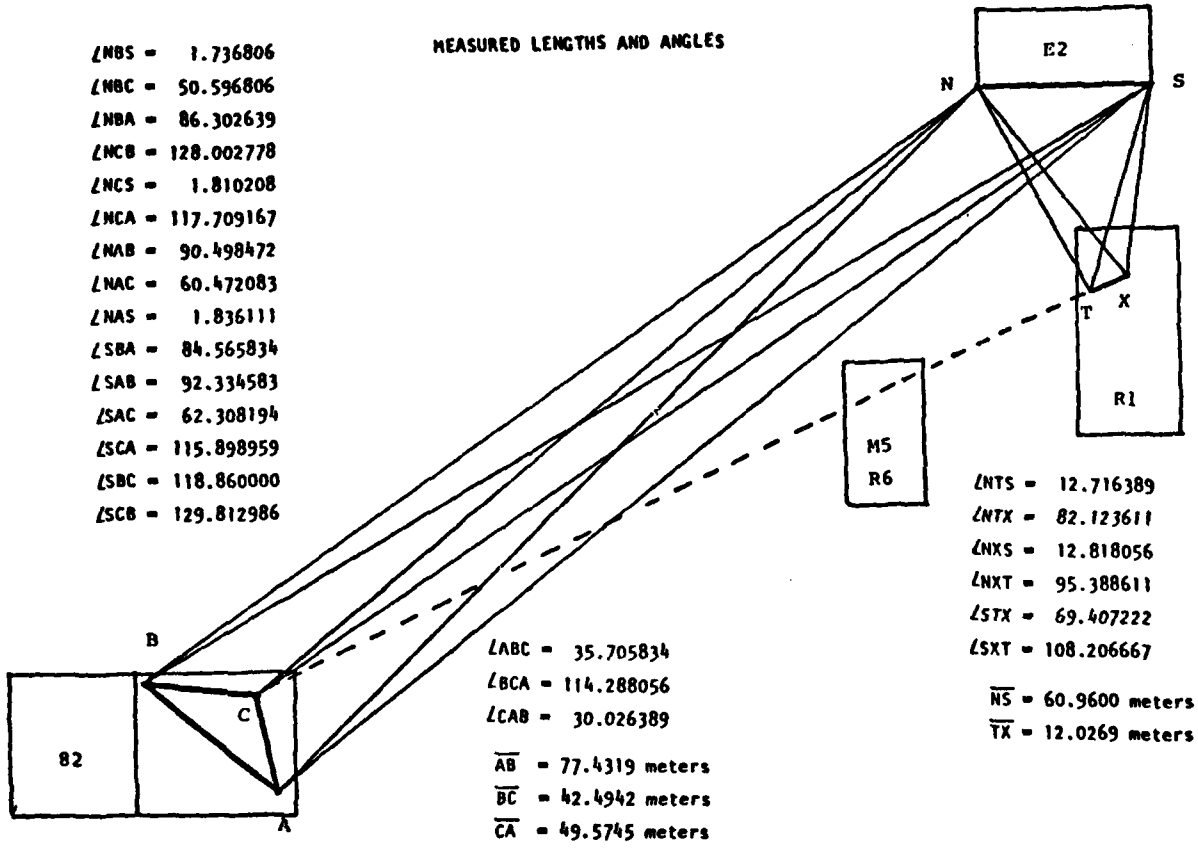

FIGURE 15. BUILDING 82 VERIFICATION GEOMETRY AND MEASUREMENTS

TABLE 9- TEST SUMMARY

RECEIVER LOCATION	PARAMETERS	MEASUREMENTS		DIFFERENCE	
		DBAS	SURVEY	MEASURED	THEORETICAL
R6	RANGE	590.7	592.5	1.8	6
	ELEVATION	13.9	5.1	8.8	20
82	RANGE	1185.1	1193.4	8.3	6
	ELEVATION	-21.8	-4.9	16.9	20

5.0 CONCEPTUAL DESIGN

Some aspects of the conceptual design have been driven by the experience gained in testing the breadboard model. The breadboard model described in Section 3 utilized an F/1 optical system with a field of view of twenty degrees. This large field of view produced excessive background noise causing the signal to noise ratio to be much lower than anticipated. In addition, there was a fixed angular separation between the upper and lower detector slits. There were situations where it was possible to detect the laser pulse with the lower detector; but because of atmospheric conditions, it was impossible to detect the laser pulse with the upper detector. If it had been possible to change the angle of separation between the detectors from 20° to 10° in these cases, range measurements could have been obtained. Therefore, the receiver conceptual design tended toward two separate telescopes with separate detectors so that this angle could be changed to meet the varying weather conditions. It would then be possible to increase the F number by making the focal length of the optics larger, thereby reducing the background noise.

In the breadboard, three slits were used with the center slit placed at an angle to provide suitable azimuthal resolution for determining the exact angle to the laser transmitter. However, the third slit can be eliminated as is shown in Figure 16. If two slits are used then

- o Rotate reciever in azimuth until
- o Receiver detects laser beam by one side of slit.
- o Record azimuth reading (A_1)
- o Continue rotating in azimuth until
- o Laser pulse ceases to be detected.

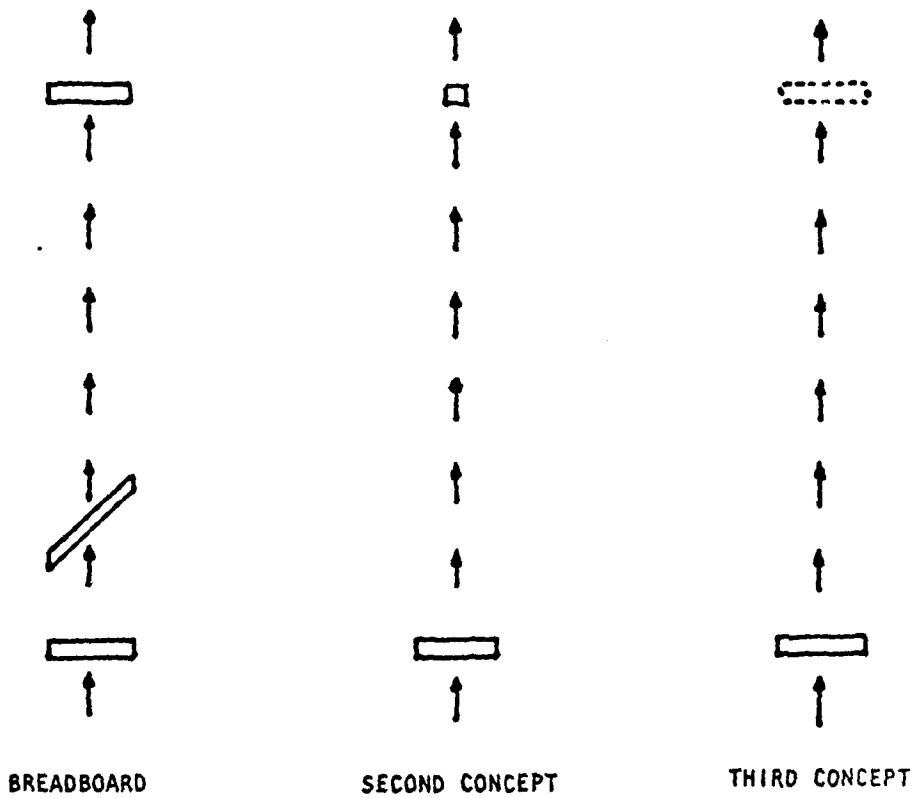

FIGURE 16. DETECTOR ARRANGEMENT

- o Record azimuth reading (A_2)
- o Rotate receiver to $A = (A_1 + A_2)/2$
- o Now laser pulse image will be directly in center of slit.

Carrying this process one step further, and considering the fact that in any system it will be necessary to have a communications link between the laser site and the receiver site, then it will be possible to eliminate one of the slits, and perform the complete process with one telescope and one slit detector by using two elevation angles in sequence with a sync signal. The sync signal can be transmitted to the receiver from the transmitter and the time difference measured between the receipt of the sync pulse and the receipt of the laser pulse.

The original concept was to use a single telescope and detector mounted on an az-el mount which in turn was mounted on an x-y gimbaled mount. The x-y mount was to be used to level the az-el mount as was done manually with the breadboard. Figure 17 illustrates the receiver in block diagram form. Another double gimbal arrangement, shown in block diagram form in Figure 18 was for the laser transmitter. At the interim technical briefing it was suggested by HELSPO that consideration be given to putting both receiver and transmitter on each end of the DBAS. A block diagram of this arrangement is shown in Figure 19. A packaging concept is shown in Figure 20.

Further investigation of the overall system operation indicated that the second set of gimbals was redundant, since the computer could transform from the transmitter and receiver coordinates directly to the vehicle coordinates. The mathematics for this transformation is covered in Appendix B.

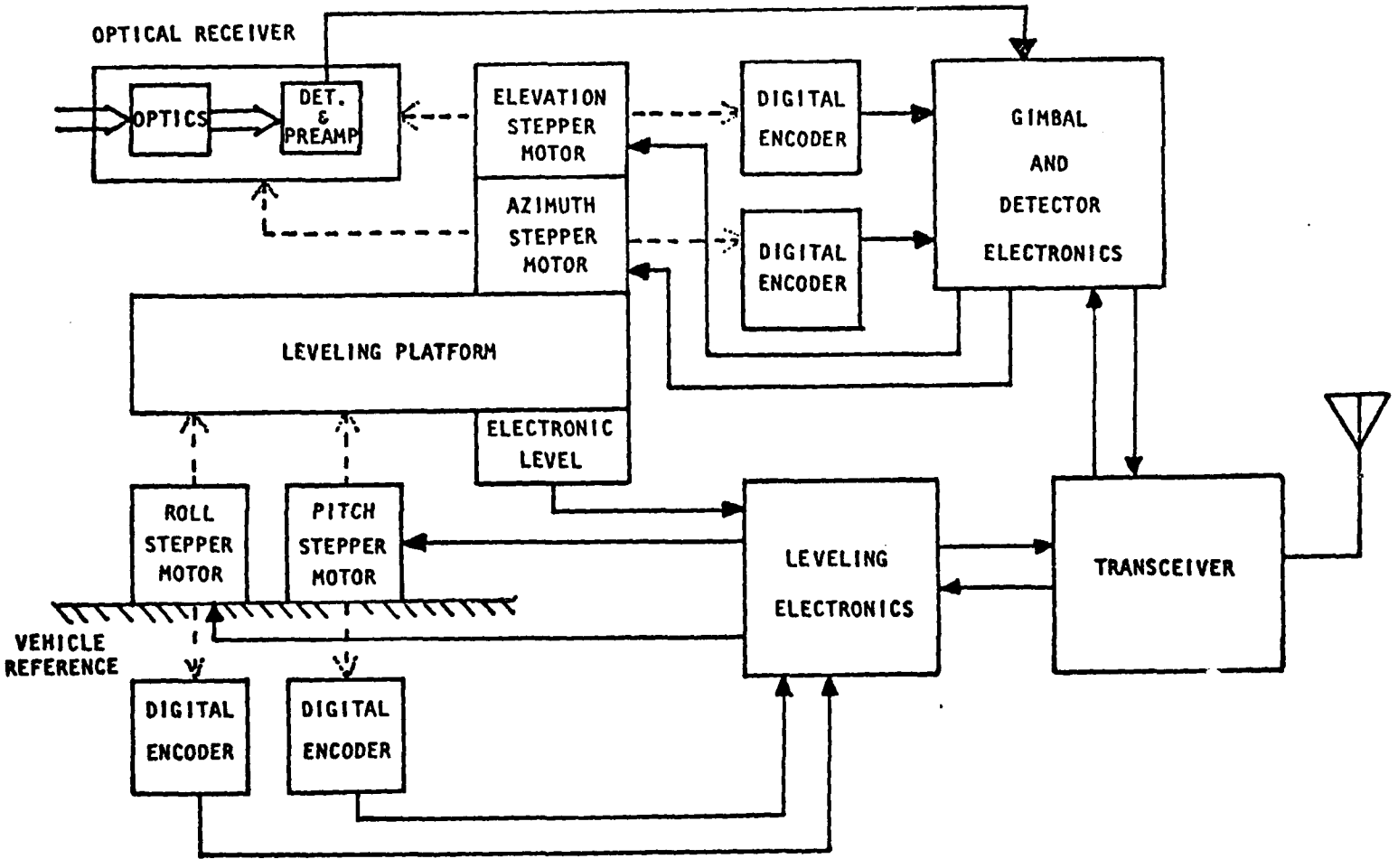

FIGURE 17. BASIC BLOCK DIAGRAM OF OPTICAL RECEIVER UNIT

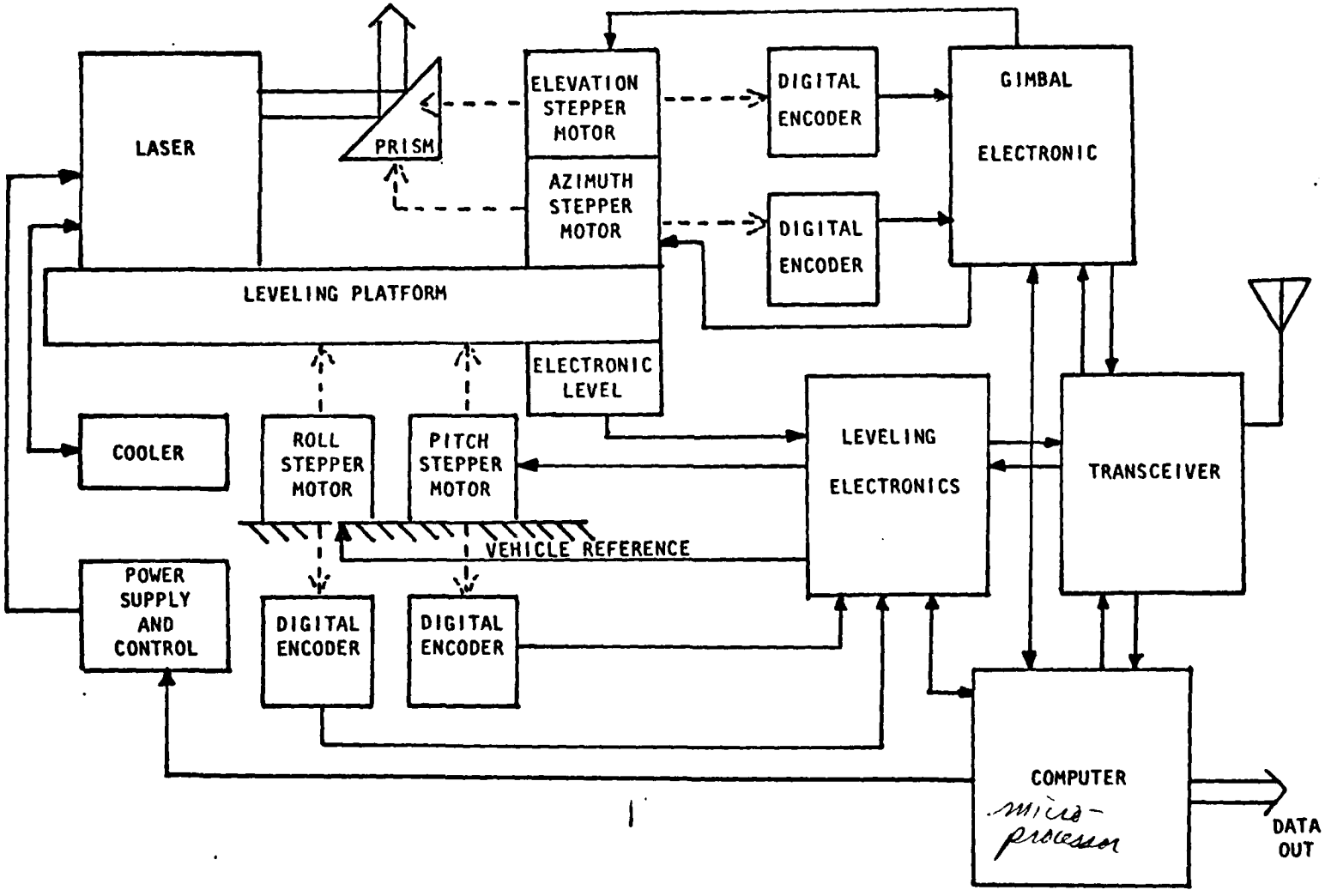

FIGURE 18. BASIC BLOCK DIAGRAM FOR LASER TRANSMITTER UNIT

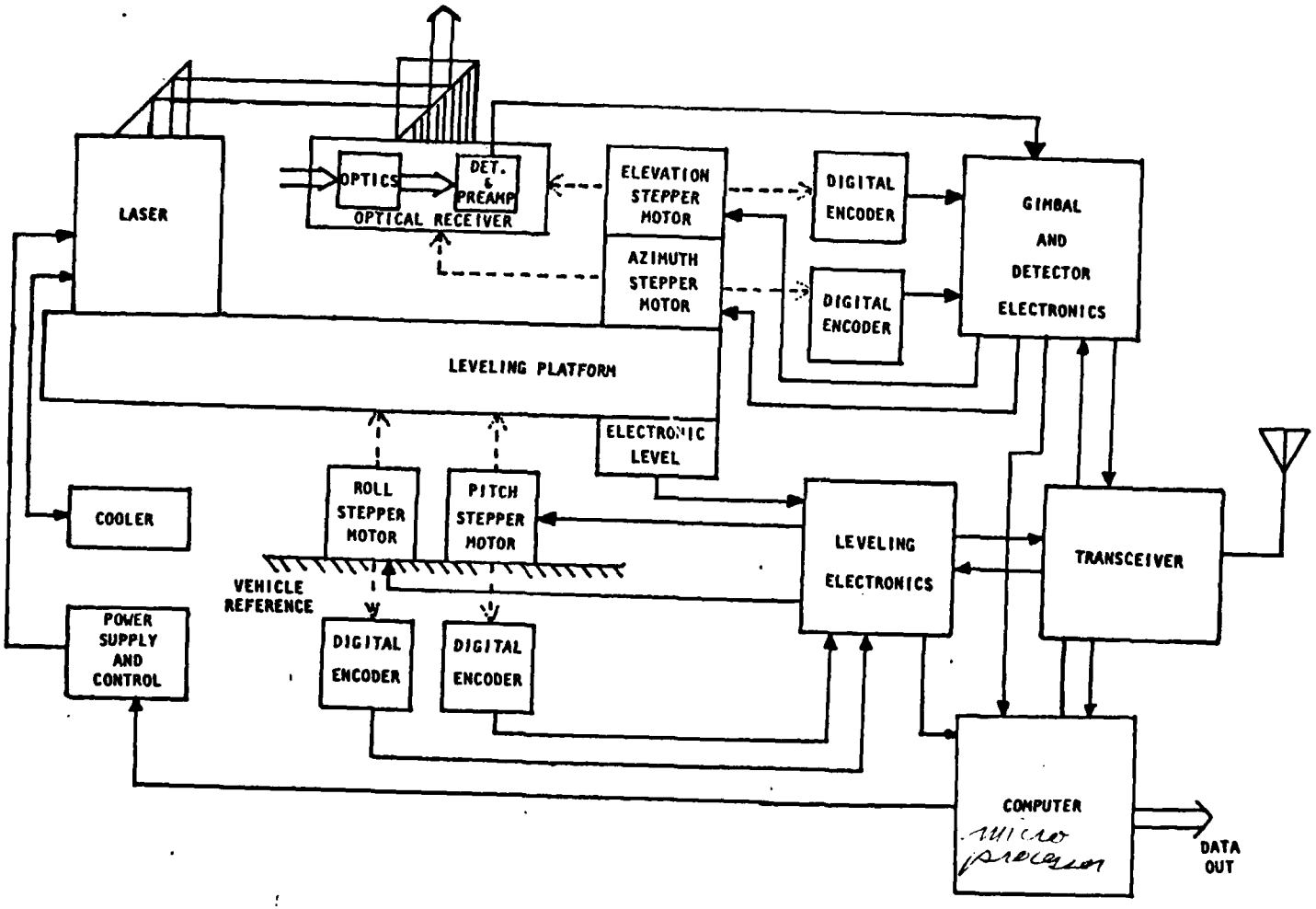

FIGURE 19. BLOCK DIAGRAM OF COMBINED UNIT

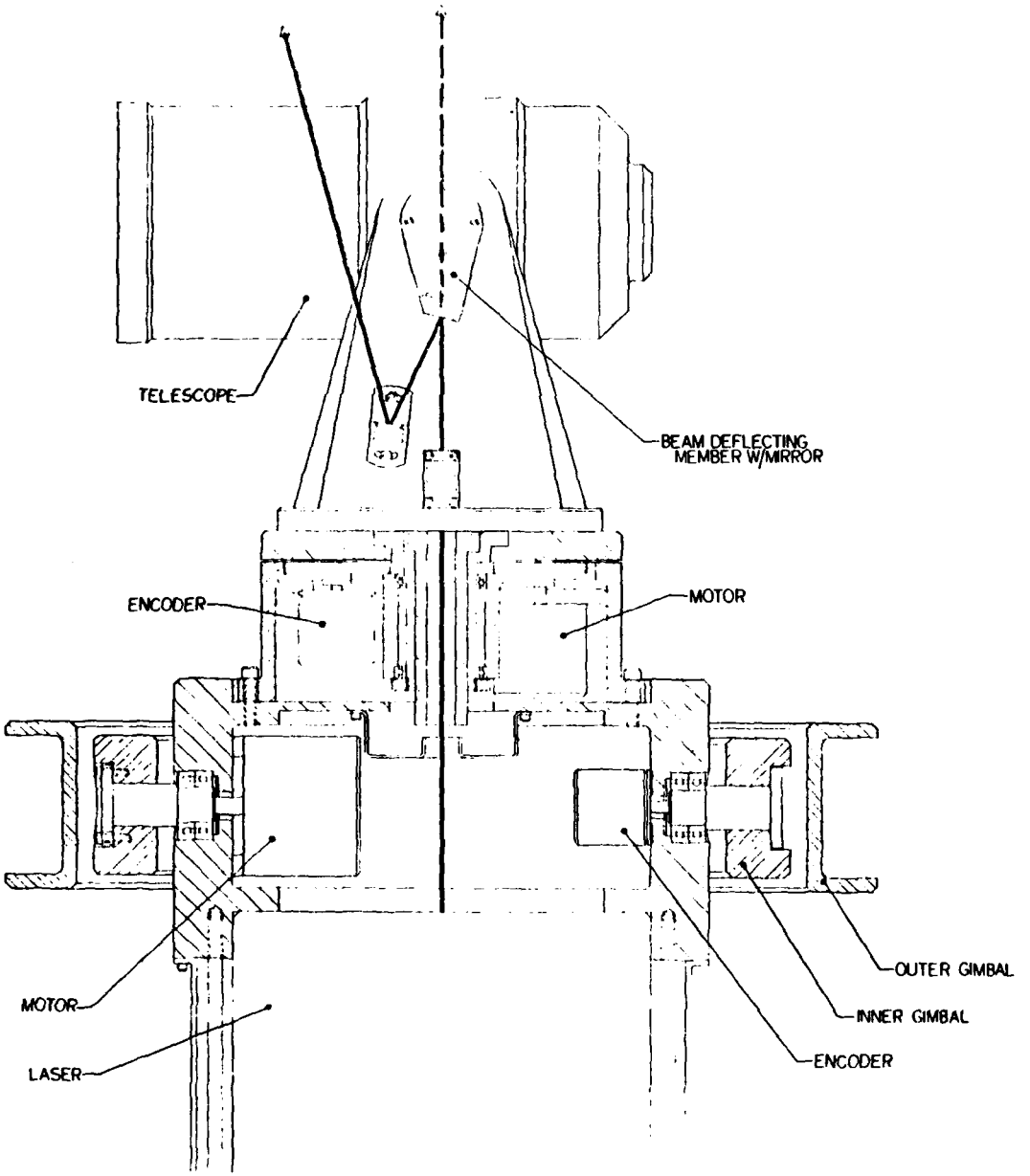

FIGURE 20. DOUBLE GIMBAL SET CONFIGURATION

One packaging approach was to eliminate the az-el mount and use only the x-y gimbal set to perform the operation. The packaging for this is shown in Figure 21. However, in order for this to work properly, the slit detector had to be replaced by a circular detector to avoid geometric problems.

Another (and the selected approach), was to use only the az-el mount which allowed keeping the slit detector. The packaging concept for this configuration is shown in Figure 22. A block diagram is shown in Figure 23.

Mounting the DBAS receiver telescope on the beam director of the HELWS was considered, but rejected for several reasons. (1) the DBAS units could not then be used to provide alignment of other field equipments, such as missile batteries or artillery batteries. (2) The acquisition radar needs a DBAS unit, and thus two design efforts would be required. (3) alignment between vehicles must be periodically checked during an engagement due to possible settling of the vehicles. This indicates that the DBAS unit should be separated from the beam director.

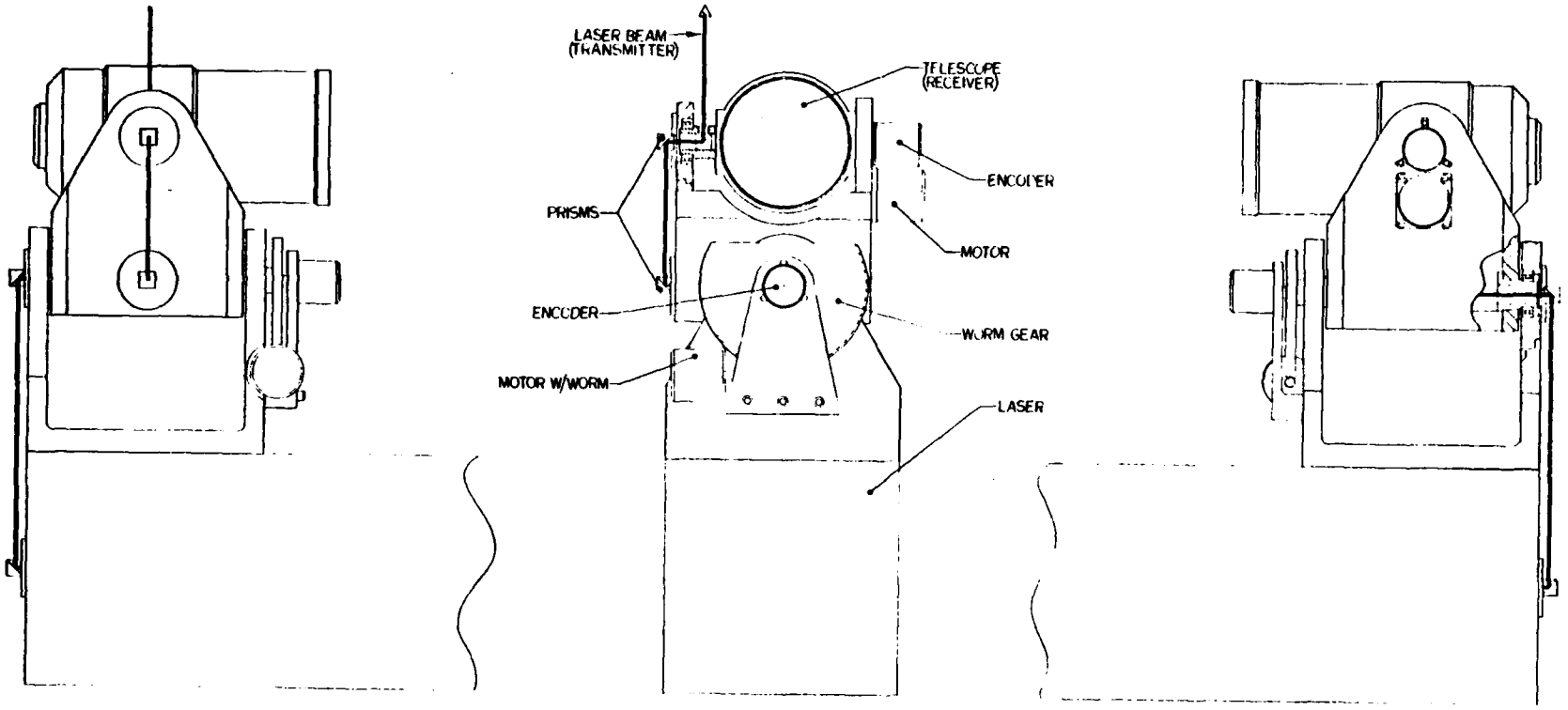

FIGURE 21. X-Y GIMBAL SET CONFIGURATION

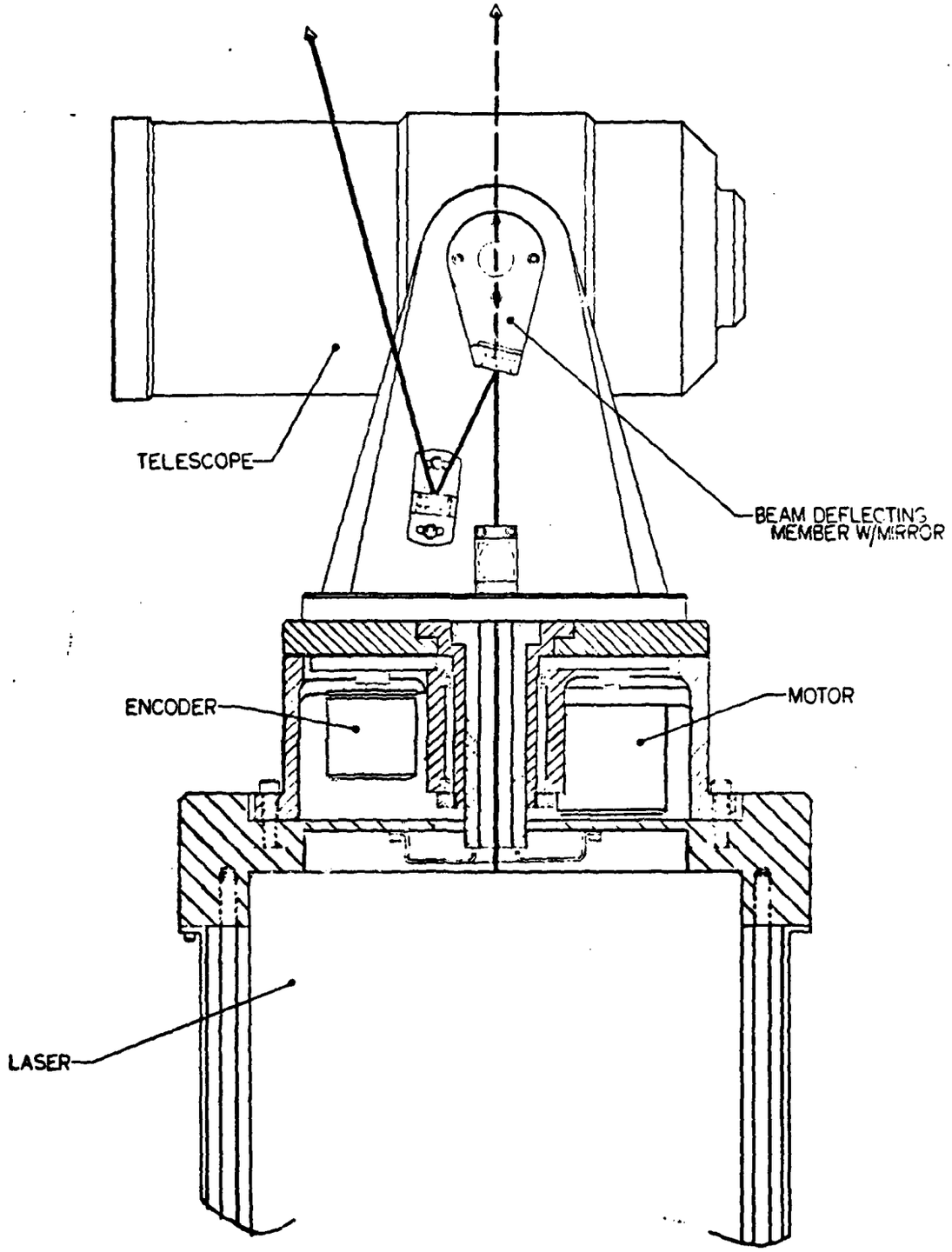

FIGURE 22. FINAL CONFIGURATION

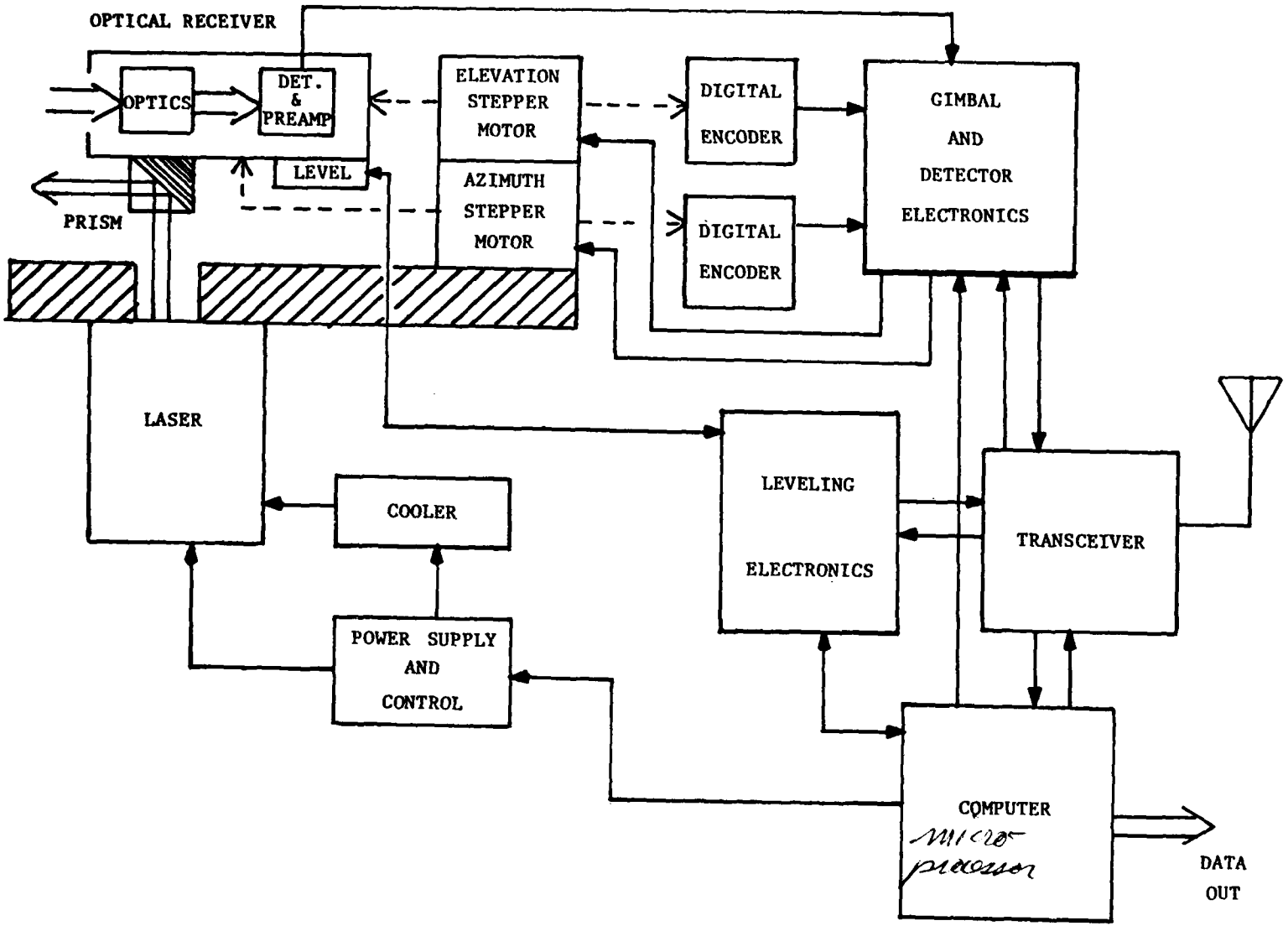

FIGURE 23. BASIC BLOCK DIAGRAM OF FINAL CONCEPT

5.1 OPERATION

After the high energy laser weapons and the acquisition radar are in position around the asset to be defined, the DBAS is used to achieve alignment. One possible sequence of operation is as follows:

1. That portion of DBAS located on the acquisition radar will be used as the laser transmitter. The laser beam output is leveled by means of the leveling device located on the "instrument", causing the laser beam to be directed along the local vertical.
2. The DBAS components located on the high energy laser weapons (the receiver) are likewise leveled.
3. The angular readouts (i.e., the A_0 and E_0 in Appendix B.) of the leveled positions are fed into the computer and stored.
4. The computer determines the coordinate transformation matrices (equations (1) and (2), Appendix B.) and instructs the receiver gimbal system to begin an azimuthal (about the local vertical) search for the vertically directed laser beam pulses (with an elevation angle just sufficient to clear any intervening obstructions).
5. When the laser beam pulses are first detected at one edge of the detector slit, the gimbal angle readouts are stored in the computer's memory. As the receiver continues to rotate in azimuth about the vertical, the laser pulse reception will stop when the laser pulse image falls off the other edge of the detector slit. The gimbal positions for this condition are also stored in the computer memory. The computer then calculates a point midway between the two readings and directs the receiver to point in that direction. At this point

the receiver is aligned in azimuth with the vertically directed laser beam. The receiver gimbal angles are now recorded and stored in the computer.

6. As the laser pulses are directed vertically they are preceded in time by a synchronization pulse coming from the communications link. The time difference between the receipt of the sync pulse via the comm link by the receiver and the receipt of the laser pulse from the receiver detector is measured. This process is repeated several times and a time average stored in the computer.
7. The elevation angle of the receiver is increased by approximately 20 degrees and the process repeated. (This angle will be a function of the weather.) The first time interval measurement is subtracted from the second time interval measurement thus providing a ΔT measurement for use in the DBAS equations. This ΔT measurement is used to calculate the horizontal range between the optical receiver and the laser pulse transmitter (see Equation (8), Section 2.2).
8. The laser beam is now tilted 30 degrees and rotated about the vertical axis. A procedure similar to that described for aligning the receiver with the transmitter is performed with the tilted transmitter beam azimuth angular measurements being stored in the computer as the beam is first detected on one side of the receiver slit and is just lost on the other side. The transmitter is then directed to a point midway between these two sets of readings. Now the transmitter is aligned directly with the receiver.

9. A series of ΔT measurements made between the sync pulse and the received laser pulse.
10. The receiver is tilted down in elevation to approximately the original elevation angle and another series of measurements made. The difference between these two sets of readings is used, along with the previously calculated horizontal range, to compute the vertical displacement between the transmitter and receiver sites (see Equations (9) and (11), Section 2.2).
11. The gimbal angles at both the transmitter and receiver are read and stored in the computer in order to provide the additional information necessary to compute the transformation matrices, so that pointing angles at the radar can be transferred to the high energy laser weapons.
12. This process is repeated for each of the other high energy laser weapons, DBAS units.

This operational process is shown in flow diagram form in Figure 24.

Since the units located on the radar and the HEL weapons will be identical in configuration, it will be possible to provide a verification of the transformation by using the weapons systems DBAS components as the pulse laser transmitters and to use the radar DBAS components as the receivers.

The communications link between the units must be a two way link so that the data obtained at the receiver locations can be sent to the transmitter location for use in the computer.

For a highly reliable system each of the DBAS units could contain separate computers, so that in the event of a failure of one computer or one component of the system, the calculations could be accomplished at another DBAS location.

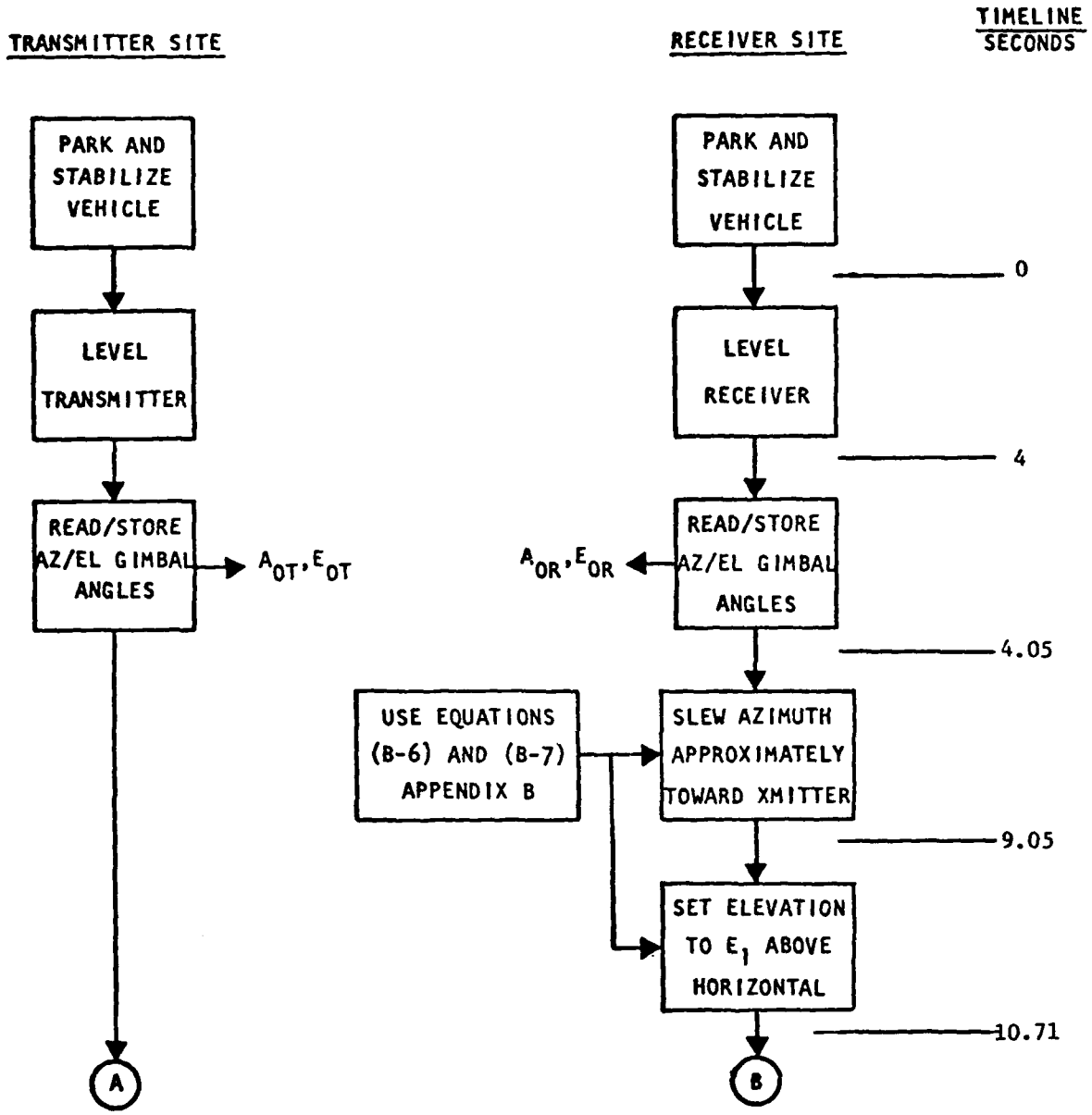

FIGURE 24(a). DBAS FUNCTIONAL FLOW

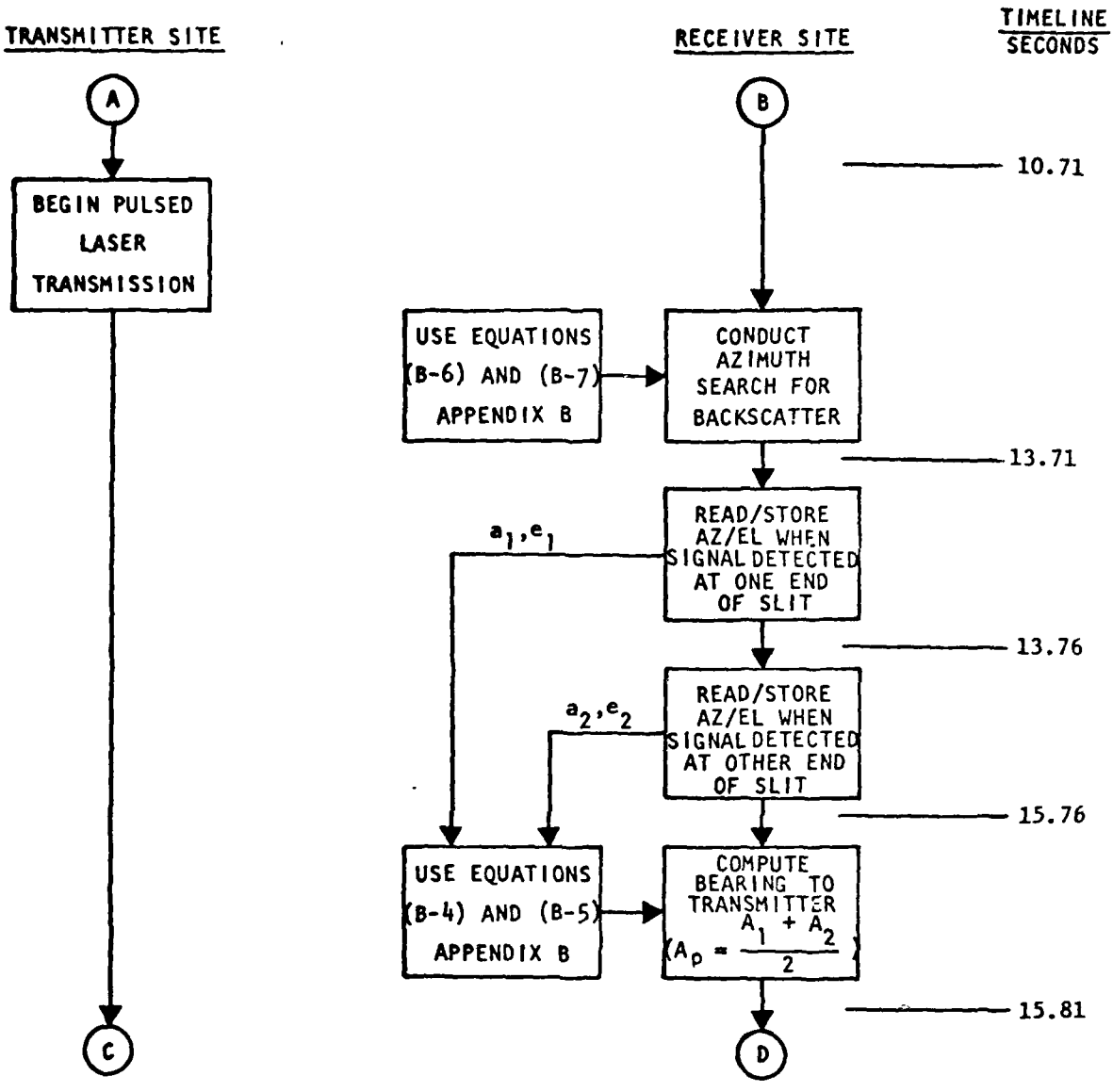

FIGURE 24(b). DBAS FUNCTIONAL FLOW (CONTINUED)

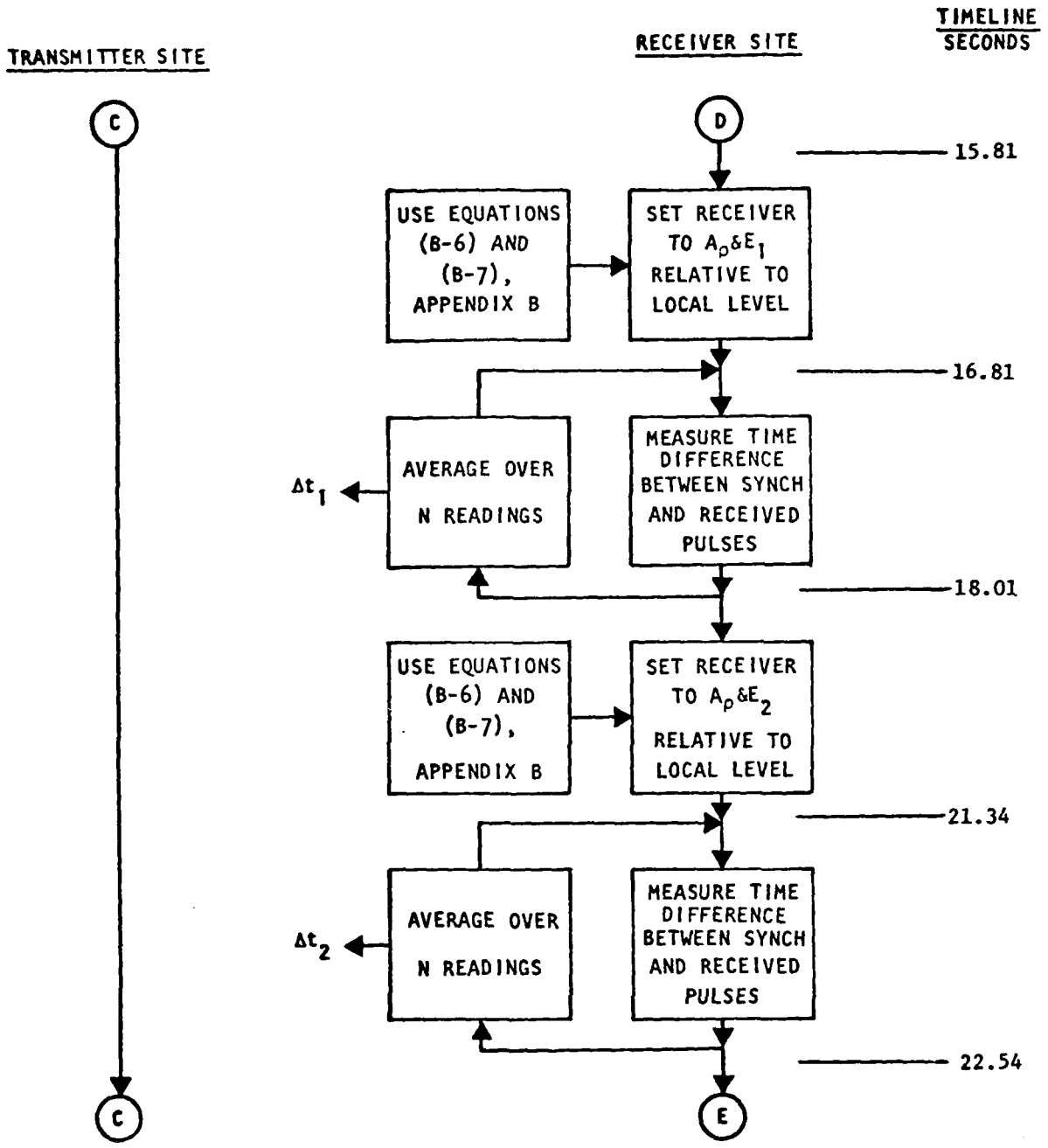

FIGURE 24(c). DBAS FUNCTIONAL FLOW (CONTINUED)

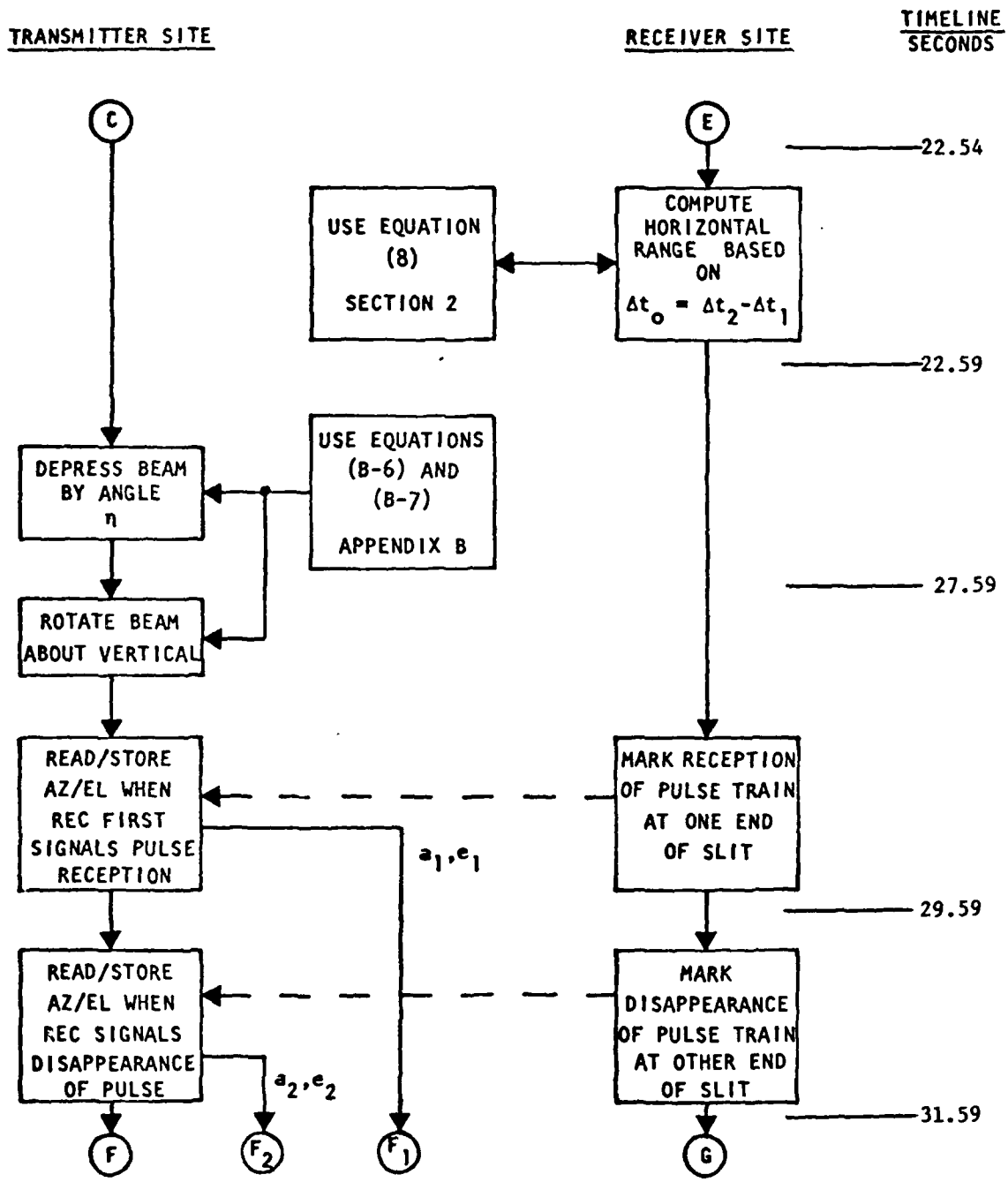

FIGURE 24(d). DBAS FUNCTIONAL FLOW (CONTINUED)

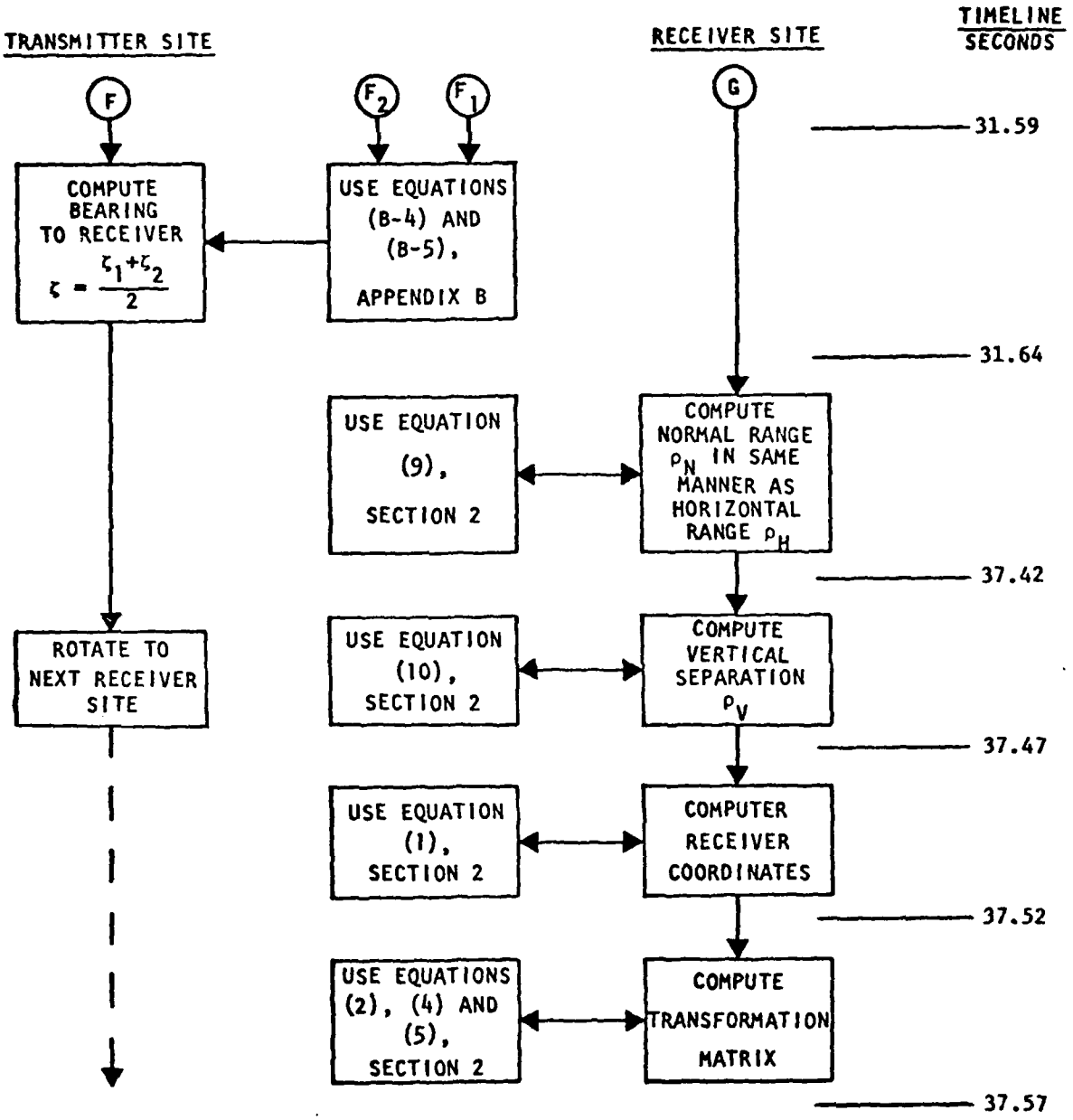

FIGURE 24(e). DBAS FUNCTIONAL FLOW (CONTINUED)

5.2 TRANSMITTER

The laser transmitter consists of a pulse laser, its power supply, its cooler, and the optics necessary to direct the beam through the gimbal system.

5.2.1 Laser

The laser selected for the DBAS concept presented here is a Nd:YAG laser pulsed at 10 pps with a peak pulse output energy of 200-400 MJ. The performance parameters of this laser are listed in Table 10.

TABLE 10. LASER PERFORMANCE PARAMETERS

TYPE	Nd:YAG
OPERATION	Mutlimode
BEAM SIZE	6-7mm
BEAM DIVERGENCE	<5mr
PULSE ENERGY	200-400 mJ
PULSE LENGTH	15-25ns
PULSE RATE	4-10 pps
PULSE JITTER	<2ns
SWITCHING METHOD	Q-switched pockelcell
SIZE (MAX)	20cmx20cmx60cm
WEIGHT (LASER UNIT)	<12 kg
COOLER	Closed cycle water
WEIGHT (COOLER AND POWER SUPPLY)	≈200 kg

5.2.2 Optics

The optics for the transmitter, in addition to the laser head optics, consists of a series of mirrors for directing the laser beam through the gimbal axes so that it can be directed by the gimbal set. Figure 25 shows schematically how this is accomplished.

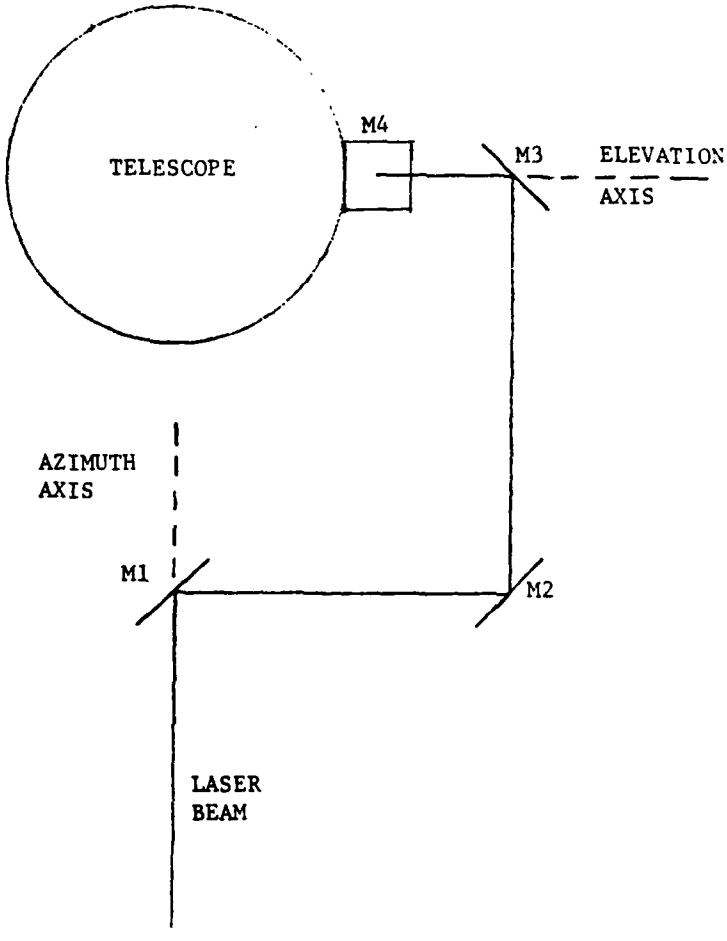

NOTE:
MIRRORS M1, M2 AND M3 ARE STATIONARY WITH RESPECT TO AZIMUTH AXIS.

MIRROR M4 IS STATIONARY WITH RESPECT TO ELEVATION AXIS.

FIGURE 25. TRANSMITTER OPTICAL SCHEMATIC

5.3 RECEIVER

The conceptual design of the receiver is predicated on the discussion in Section 5.0. Thus, by removing two of the three slits, the field of view was decreased substantially, making the receiver package smaller. The salient parts of the receiver are:

- o Optics
- o Detector
- o Preamplifier
- o Housing

5.3.1 OPTICS

The receiver optical design is a conventional cassegrain telescope with a paraboidal primary and a hyperboloidal secondary. By going from a three detector optical system, as used in the breadboard, to a single detector system, it was possible to go from an F/1 optic to an F/8 optical system and thus reduce the background noise and increase the system S/N.

Figure 26 shows the optical schematic while Table 11 lists the pertinent data for the components of the optical system.

TABLE 11. OPTICAL SPECIFICATIONS

PRIMARY MIRROR - PARABOLOIDAL	
DIAMETER	140mm
FOCAL LENGTH	300mm
SURFACE	λ/10
COATING	HIGH REFLECTANCE SILVER
SECONDARY - HYPERBOLOIDAL	
DIAMETER	36mm
FOCAL LENGTH	-110mm
SURFACE	λ/10
COATING	HIGH REFLECTANCE SILVER
TELESCOPE	
MIRROR SEPARATION	223mm
BACK FOCAL DISTANCE	256.666mm
EFF, FOCAL LENGTH	1000 mm

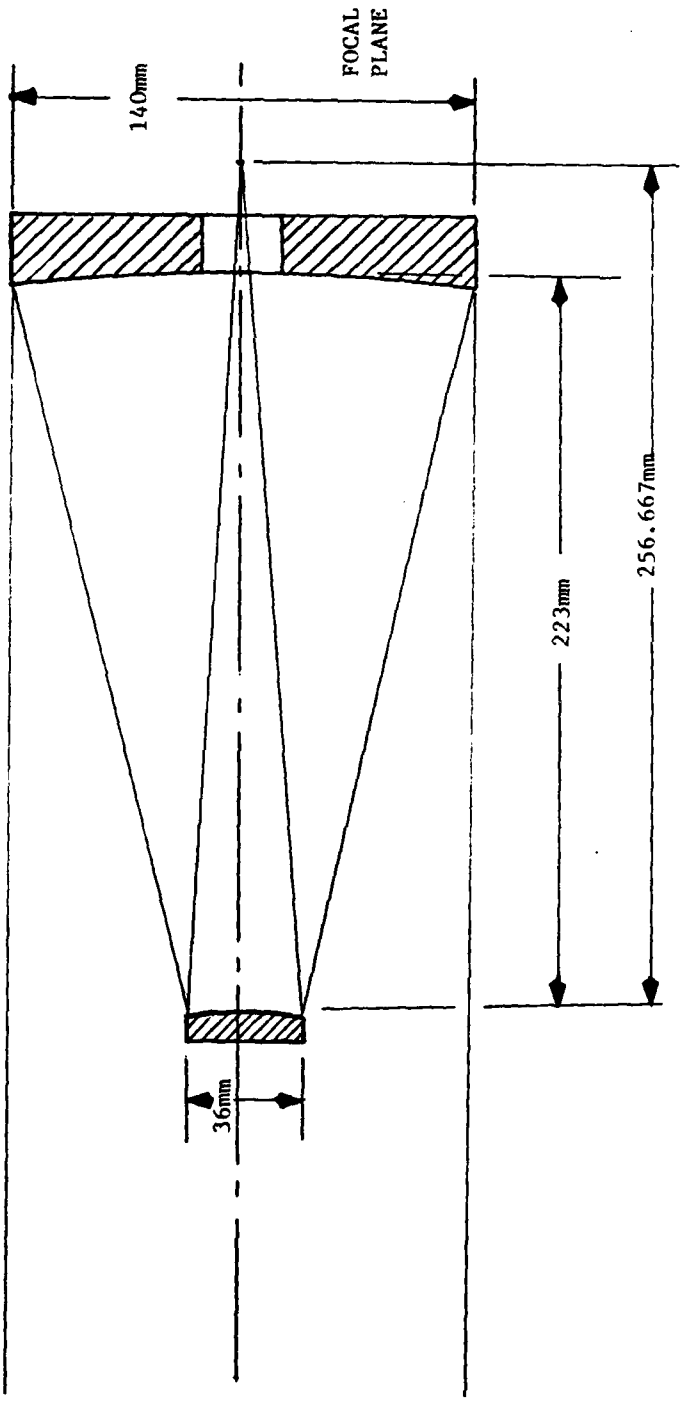

FIGURE 26. RECEIVER OPTICAL SCHEMATIC

5.3.2 DETECTOR

The detector for the receiver must have good response at the wavelength of the Nd:YAG laser which is 1.06 m. Silicon detectors are fabricated which peak at this wavelength. No preliminary selection has been made at this time, because it would be better to have a detector fabricated to a specified size and shape to reduce noise. Table12 gives a simplified performance specification of such a detector. Figure 27 shows a typical response curve for such a detector.

TABLE 12- DETECTOR SPECIFICATION

D^*_λ (1.06λm, 270, 1)	$3x10^{12}$	$cm(Hz)^{1/2}{}_w{}^{-1}$
NEP_λ (1.06 m, 270, 1)	$3x10^{-13}$	watt
Quantum Efficiency	50	%
Operating Voltage	TBD (60)*	volts
Leakage Current	TBD (1)*	μa
Capacitance	TBD (4)*	pf
Rise Time	TBD (5)*	ns
Active Area	1x10	mm

*Suggested values, open for negotiation

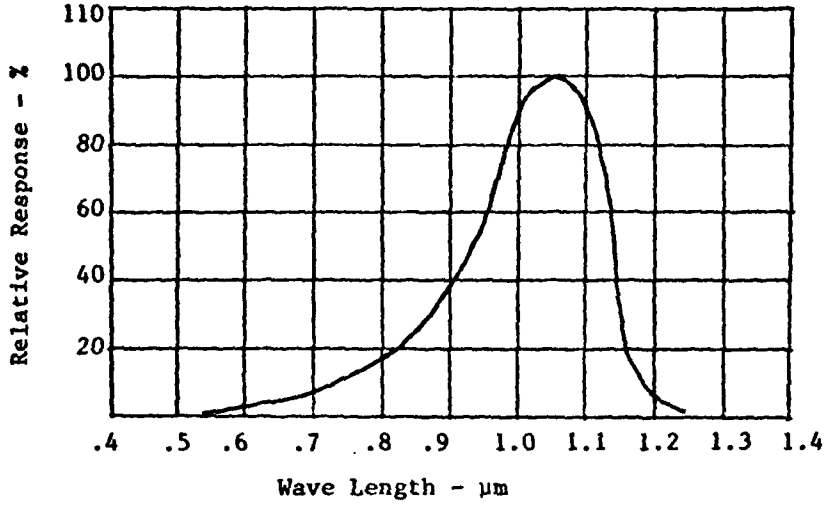

FIGURE 27. DETECTOR SPECTRAL RESPONSE

5.3.3 Signal-to-Noise Estimate

Using the scattering equations presented in Appendix A, a family of curves can be plotted which relate the S/N ratio at several DBAS ranges to the visibility range. Figure 27a shows such a plot for DBAS ranges of 1 Km, 2Km, and 3 Km with telescope elevation angles between 10° and 30°. A telescope aperture of 126 cm^2, a transmitter pulse energy of 100 mJ, and a wavelength of 1.064 μm were used in the calculation of these results.

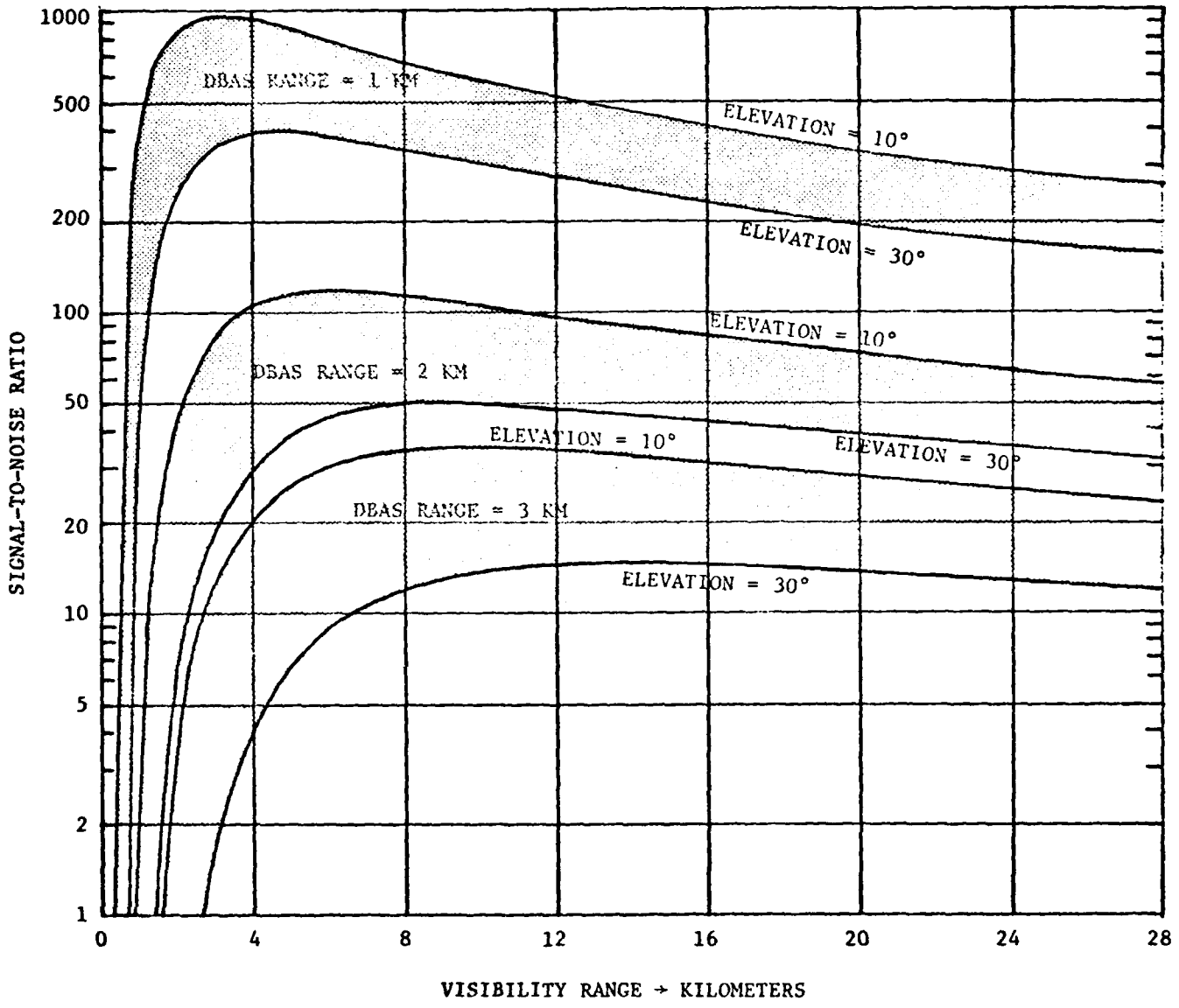

FIGURE 27a. SIGNAL-TO-NOISE AS A FUNCTION OF VISIBILITY

5.4 ELECTRONICS

The electronics of DBAS are concerned with numerous tasks. These are:

- o Laser Power Supply
- o Sync Pulse Generation
- o Laser Trigger Pulse
- o Laser Transmit Pulse Detector
- o Sync Receiver
- o Laser Pulse Receiver Detector Preamp
- o Timing Measurements
- o Leveling Sensor and Electronics
- o Shaft Angle Encoders
- o Range, Altitude, and Coordinate Transformation Computation
- o Gimbal Motor Drive
- o Communications System

A laser power supply would be part of the laser package procured from the laser manufacturer.

The sync pulse generator provides a pulse 10 times a second and is the zero time indicator for the DBAS. This pulse is used to provide a trigger for the laser and is transmitted via to communications system to the receiver. Figure 28 shows a typical pulse sequence in the DBAS. The difference in time of receipt of laser pulses at the receiver for the two elevation angles, is by inspection of Figure 28.

$$\Delta T = (T_{RL}' - T_L') - (T_{RL} - T_L)$$

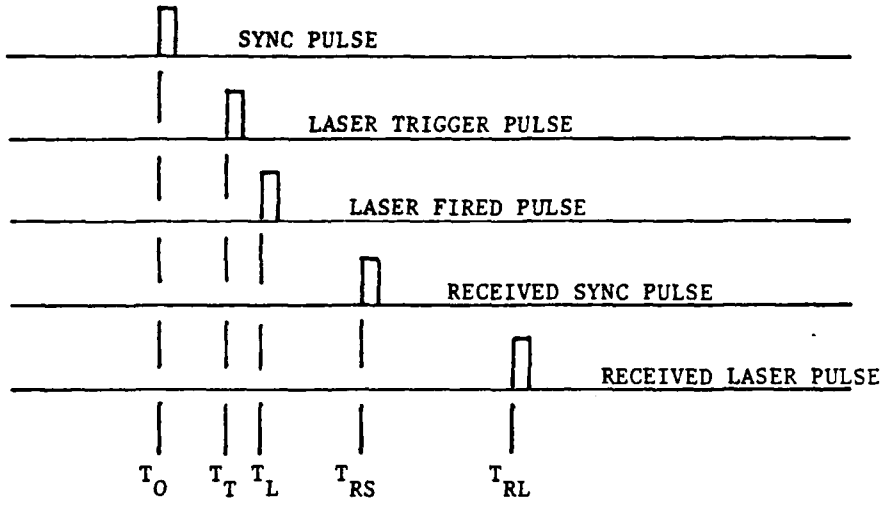

(a) PULSE SEQUENCE AT ELEVATION ANGLE E_1

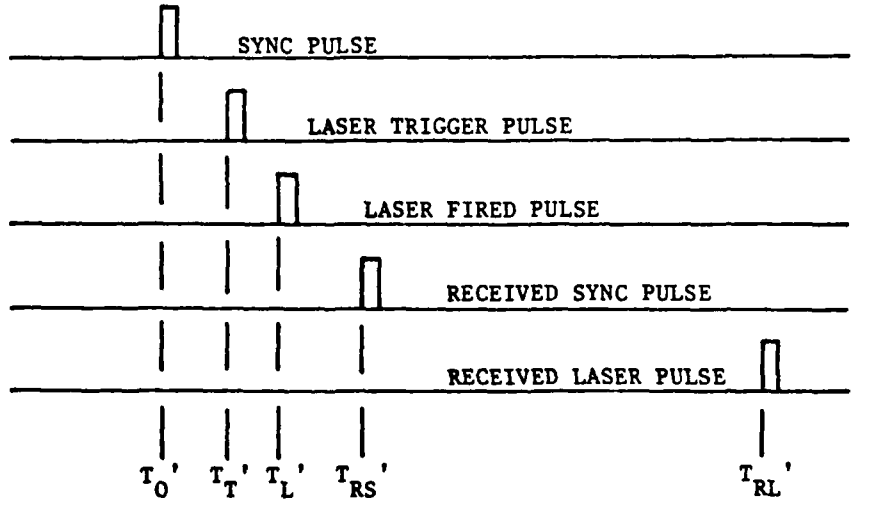

(b) PULSE SEQUENCE AT ELEVATION ANGLE E_2

FIGURE 28. PULSE SEQUENCE TIMING DIAGRAMS

These times occur at opposite ends of DBAS and are not directly measurable. However, in the transmit mode the system time counter reads ($T_L - T_0$) (or ($T_L' - T_0'$)) which, since T_0 (or T_0') is zero time reference, is simply T_L (or T_L').

In the receiver mode the counter reads ($T_{RL} - T_{RS}$) (or ($T_{RL}' - T_{RS}'$)). However, since $T_{RS} = T_{RS}'$ then

$$\Delta T = [(T_{RL}' - T_{RS}') - T_L'] - [(T_{RL} - T_{RS}) - T_L]$$

Thus, the ΔT is simply the difference of the 2 counter readings at elevation E_1 minus the difference of the 2 counter readings at elevation E_2.

The laser trigger pulse is delayed from the sync pulse in order to have a measurable time between when the sync pulse is received at the optical receiving unit and when the backscattered laser pulse is received at the optical receiving unit.

The purpose of the laser transmit pulse detector is to provide the pulse at the time T_L. This is necessary since the pulse timing jitter with respect to the trigger pulse can be between as large as 10 - 20 ns.

Part of the communications system is used to provide the transmittal of sync pulse and the reception of the sync pulse. This pulse can be impressed on the normal communications signals and stripped off by a special electronic circuit.

The laser pulse receiver is described in the previous section.

Timing measurements are provided by high speed timing counters such as were used in the breadboard.

A level sensor, such as shown in Figure 29 will provide signals which can be used to drive the gimbal motors until the level sensor output in both axes are zero.

The shaft angle encoders provide angular measurements in 16 bit digital form for a resolution of 0.0959 milliradians. The zero position of these readouts present two axes of the vehicle that DBAS unit is mounted on. Computations of horizontal range, vertical separation, and coordinate transformations take place in a special purpose microprocessor. This microprocessor also provides the control functions for the DBAS including the gimbal motor drive signals.

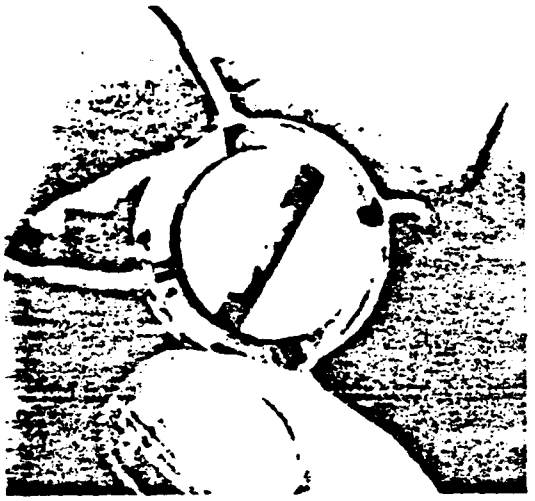

The Tiltmeter Sensor

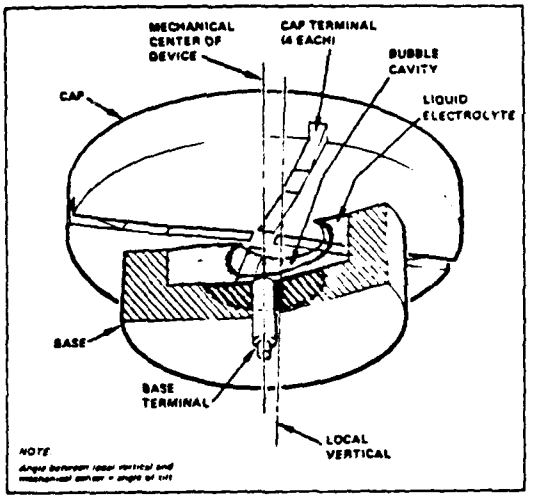

Sensor Assembly

FUNCTIONAL

- RMS Resolution Limit: 1.4×10^{-3} arc second or 8×10^{-9} radians at 1-Hz bandwidth
- Stability: Less than 0.08 arc second in 20 days
- Frequency Response (Tilt and Acceleration at 70°F): Flat within 3 db from dc to 1 Hz; -40 db per decade from 1 to 10 Hz

PHYSICAL

- Sensor Dimensions: 2-in. diameter x 2 in. long
- Electronics Unit

  Design configuration can be varied according to application.

FIGURE 29. LEVEL SENSOR

5.4.1 ERROR ESTIMATE

The basic errors to be expected in field equipment consist of timing errors and angular measurement errors. Timing errors are due to signal-to-noise on the received pulse and resolution of the timing counters. By designing the receiver electronics so that the rise time of the electrical pulse is 10 nanoseconds or less, and with a S/N ratio of 5, the inherent RMS timing error is 2.24 nanoseconds. Assuming the counter resolution to be 2 nanoseconds, then the overall RSS timing error is 3 nanoseconds. Angular measurement errors are basically dependent upon the resolution of the angular encoders. The proposed encoders have a 16 bit resolution, or approximately $\pm$.005° accuracy.

Using these error estimates in the equations for ρ_h and ρ_v, on pages 10 and 12, gives a 1σ ρ_h error of 0.78 meters and a 1σ ρ_v error of 3.06 meters.

5.5 UNIQUE PROBLEMS

The weather is the most unique problem to the DBAS, since if the weather is too clear, the range is less; if too hazy, the range is less. This problem is not alleviated by going to the 1.06μm wavelength. However, by going to a smaller field-of-view sensor, the difficulties are partially overcome, since the background noise is decreased. In addition, the proposed conceptual design uses a higher energy per pulse laser than the breadboard DBAS, providing a larger margin for operation in foul weather.

Other possible areas of difficulty are, in general, concerned with problems which are amenable to engineering solution, such as:

- o Cooling
- o Ruggedness
- o Safety
- o Integration with Vehicle
- o Covertness

Cooling of the Nd:YAG laser is not expected to be a critical problem for several reasons. First, closed loop cooling systems have previously been used with Nd:YAG lasers, secondly, the operational "on" time for any alignment sequence is relatively short. These two considerations, along with the fact that the average power is quite low when the laser is running relegates this problem to one of making sure that the system is designed with it in mind.

Many Nd;YAG lasers have been built for field use, and so have other electro-optical systems. Mechanical ruggedness for the DBAS is a requirement and will be dealt with in the mechanical design. Exposed optical elements present a cleanliness problem that can be solved by providing dust covers and proper maintenance procedures.

Safety is dealt with by using proper procedural techniques and by making DBAS completely automatic.

Integration of DBAS with the vehicle is suggested as a possible problem because it has to be mounted in such a way as to have full 360° clear azimuthal field of view. In addition, it has to be aligned with the vehicle coordinate system.

Covertness is partially accomplished by using the 1.06 m wavelength. Nevertheless, if DBAS can sense the laser backscatter, certainly other instruments also could. Such detection can be minimized by using DBAS sparingly and on a non-periodic schedule.

5.6 WEIGHT

The DBAS unit total weight including the laser, laser cooler, laser power supply, and electronics would be approximately 250 Kg. If it were possible to operate the laser for short durations without the cooling system (not investigated) this weight may drop to 150 Kg.

If the laser were not included, the DBAS unit weight would be about 40 Kg including electronics and microprocessing equipment.

A further possibility would be to design the DBAS so that a field target designator/range finder (TDR) could be interfaced with the DBAS mount to provide the laser pulses; however, the pulse power output of known TDR's is lower than that necessary to achieve a 3 km range for DBAS.

6.0 DEVELOPMENT RECOMMENDATIONS

The purpose of this section is to establish guidelines for developing an operational militarized version of the Directed Beam Alignment System. Detailed schedule and cost data for the experimental prototype development are given.

This report for the current DBAS Project includes a system level conceptual design for an automatic militarized DBAS. The next program phase would be to convert this concept into a detailed design from which an experimental prototype could be fabricated and tested. This experimental prototype would contain all of the necessary feasibility operational features but would not be completely automatic in operation. The test effort for this model should demonstrate, not only range and altitude measuring capability, but the ability to hand over target coordinates from one site to another site. Initially, this could be accomplished using stationary targets (in order not to involve radar and optical tracker dynamics) followed by a full scale dynamic transfer on a moving target from an acquisition radar to an optical tracker. Once this dynamic transfer has been successfully demonstrated, a qualification model design and fabrication effort would begin, followed by full scale completely automatic performance testing, and environmental qualification testing.

Figure 30 shows an overall schedule for this complete development program recommendation.

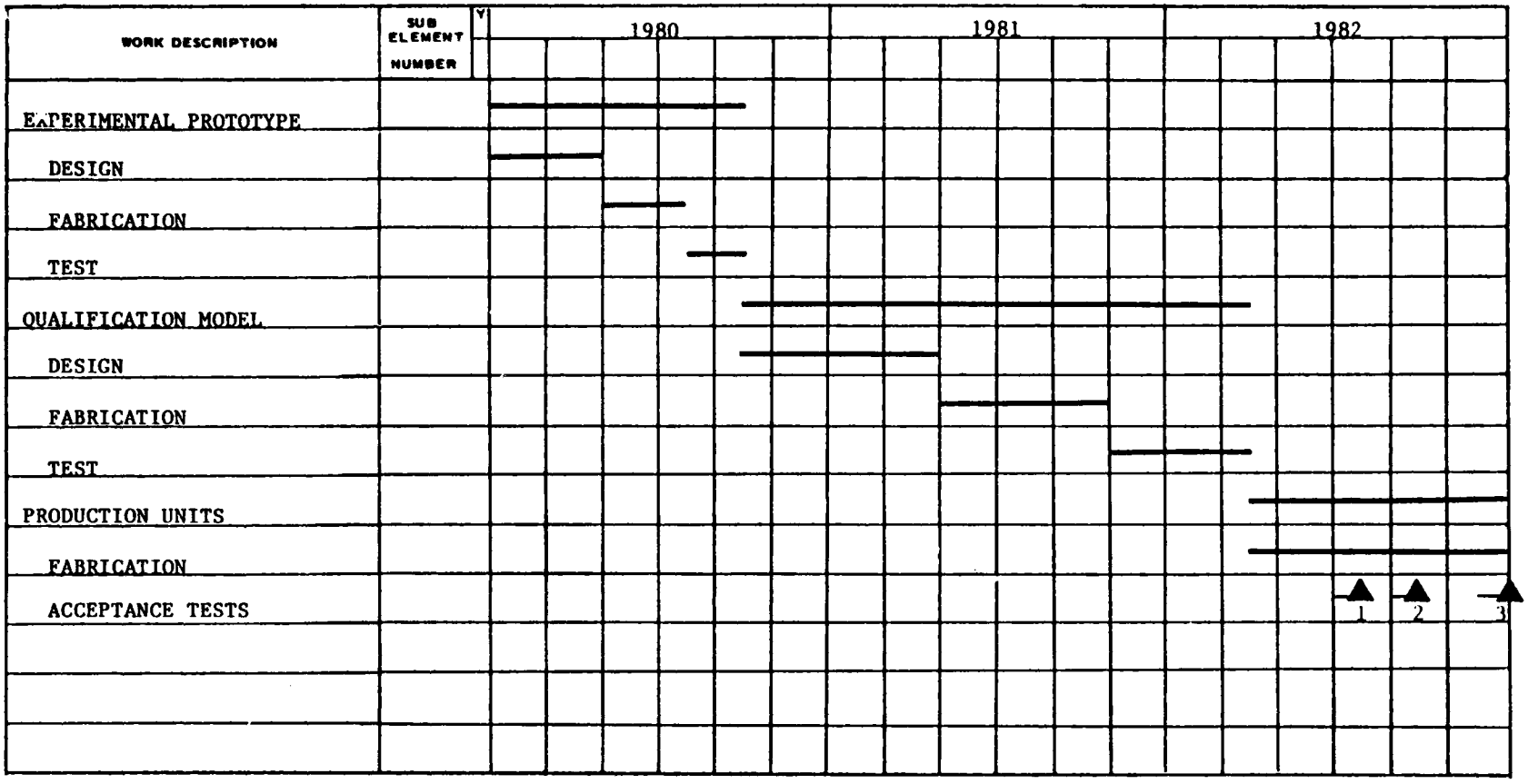

FIGURE 30. RECOMMENDED DBAS DEVELOPMENT SCHEDULE

6.1 DETAILED EXPERIMENTAL PROTOTYPE SCHEDULE

A detailed schedule for the experimental prototype is given in Figure 31. The schedule is broken into 5 major tasks: Program Management, Design, Fabrication, Assembly, and Test. In addition, the Design and Fabrication tasks are further broken into the effort required for each of the components of the DBAS assembly.

The overall schedule has been compressed into 9 months in order to keep costs minimal. To meet this compressed schedule, it will be necessary to make some early design decisions that will permit ordering long lead items for the fabrication effort. This should not be too difficult, since the experience obtained with the breadboard model provides a solid basis for these decisions.

6.2 COST ESTIMATES

The cost estimates given in this section are for the experimental prototype and are based upon past experience with similar type equipment. In an effort to keep costs as low as possible, laboratory type equipment has been assumed where it can be used without affecting operation, and only semi-automatic operation has been considered. For instance, the computer used to provide the calculations will be an existing TRW HP-9835A desk-top computer. In addition, laboratory equipment that will interface with the HP9835A on an HP-1B bus will be used whenever possible, and the control loop around the gimbals will be manually closed.

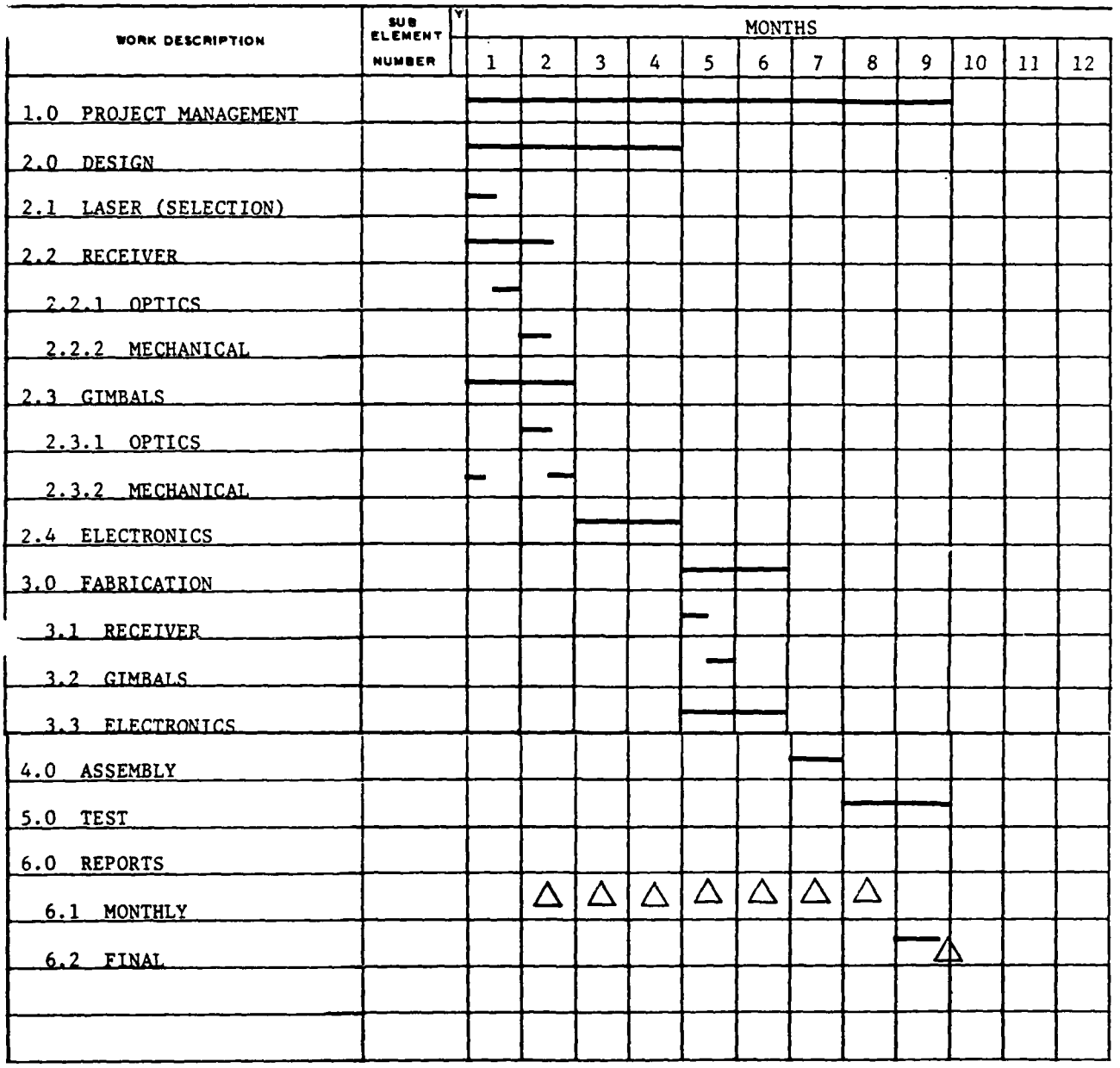

FIGURE 31. EXPERIMENTAL PROTOTYPE SCHEDULE

APPENDIX A

SCATTERING PHENOMENOLOGY

When an electromagnetic wave propagates through any passive media, energy is removed from the radiation beam. The relative amount of energy/power removed from the beam per unit length of propagation defines the extinction coefficient for the media and is

$$\gamma_{ext} = \frac{1}{P} \frac{dP}{dz}$$

where

P = transmitted power

γ_{ext} = extinction coefficient

Part of the energy which is removed is reradiated (scattered) and, therefore, it is still an electromagnetic wave and is available for detection purposes. The remaining part is absorbed by the media and converted into some other form of energy such as heat. These two parts of the extinction coefficient are symbolized by γ_{sc} for the reradiated (scattered) energy and γ_{abs} for the absorbed energy. The following relationship is valid

$$\gamma_{ext} = \gamma_{abs} + \gamma_{sc}$$

Figure A-1 defines the geometry and variables used in the aerosol scattering formalism. The amount of power scattered per unit length

$$dP = P \gamma_{sc} dz$$

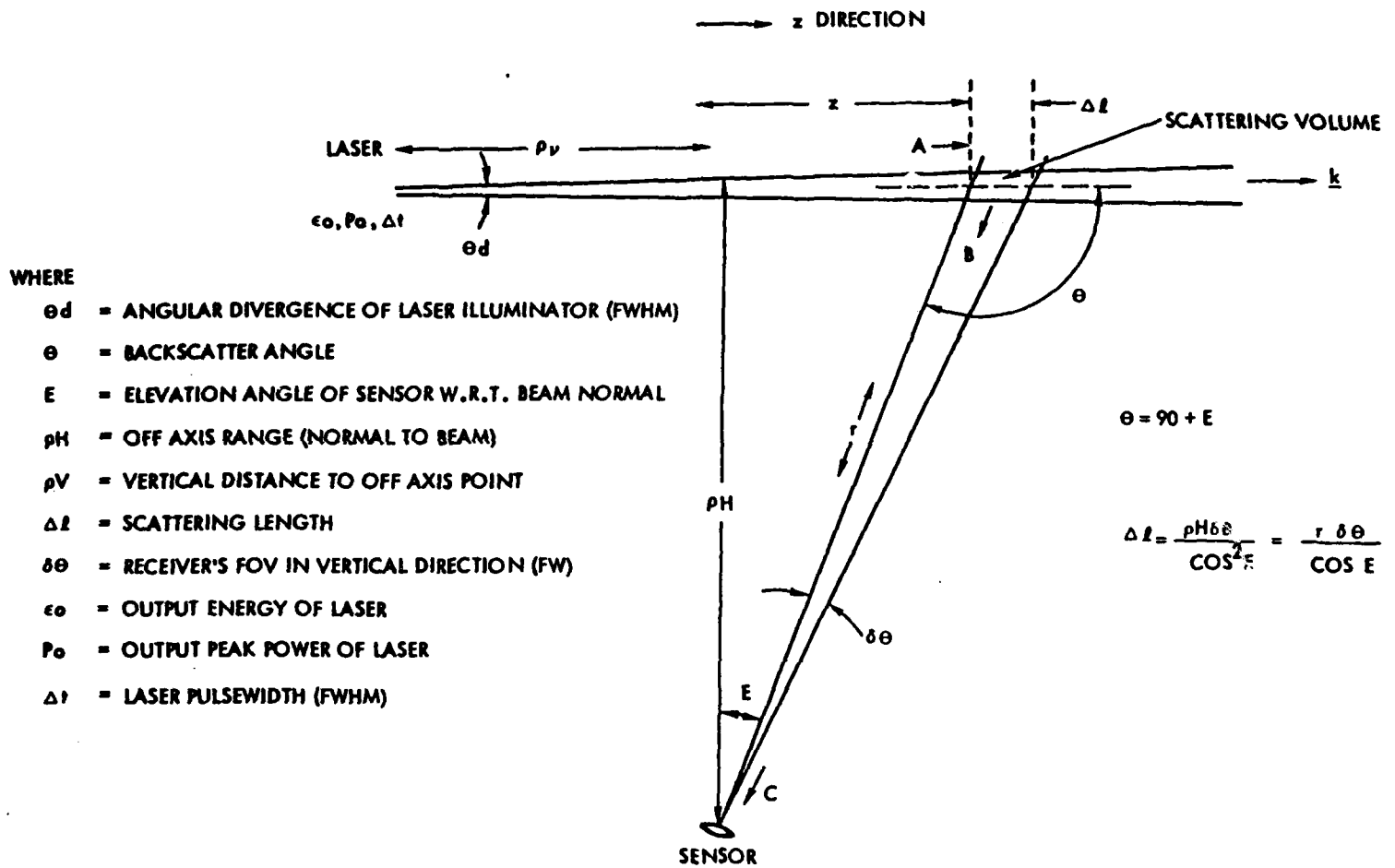

WHERE

- θd = ANGULAR DIVERGENCE OF LASER ILLUMINATOR (FWHM)
- θ = BACKSCATTER ANGLE
- E = ELEVATION ANGLE OF SENSOR W.R.T. BEAM NORMAL
- ρH = OFF AXIS RANGE (NORMAL TO BEAM)
- ρV = VERTICAL DISTANCE TO OFF AXIS POINT
- Δℓ = SCATTERING LENGTH
- δθ = RECEIVER'S FOV IN VERTICAL DIRECTION (FW)
- εo = OUTPUT ENERGY OF LASER
- Po = OUTPUT PEAK POWER OF LASER
- Δt = LASER PULSEWIDTH (FWHM)

FIGURE A-1. AEROSOL SCATTERING GEOMETRY

is redistributed over 4π steradians. For polarized laser beams there is a dependence in the redistribution as a function of ϕ the angle about the beam axis. For Rayleigh scattering (small particles) this effect can be severe at off-axis angles, θ, about 90°. Larger particles reduce this effect. Since the polarization direction of the laser is not known a priori and also the magnitude of the dependence on ϕ is small, it will be assumed that the dependence on ϕ can be neglected. The angular redistribution is then given by the normalized scattering function $F(\theta)$ where

$$\int_0^{\pi} F(\theta)\ 2\pi\ \sin\theta\ d\theta \equiv 1$$

The amount of energy scattered in the angular direction θ is

$$dP(\theta) = P\ F(\theta)\ \gamma_{sc}\ dz$$

An important element of scattering is that the correlation of the scattered wavefronts at different points in the media does not extend to neighboring particles. Therefore, the scattered light is noncoherent so that intensities at the sensor may be added rather than field strengths. This noncoherent nature reduces the magnitude of scintillation that can affect any detection statistics. In the remaining discussion, only a single scattering model is considered. This assumption means that only the radiation scattered at the intersection of the laser beam and sensor's FOV will contribute to the signal level at the sensor (see Figure A-1). Mutliple scattering is required when the ranges of interest are many times the inverse scattering coefficient ($1/\gamma_{sc}$), and scattering dominates absorption, $\gamma_{sc} >> \gamma_{abs}$.

2.2 Aerosol Scattering Formalism

Referring to Figure A-1, the equations used to predict the intensity at the sensor are derived. The power at point A, just before the scattering volume is

$$Pa(t) = P_o(t - \rho_v/c - z/c)\ e^{-\gamma_{ext}(\rho_v + z)}$$

The differential scattered power in the direction of the sensor is

$$dP_B(t) = Pa(t)\ \gamma_{sc}\ F(\theta)\ dz$$

At the sensor the incident intensity is

$$dI_c = dP_B(t - r/c)\ \frac{e^{-\gamma_{ext} r}}{r^2}$$

Combining the above results in

$$dI_c(t) = P_o[t - (\rho_v + 3 + r)/c]\ \frac{\gamma_{sc} F(\theta)}{r^2}\ e^{-\gamma_{ext}(r + z + \rho_v)}\ dz$$

A simplification is obtained from the relation

$$\rho_H = r \sin\theta = -z \tan\theta$$

from which

$$\frac{dz}{r^2} = \frac{d\theta}{\rho_H}\ (\sin^2 \theta)$$

Noting that

$$z + r = \rho_H \tan(\theta/2)$$

results in

$$dI_c(+) = P_o[t - (\rho_v + \rho_H \tan(\theta/2))/c]\ \gamma_{sc}\ F(\theta)\ \frac{d\theta}{\rho_H}\ e^{-\gamma_{ext}[\rho_v + \rho_H \tan(\theta/2)]}$$

where the total intensity is (assuming small FOV $\therefore$ ρ_v and $\rho_H = f(\theta)$)

$$Ic(t) = \int_{\theta}^{\theta} dI_c(+)$$

For an infinitesimal small field-of-view, $\delta\theta$, the incident intensity will have the same shape as the transmitted laser pulse. (A pulsed laser is assumed for the laser source.) The magnitude of the intensity will be extremely small since $Ic(t) \propto \delta\theta$. As the field-of-view is increased, the received pulse shape will be slightly distorted and the intensity level will increase; more of the beam is seen and adds up with different time delays at the receiver. A point is reached where a further increase in $\delta\theta$ does not increase the intensity level, but just increases the total energy received since the pulse will be seen longer but not take up the total spatial extent of the projected field-of-view at the beam. For a laser pulsewidth ΔT, this occurs when

$$\Delta l \quad c\ \Delta t$$

or

$$\delta\theta = \cos^2(E)\ \frac{c\Delta t}{\rho_H}$$

This equality can be used to determine the vertical FOV of the sensor.

The intensity is analytically tractable by assuming that the laser output is an impulse given by

$$P_o = E_o\ \delta(t - t_o)$$

in reality Δt = 15 - 30 ns and the results are valid. Neglecting any fixed

(non angular pulse delay) the pulse output is

$$P_o = \frac{E_o\ 2C}{\rho_H} \cos^2(\theta_o/2) \quad (\theta - \theta_o)$$

where θ_o is the off-axis angle. The resulting intensity at the sensor for the impulse function is:

$$Ic(t) = \frac{E_o\ 2c}{\rho_H^2} \cos^2(\theta_o/2)\gamma_{sc}\ F(\theta_o)\ e^{-\gamma_{ext}[\rho_v + \rho_H \tan(\theta_o/2)]}$$

Atmospheric Modeling

The atmospheric information required to assign values to γ_{sc} and γ_{ext} are obtained from Reference A-1. These values vary as a function of altitude (intersection of laser beam and sensor field-of-view). The data are only given in discrete 1 km blocks i.e., γ_{sc} for 0 - 1 km altitude, 1 - 2 km altitude, etc. The resulting data will therefore have discontinuities as the elevation angle views a position just below and just above 1 km. This discontinuity was smoothed during the process of graphing the results.

The extinction and scattering coefficients also vary as a function of meteorological visibility range as well as atmospheric model. The model chosen represents an average or below average condition. In this way, a conservative number results for the intensities.

The normalized scattering function is strongly dependent on angle. Fortunately, in the region of interest θ = 100 to 140°, the function is fairly smooth, $F(\theta) \doteq 0.01$. This case is also the lowest value of the function and is thus a worst case for assessing probabilities of detection.

Predicted Intensity

In order to evaluate the expected intensity at the receiver, the value of $I_c(t)$ was calculated for a given set of conditions. Using the variable off-axis angles, range from 1 to 3 km, and a clear and hazy atmosphere, a computer program was prepared which calculates the intensity at the receiver for the scattered ruby laser transmitter. A pulse energy of 0.100 joules was assumed, and an elevation geometry similar to that of the tests was included (elevation, -4.29 m, elevation angle, 67 mrad). The results are shown in Figure A-2. Note that at longer range, the extinction of the hazy atmosphere reduces the available scattered energy at the receiver, while at shorter range the enhancement of scattered energy due to haze is dominant. The elevation angles of practical interest lie between 15 and 25 degrees. Thus, for the test conditions, an irradiance level of about 10^{-9} w/cm^2 is predicted. For a range of 1200 m, elevation angle of 20 degrees, and medium visibility a signal-to-noise ration of about 40 is predicted for the DBAS breadboard sensor.

AD-A114 460 TRW DEFENSE AND SPACE SYSTEMS GROUP REDONDO BEACH CA F/G 20/5
DIRECTED BEAM ALIGNMENT SYSTEM TESTING PROGRAM.(U)
JUN 79 R F GATES DAAK40-79-C-0018
UNCLASSIFIED TRW-33556 NL

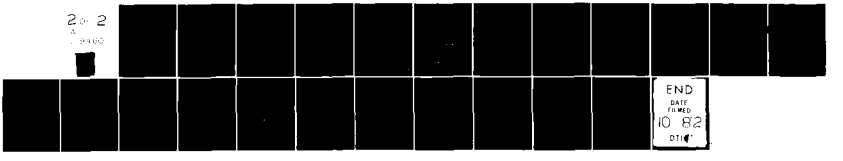

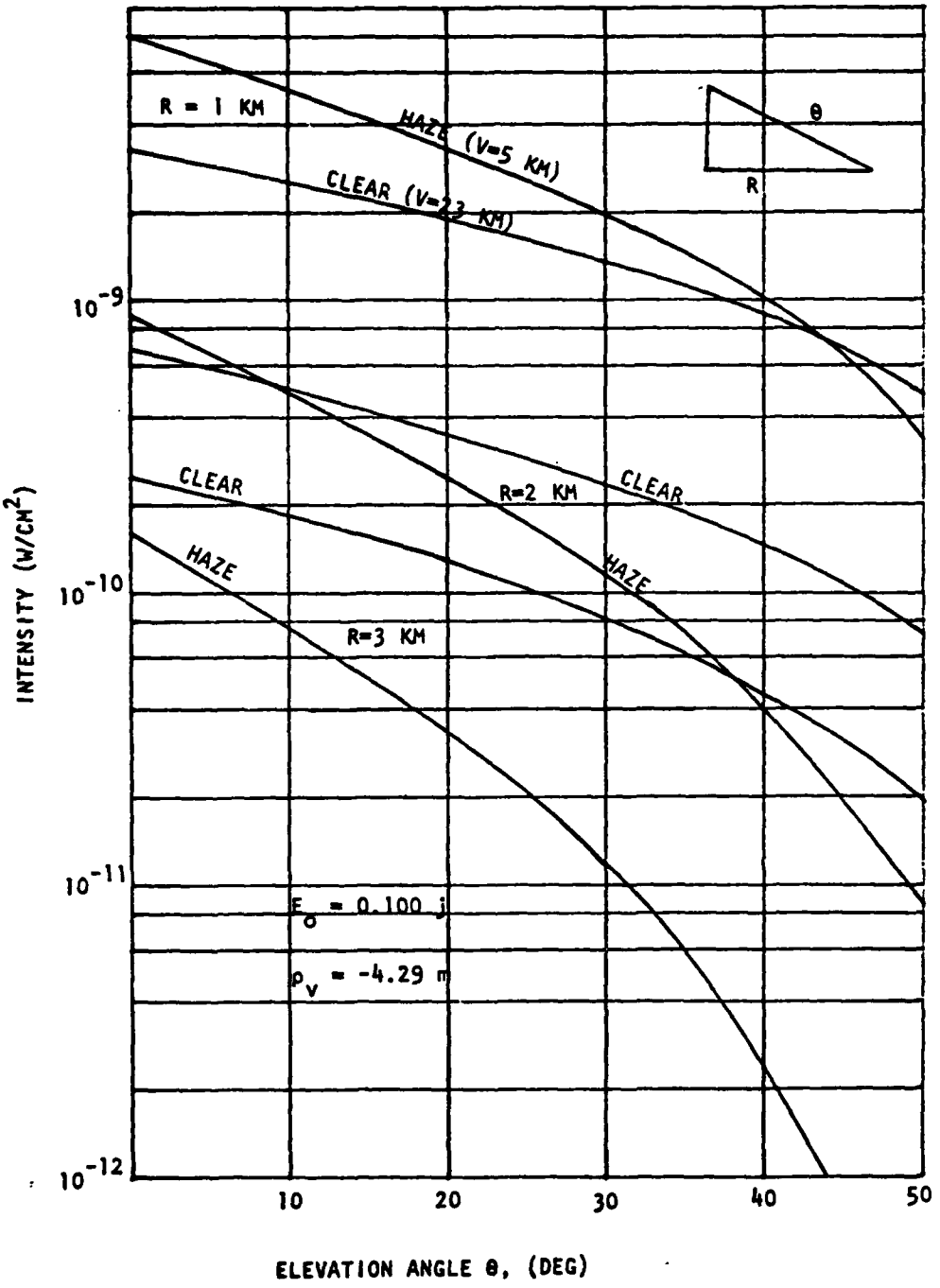

FIGURE A-2. PREDICTED INTENSITY AT THE RECEIVER

APPENDIX B

TWO GIMBAL DBAS EQUATIONS

In Section 5.1, a two-gimbal mechanization was proposed in lieu of the four-gimbal arrangement illustrated in Figure 2, Section 2. The equations necessary to achieve equivalence between the two-and four-gimbal mechanizations are summarized below.

Vehicle Attitude Relative to Local Level

In the four-gimbal mechanization, the leveling sensor was installed on the "instrument mounting plate". For the two-gimbal implementation, the leveling sensor would now be mounted directly on the instrument (i.e., either the transmitter or receiver). Assuming an azimuth and elevation gimballing order from the vehicle to the instrument, the vehicle orientation with respect to local level is given by

$$\begin{bmatrix} X \\ Y \\ Z \end{bmatrix}_V = \begin{bmatrix} \sin E_o \cdot \cos A_o & -\sin A_o & -\cos E_o \cdot \cos A_o \\ \sin E_o \cdot \sin A_o & \cos A_o & -\cos E_o \cdot \sin A_o \\ \cos E_o & 0 & \sin E_o \end{bmatrix} \begin{bmatrix} X \\ Y \\ Z \end{bmatrix}_L \qquad \text{(B-1)}$$

where A_o = azimuth gimbal reading when the instrument is leveled

E_o = elevation gimbal reading under the same consition

Instrument Azimuth(A) and Elevation (E) with Respect to Local Level

Let a and e be respectively the azimuth and elevation angle readouts relative to the vehicle axes. Then

$$\begin{bmatrix} X \\ Y \\ Z \end{bmatrix}_I = \begin{bmatrix} \text{sine}\cdot\text{cosa} & \text{sine}\cdot\text{sina} & \text{cose} \\ -\text{sina} & \text{cosa} & 0 \\ -\text{cose}\cdot\text{cosa} & -\text{cose}\cdot\text{sina} & \text{sine} \end{bmatrix} \begin{bmatrix} X \\ Y \\ Z \end{bmatrix}_V \tag{B-2}$$

$$= \begin{bmatrix} \text{se}\cdot\text{sE}_o\cdot\text{c}(a-A_o)+\text{ce}\cdot\text{cE}_o & \text{se}\cdot\text{s}(a-A_o) & -\text{se}\cdot\text{cE}_o\text{c}(a-A_o)+\text{ce}\cdot\text{sE}_o \\ -\text{sE}_o\cdot\text{s}(a-A_o) & \text{c}(a-A_o) & \text{cE}_o\cdot\text{s}(a-A_o) \\ -\text{ce}\cdot\text{sE}_o\cdot\text{c}(a-A_o)+\text{se}\cdot\text{cE}_o & -\text{ce}\cdot\text{s}(a-A_o) & \text{ce}\cdot\text{cE}_o\cdot\text{c}(a-A_o)+\text{se}\cdot\text{sE}_o \end{bmatrix} \begin{bmatrix} X \\ Y \\ Z \end{bmatrix}_L \tag{B-3}$$

where the subscript I refers to the instrument axes, and s and c are shorthand notation for sin and cosine respectively.

From the third row of (B-3), the equivalent instrument Z-axis orientation with respect to local vertical is

$$\sin E = \sin e \cdot \sin E_o + \cos e \cdot \cos E_o \cdot \cos(a-A_o) \tag{B-4}$$

$$\tan A = \frac{\cos e \cdot \sin(a-A_o)}{\cos e \cdot \sin E_o \cdot \cos(a-A_o) - \sin e \cdot \cos E_o} \tag{B-5}$$

Instrument Azimuth and Elevation Drive Commands

Because of the two-axis gimballing, it is now necessary to drive both axes relative to the vehicle in order to achieve the desired azimuth (A_d) and elevation (E_d) relative to local vertical. The necessary equations can be obtained by inverting equations (B-4) and (B-5) and are

$$\sin e_c = \text{sinE}_d\cdot\text{sinE}_o - \text{cosE}_d\cdot\text{cosA}_d\cdot\text{cosE}_o \tag{B-6}$$

$$\tan(a_c - A_o) = \frac{\text{cosE}_d\cdot\text{sinA}_d}{\text{sinE}_d\cdot\text{cosE}_o + \text{cosE}_d\cdot\text{cosA}_d\cdot\text{sinE}_o} \tag{B-7}$$

APPENDIX C

TEST PLAN

AND

ERRATA SHEET

TRW
DEFENSE AND SPACE SYSTEMS GROUP
ONE SPACE PARK • REDONDO BEACH • CALIFORNIA 90278

INTEROFFICE CORRESPONDENCE

TO: Distribution

CC: O. Imai
P. Kendall
O. Momary

DATE: 26 January 1979
6500.79.RG-002

SUBJECT: DBAS Test Plan - 6500.78.08-013

FROM: R. F. Gates

BLDG	MAIL STA.	EXT.
R3	2182	64174

ERRATA:

Page 7

E_1 = the optical angle between horizontal and 1st slit.

E_2 = the optical angle between horizontal and 3rd slit.

Page 14

Add to end of second line ", in the horizontal plane,"

Page 16

Second equation is missing "squared" sign on second term on right side of equals sign. $x^2(\frac{\sin A_1}{\sin A_2})^2$

Fourth equation is missing "prime" sign on S_2 (S_2').

6500.78.08-013
Total Pages: 18

Received 15 Jan 79 DLW

TEST PLAN

FOR

DIRECTED BEAM ALIGNMENT SYSTEM

20 DECEMBER 1978

PREPARED BY: RF Gates for
R. F. Gates

APPROVED BY: PE Kendall
P. E. Kendall

APPROVED BY: David H Gray 17 Jan 79
MIRADCOM COTR

CONTRACT NUMBER DAAK40-79-C-0018
CDRL A004
SALES NUMBER 33556

PREPARED FOR

U.S. ARMY MISSILE RESEARCH AND DEVELOPMENT COMMAND
HIGH ENERGY LASER SYSTEMS PROJECT OFFICE
REDSTONE ARSENAL, ALABAMA 35809

TRW
ONE SPACE PARK
REDONDO BEACH, CA 90278

TABLE OF CONTENTS

PAGE

1.0 Introduction 1
1.1 Purpose of Test Plan. 1
1.2 Objectives. 1
1.2.1 Sensitivity and Range. 3
1.2.2 Accuracy 3
1.2.3 Communications 3
1.2.4 Data Reduction and Analysis. 3
2.0 Test Facilities. 6
2.1 Equipment 6
2.2 Test Sites. 8
3.0 Tests. 8
4.0 Verification 11

LIST OF FIGURES

Figure 1. DBAS Components (Artists Concept) 2
Figure 2. Section View of Optical Receiving Unit 3
Figure 3. ORU and Computing Equipment Block Diagram . . . 5
Figure 4. Range and Elevation Equations. 7
Figure 5. Flow Chart 8
Figure 6. Site Locations 10
Figure 7(a). Geometry for Horizontal Range Determination . 12
Figure 7(b). Geometry for Altitude Difference Determination 12
Figure 8. Space Park Transmitter Location. 13
Figure 9. Verification Geometry. 15

1.0 INTRODUCTION

The Directed Beam Alignment System (DBAS) concept was developed by TRW's Laser Systems Group during 1977-78 IR&D sponsorship. The concept was to provide a fast, simple, accurate, and reliable technique for determining relative alignment information, both metric and angular, between several field vehicles separated by up to 3 kilometers with line-of-sight obstructions. After analytically demonstrating feasibility, TRW designed and fabricated a DBAS breadboard, also under company sponsored IR&D. The present contract is to provide system performance testing of this completed breadboard model.

1.1 Purpose of Test Plan

This test plan is for the purpose of outlining the actual tests that will be performed with the DBAS. The DBAS, Figure 1, consists of a Laser Transmitter Unit (LTU) at one location and an Optical Receiving Unit (ORU) at the second location. The LTU is comprised of a pulsed laser and an optical assembly for directing the beam vertically. The optical assembly is mounted on a plate which has two axes of gimbal freedom relative to a level reference plate. The ORU, Figure 2, consists of a Bouwers lens with 3 slit apertures located in the focal surface. Fiber optics direct the radiant energy from the slits to the photodetectors. The slits are arranged so that the two outside slits are normal to the vertical, while the center slit is at an angle. The receiver focuses and detects the vertically traveling laser pulse backscatter in sequence in each of the three slits. The time difference between the pulses from the two horizontal slit detectors will provide range information while the time between the lower horizontal slit and the angled slit provides azimuth information. The receiver can then be azimuthally positioned to provide accurate azimuthal information.

1.2 Objectives

The objective of the testing program is to provide experimental proof of the validity of the concept, and in addition to provide data that can be utilized in the conceptual design of a militarized automated DBAS. In particular, attention will be centered on sensitivity, range, accuracy, communications and data reduction and analysis requirements.

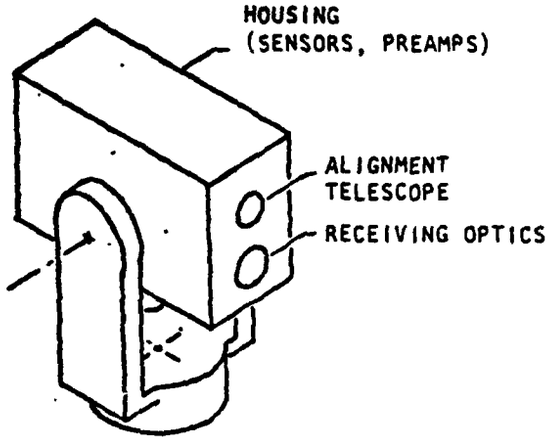

A) OPTICAL RECEIVING UNIT (ORU)

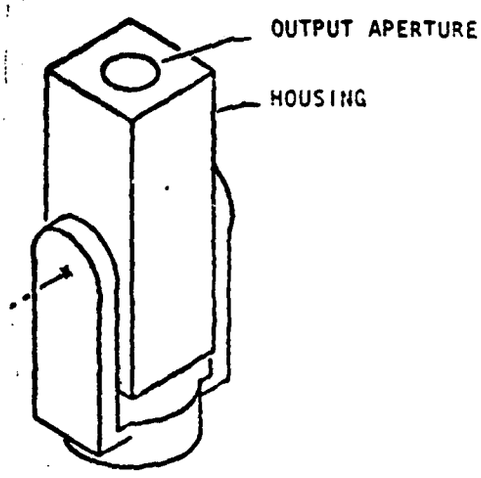

B) LASER TRANSMITTER UNIT (LTU)

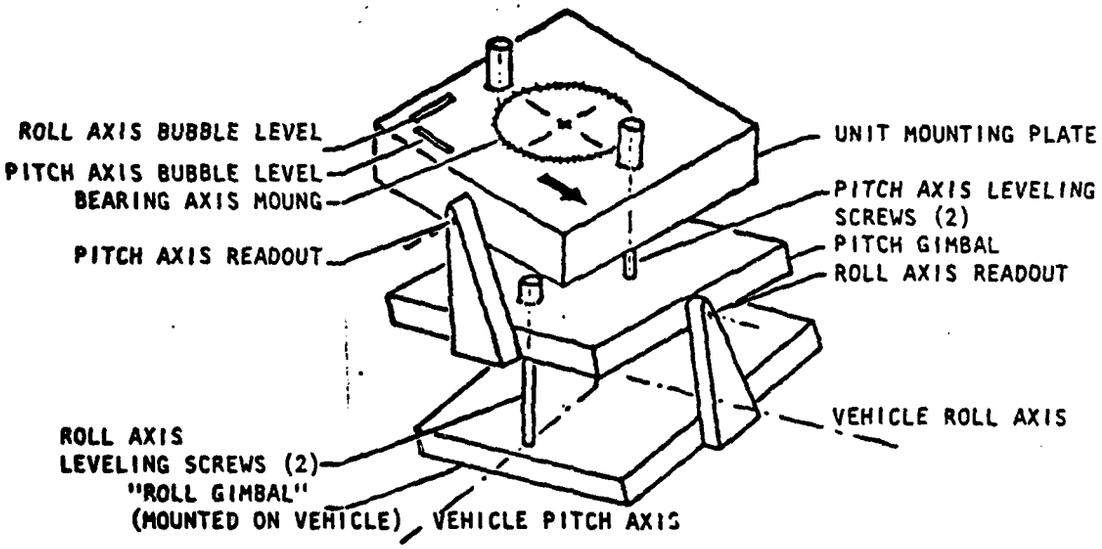

C) UNIT MOUNTING ASSEMBLY (UMA)

FIGURE 1 - DBAS COMPONENTS (ARTISTS CONCEPT)

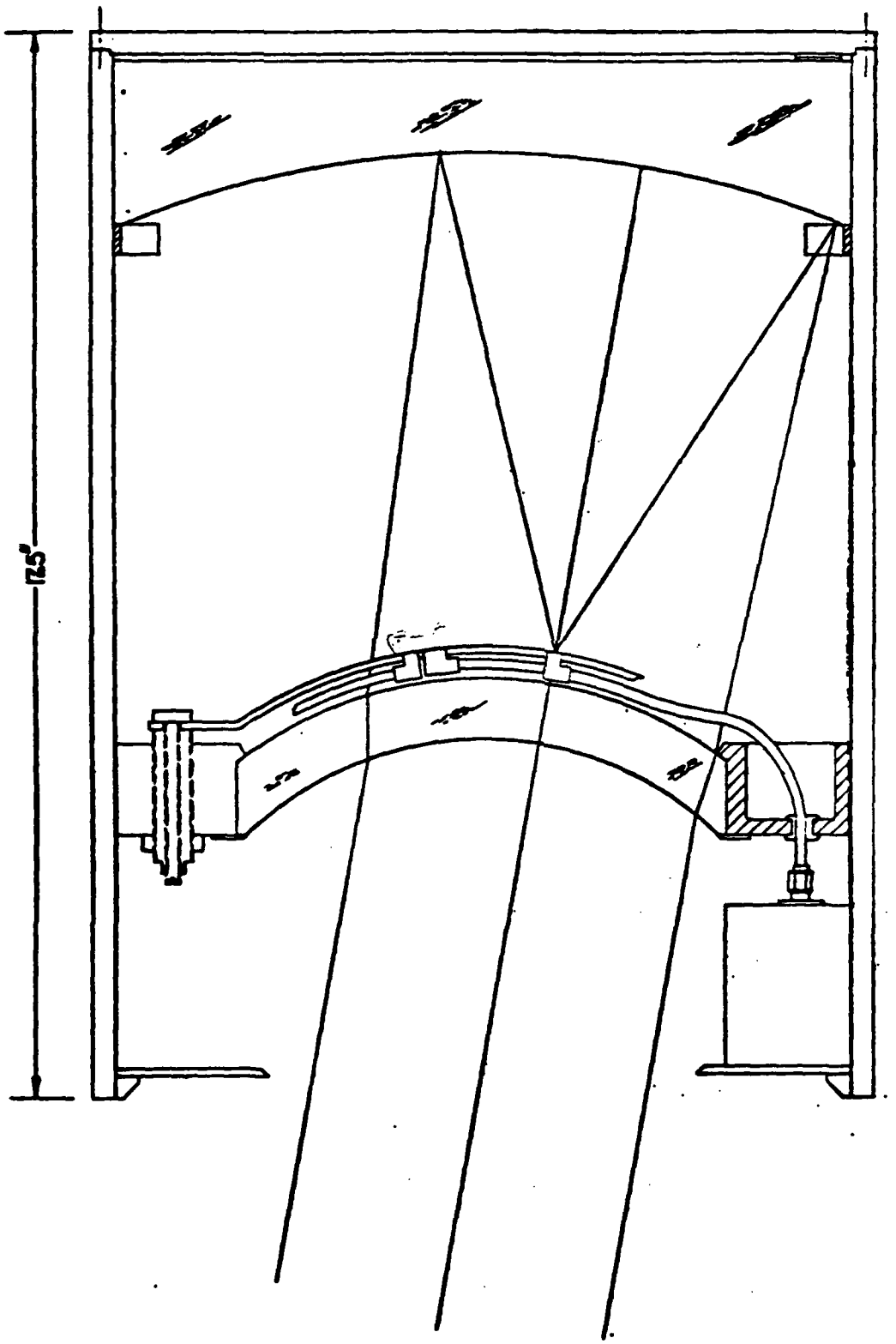

FIGURE 2. SECTION VIEW OF OPTICAL RECEIVING UNIT

1.2.1 Sensitivity and Range

The range of the DBAS is directly affected by the sensitivity of the receiver. Since the backscatter that the receiver detects can be considered an isotropic source, the inverse square law for received energy is valid. Therefore, the more sensitive the receiver the longer the range. The receiver can be made more sensitive by enlarging the receiver optical aperture, but there is a practical limit to this. Thus, using the DBAS breadboard it will be possible to determine the optimum receiver optics dimensions for maximum range of operation for use in Task 3 design effort.

Minimum range is a function of the ability to provide accurate timing measurements between pulses. Tests will be run to determine what this time is.

1.2.2 Accuracy

The accuracy of the DBAS is a function of the signal to noise ratio (sensitivity) and how it affects the accuracy of the timing measurements. The rise time of the received pulses affects the accuracy of the timing measurements. Noise on the received pulses will cause the time at which the pulse crosses the circuit threshold to occur either before or after the true zero noise time. The larger the signal to noise, the smaller this effect will be. In the case of a fixed threshold, the signals from the slits will get progressively smaller and the S/N will get less. Thus, the uncertainties in the time threshold crossing get larger with each slit. By taking a number of samples, the effects of noise can be reduced, thus the timing error (ΔT_e)

$$\text{is} \quad \Delta T_e = \Delta t_e / \sqrt{N}$$

where Δt_e is the per pulse timing error and N is the number of samples.

There is a practical limit to the number of samples that can be taken with the breadboard equipment. This is due to the low repetition rate of the Ruby laser (4 ppm) utilized for the tests. Thus, it would be unwise to extend the measurement period for more than several minutes, making the maximum number of samples to be 8 or 9 for these tests. In an operational system with a laser pulse rate of 10 pps, as many as 100 pulses could be used to reduce the noise effects by a factor of 10. The validity of this sampling technique will be verified during test.

1.2.3 Communications

Since the DBAS breadboard is not a fully automated system, walkie-talkie communications will be maintained between the LTU and the ORU at all times.

1.2.4 Data Reduction and Analysis

The output of the ORU will be directly input into a pair of HP high speed timing counters. The counter outputs will be input to an HP 9825A desktop computer and the appropriate calculation made in real time. Figure 3 shows a block diagram of both the ORU and the computing equipment.

Data acquisition consists of the measurements of Δto, $\Delta t2$ with the source laser pointed vertically and Δton, $\Delta t2n$ with the source laser at a slant angle of n degrees. The above transit times can be averaged for any number of measurements to reduce the effects of noise or other disturbances (Section 1.2.2 above). These RSS times are then used along with the system constants E_1, E_2, C to compute (see Figure 4) the relative range and elevation between the source laser and the receiver. A 9825A calculator is used to collect the time measurements from two HP5345 counters, perform data averaging, compute the range and elevation and display the results (by LED display as well as hard copy). The flow diagram shown in Figure 5 describes the procedure by which a complete set of measurements are made and the results displayed.

2.0 TEST FACILITIES

2.1 Equipment

The equipment required for the DBAS tests consists of certain special purpose equipment and some general purpose equipment. The TRW receiver design will be used with its present mounting (azimuth and elevation rotary mounts). Transmitter characteristics are given below, along with a detailed list of equipment.

Receiver

- o TRW Breadboard Design
  - o Bouwers Concentric Telescope with Fiber optic focal plane relay
  - o Avalance photodiode detectors and preamplifiers (RCA C30911E)

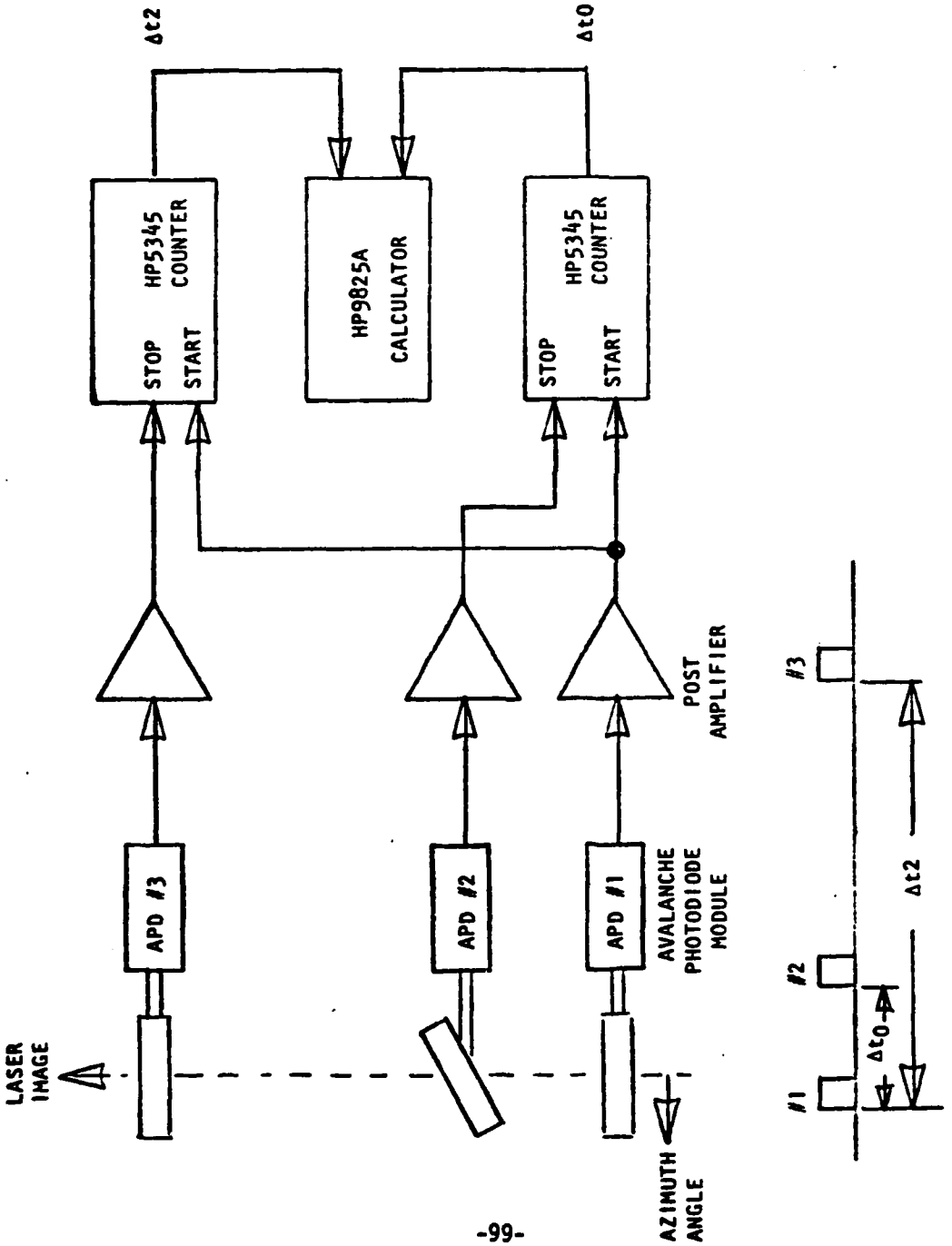

FIGURE 3. ORU AND COMPUTING EQUIPMENT BLOCK DIAGRAM

$$\overline{\Delta t_0} = \frac{1}{N} \sum_{i=1}^{N} \Delta t_{0i}$$

AV DATA

$$\overline{\Delta t_\eta} = \frac{1}{N} \sum_{i=1}^{N} \Delta t_{\eta i}$$

$$\text{RANGE} = \rho_H = \frac{C \cdot \overline{\Delta t_0} \cdot \cos E_1 \cdot \cos E_2}{\sin(E_2 - E_1) + \cos E_1 - \cos E_2}$$

$$\rho_N = \frac{C \cdot \overline{\Delta t_\eta} \cos(E_1 - \eta) \cos(E_2 - \eta)}{\sin(E_2 - E_1) + \cos(E_1 - \eta) - \cos(E_2 - \eta)}$$

$$\text{ELEVATION} = \rho_V = \frac{(\rho_N - \rho_H \cos \eta)}{\sin \eta}$$

where,

E_1 = the optical angle between 1st and 2nd slit

E_2 = the optical angle between 1st and 3rd slit, and

C = the velocity of light

AZIMUTH ERROR COEFFICIENT

$$A_0 = \frac{\overline{\Delta t_0}}{\overline{\Delta t_{20}}} 0$$

$$A_\eta = \frac{\overline{\Delta t_\eta}}{\overline{\Delta t_{2\eta}}} 0$$

FIGURE 4. RANGE AND ELEVATION EQUATIONS

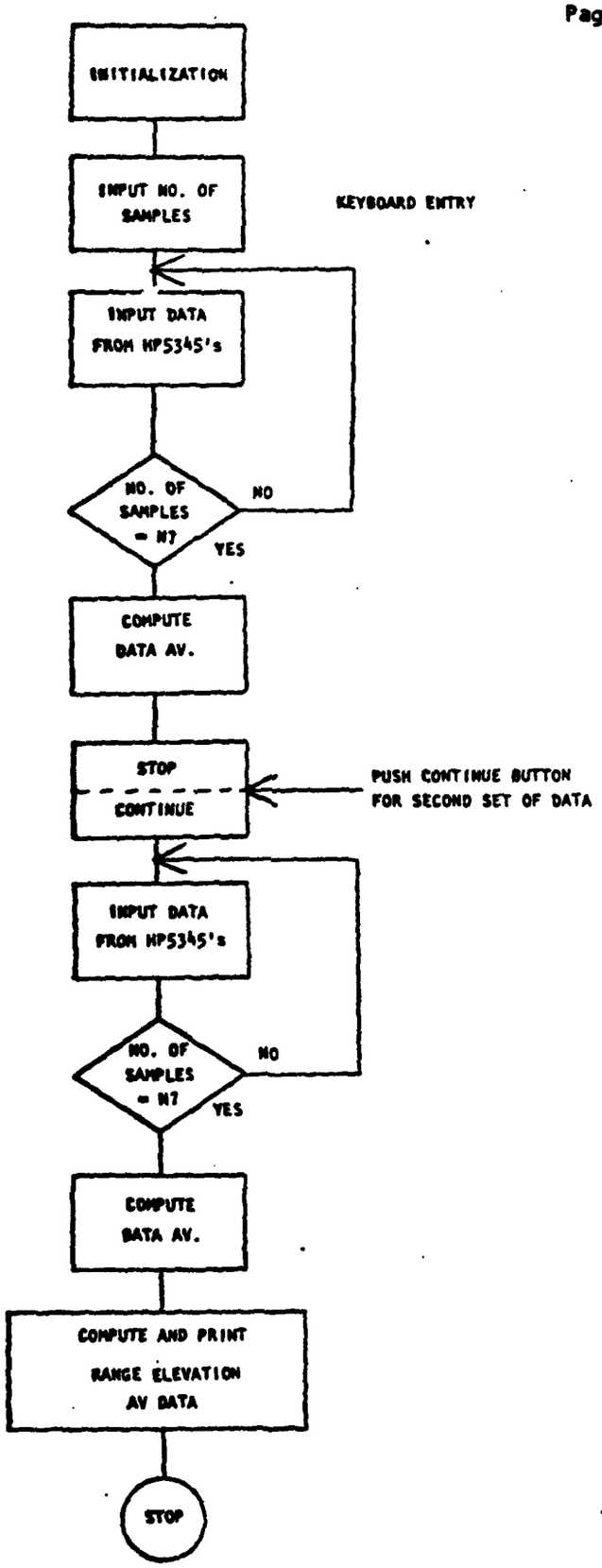

FIGURE 5. FLOW CHART

- Two 6 volt power supplies (HP 721A)
- Azimuth/Elevation Rotary Mounts

Transmitter

- Pulsed Ruby Laser 6943 Å
  - 4 ppm
  - 100 mj/pulse
  - 20 nsec/pulse
  - Beam Diameter - 6 mm
  - Beam Divergence <2 mrad

Electronic Support Equipment

- Two Electronic Counters (HP 5345)
- Computer (HP 9825)
- Oscilloscope (Tektronix 545)

Other Related Equipment

- TK-3 Theodolite
- Tripod

2.2 Test Sites

Tests will be conducted in the vicinity of TRW's Redondo Beach facility. The transmitter location will be the rooftop of Building R-1 of TRW's Space Park complex.

The ORU will be mounted in a van and transported to several locations shown on the map in Figure 6. The approximate ranges to the four locations shown are:

A ≈ 1.3 km
B ≈ 1.6 km
C ≈ 2.1 km
D ≈ 3.0 km

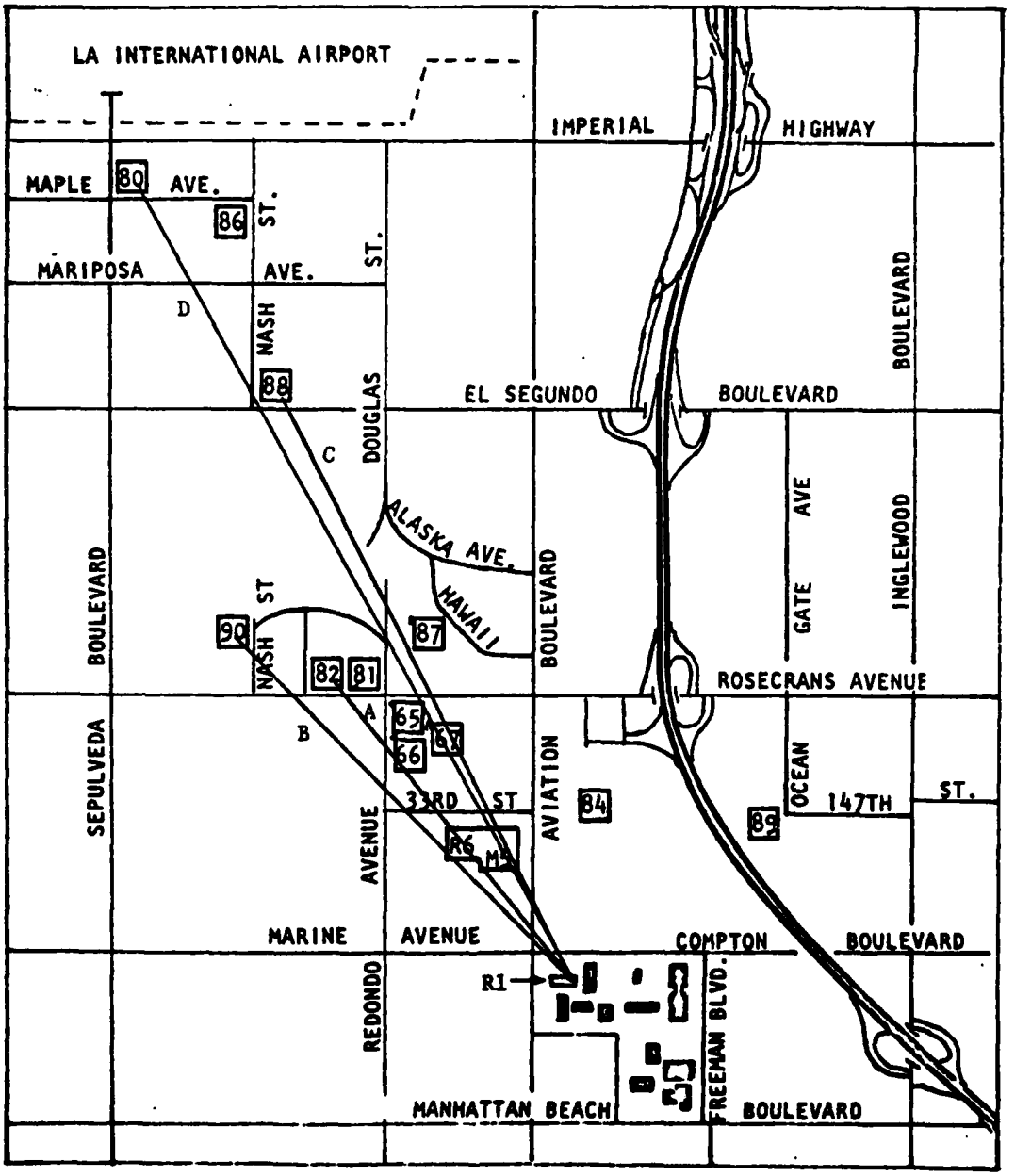

FIGURE 6. SITE LOCATION

A fifth site with a much shorter range may be added to the list to verify minimum range operation. Receiver locations are to be selected on the basis of range, power availability, line of sight, and site survey capability.

3.0 TESTS

The LTU will be located atop building R-1 and leveled for all tests. It will be placed so that both upper corners of building E-2 are visible and azimuth and elevation angle readings can be made as shown in Figure 7. The ORU will be located at each of the selected sites and leveled. Since The ORU is not automated, a technician has to be in attendance with it. The van will rock if the technician moves, thus destroying the accuracy of the measurements. To eliminate this problem, the van will be jacked up and supported off of its suspension. Both units will be nominally set-up so that they are approximately pointed toward each other. The laser is fired and the beam directed vertically. Measurements are made at the ORU after the ORU is precisely aligned in azimuth. Several readings will be made to verify angular accuracy. At this time a sighting is taken on two landmarks that are visible from each site and have a known separation. These measurements, coupled with the known azimuth, are sufficient to provide verification of the directed beam measurement results. (See Section 4.) The LTU prism assembly is now tilted so that the beam is 15° off vertical and pointed in the general direction of the ORU. Readings are taken at the ORU and the prism azimuth angle adjusted to bring the laser azimuth direction exactly in line with the ORU. This is accomplished manually using the walkie-talkies to communicate. Several readings will be made and averaged for this configuration.

After these tests have been made and verified at the Building 82 site, the van will be relocated at the next site.

4.0 VERIFICATION

It is necessary to have an independent measurement of the range and elevation in order to prove that the DBAS measurements are valid. It is proposed to use straight forward trigonometry measurements to do this. Figure 8 shows the relationships between the LTU on the roof of Building R-1, the ORU on the roof of Building 82, and the top of Building E-2. The

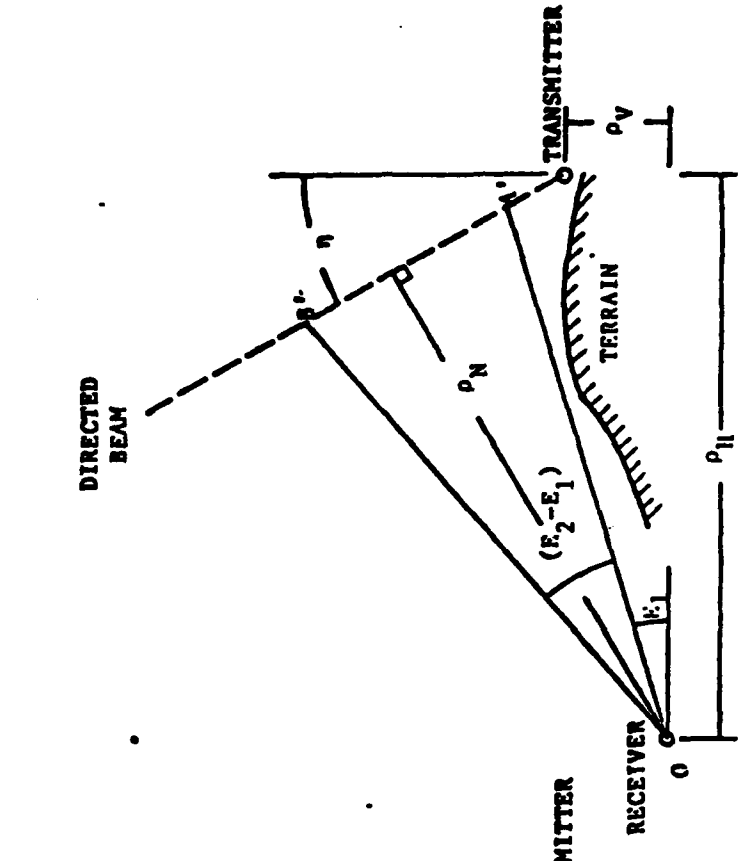

FIGURE 7(b). GEOMETRY FOR ALTITUDE DIFFERENCE DETERMINATION

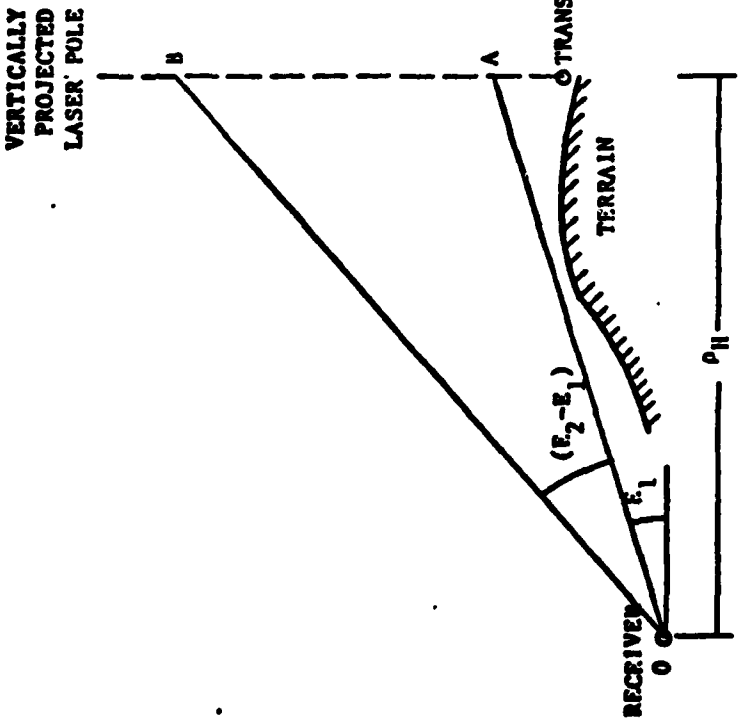

FIGURE 7(a). GEOMETRY FOR HORIZONTAL RANGE DETERMINATION

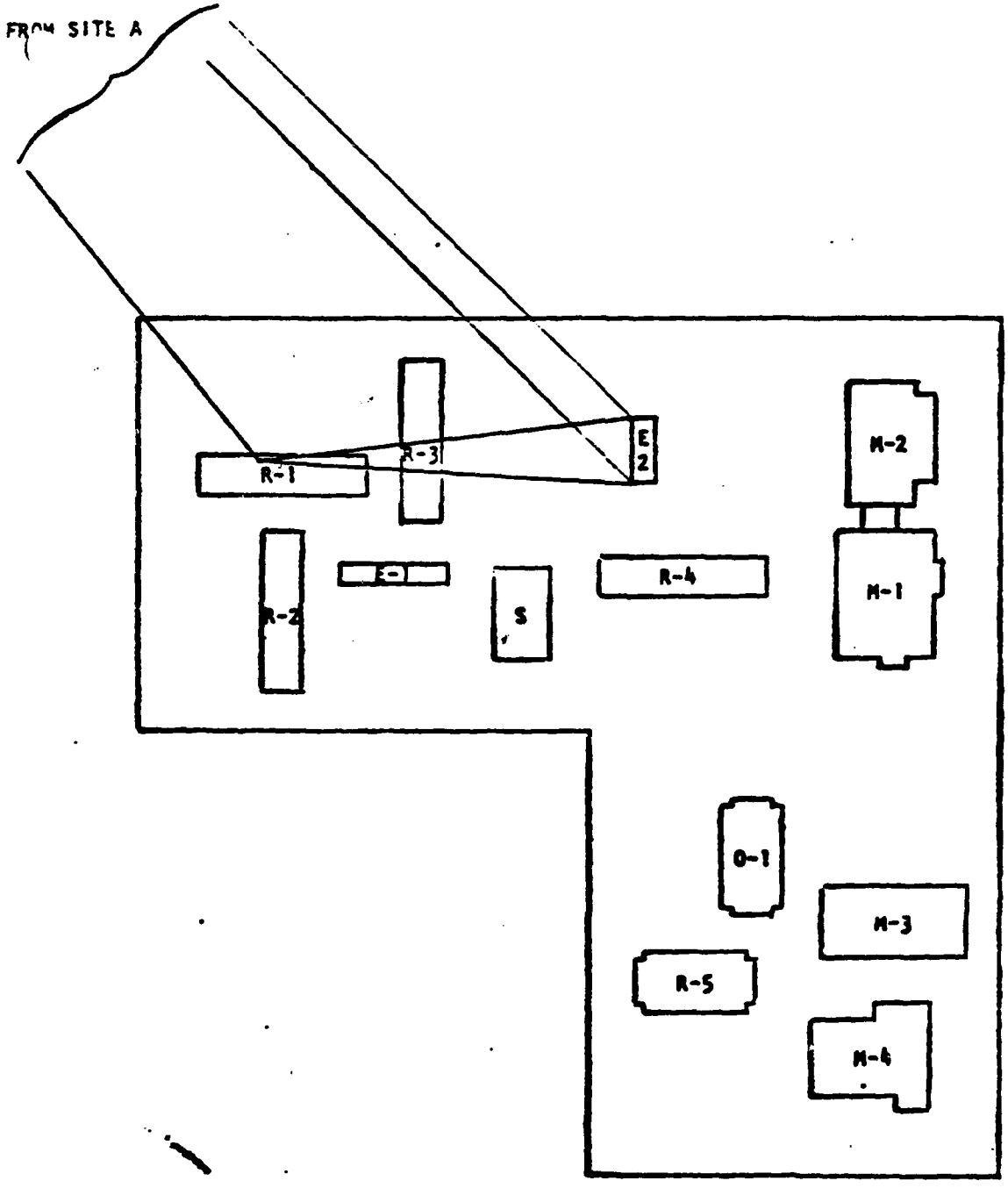

FIGURE 8. SPACE PARK TRANSMITTER LOCATION

LTU and the ORU cannot make visual contact, but both can see the top of Building E-2. The angles A_1, A_1^1, A_3, and A_3^1 (Figure 9) can be measured directly using alignment telescopes attached directly to the ORU and the LTU (or independent TK-3 theodolite measurements). The obscured line-of-sight direction between the two sites is known after the DBAS measurements have been made because part of the test procedure (Section 3) is to accurately align both the ORU and the LTU so that they are pointing directly at each other. The distance (d) can be measured between two points on the parapet on the roof of E-2. These five measurements can be used to solve for the distance ($S_1 = X$) between the LTU and the ORU as follows.

Given: A_1

A_1^1

A_3

A_3^1

d

Find:

$$A_2 = 180 - A_1 - A_3$$

$$A_2^1 = 180 - A_1^1 - A_3^1$$

$$S_2 = X \frac{\sin A_3}{\sin A_2}$$

$$S_2' = X \frac{\sin A_3'}{\sin A_2}$$

$$S_3 = X \frac{\sin A_1}{\sin A_2}$$

$$S_3 = X \frac{\sin A_1'}{\sin A_2'}$$

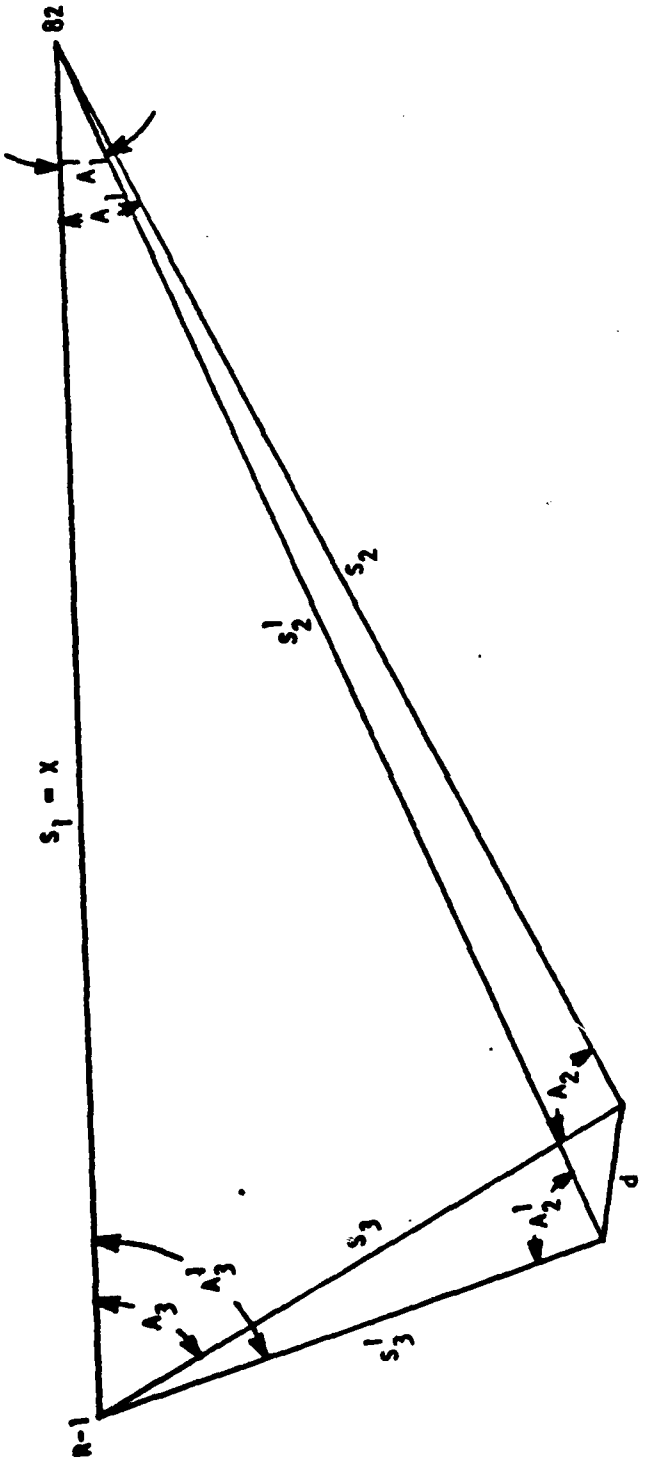

FIGURE 9. VERIFICATION GEOMETRY

$$d = \sqrt{S_3'^2 + S_3^2 - 2S_3' S_3 \cos(A_3' - A_3)}$$

or

$$d^2 = X^2\left(\frac{\sin A_1'}{\sin A_2'}\right)^2 + X^2\left(\frac{\sin A_1}{\sin A_2}\right) - 2X^2 \frac{\sin A_1' \sin A_1}{\sin A_2' \sin A_2} \cos (A_3' - A_3)$$

Rearrange and take square root of both sides gives:

$$X = \frac{d}{\sqrt{\left(\frac{\sin A_1'}{\sin A_2'}\right)^2 + \left(\frac{\sin A_1}{\sin A_2}\right)^2 - 2\frac{\sin A_1' \sin A_1 \cos(A_3' - A_3)}{\sin A_2' \sin A_2}}}$$

(X is the horizontal distance between the LTU and the ORU.) To find the vertical separation between them, the elevation angles E_3' and E_1' have to be measured at the same time A_3' and A_1' are measured.

Thus vertical separation = $S_3' \tan E_3' - S_2 \tan E_1'$

or

$$\rho_V = \frac{Si}{\sin A_2} [\sin A_1' \tan E_3' - \sin A_3' \tan E_1'].$$

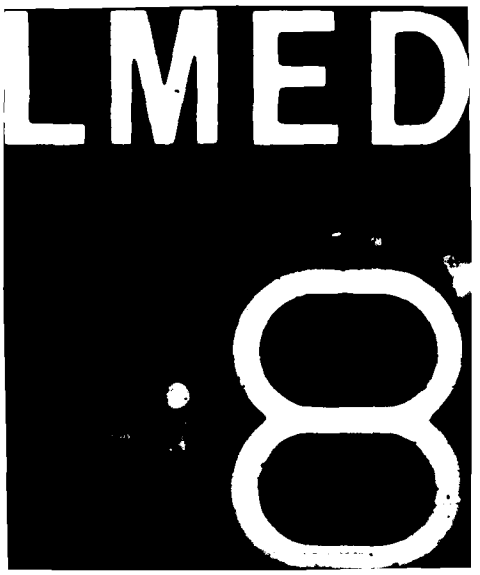
LMED
8